



Norwegian University of
Science and Technology

Long Term Analysis of Semi Submersible Offset

Sindre Schafroth
Sandbakken

Marine Technology

Submission date: June 2016

Supervisor: Sverre Kristian Haver, IMT

Co-supervisor: Kjell Larsen, IMT

Norwegian University of Science and Technology
Department of Marine Technology



Department of Marine Technology

Master Thesis
for
Stud. tech. Sindre Schafroth Sandbakken

Long Term Analysis of Semi Submersible Offset

Langtids-forsyvningsanalyse av en halvt nedsenkbar plattform

Background

Characteristic loads and loads effects for offshore structures are generally defined by the annual probability of exceedance. ULS characteristics are defined by an annual exceedance probability, q , of 10^{-2} , while ALS characteristics are defined by $q_{ALS} = 10^{-4}$. In order to estimate characteristic loads in a consistent way, a long term response analysis accounting properly for all inherent randomness are – in principle – required. Design of mooring lines differs from structural design in the sense that the characteristic line load is not defined in terms of a required maximum permissible annual exceedance probability. Instead, the characteristic line load for design is taken to be the expected 3-hour maximum in the 100-year storm event. However, it may be of interest to calculate the probability of exceeding the characteristic line load and that would require a long term response analysis.

Long term response analysis can be carried out using an all sea state approach or a peak-over-threshold approach. In this master thesis, focus is to be given using the peak-over-threshold approach. This means we shall only include storm events exceeding selected thresholds in terms of significant wave height or, possibly, in terms of wind speed if wind speed is considered to be the most important weather characteristic. Whether or not one shall include all storms above

threshold or restrict analysis to storms within selected direction sectors is a subject the candidate shall address in view of his selected problem.

The necessary weather information will be given by the Norwegian hindcast database, NORA10, giving weather characteristics every third hour from 1957 – 2014. The study can be done for Haltenbanken weather condition.

Sub-division of tasks

1. Define the problem to be analyzed. It is left to the candidate to select problem, but it shall be a problem depending both on wave and wind conditions. It is also expected that the problem is of a non-linear nature, i.e. in order to identify the short term variability of the response in a given weather condition time domain simulations using SIMA (SIMO) (or equivalent programs) are required.
2. Describe in detail the steps necessary when doing a long term analysis by the peak-over-threshold approach. In order to establish the distribution function for storm maximum (a storm is here a sequence of 3-hours stationary weather conditions) a number of 3-hour simulations are required for each storm step. If we neglect the direction and directional change during the storms, each storm step is characterized by significant wave height, H_s , spectral peak period, T_p , and wind speed, W . Then it is possibly cost efficient to do a number of 3-hour simulations of all possible combinations of H_s , T_p and W with reasonable resolution covering the actual sample space. Select for example a Gumbel distribution for the 3-hour maximum response of a given combination of H_s , T_p and W and estimate the Gumbel parameters using method of moments. Do this for all combinations and fit continuous function for the Gumbel parameters. The analysis of each storm can now be done using the response surfaces.
3. For a selected threshold, establish the step maximum response distribution for all steps using the response surfaces. Thereafter the storm distributions can be determined for each storm. Assume that the storm maximum distribution can be modelled as a conditional distribution given the most probable largest storm response. Investigate if this

conditional distribution is varying much between the included storms.

4. Fit a probabilistic model to the most probable largest storm response. This variable is now merging the long term variability in H_s , T_p and W into a single parameter valid for the selected response quantity. Perform a long term analysis by the following integral:

$$F_{Y_s}(y) = \int_{\tilde{y}} F_{Y_s|\tilde{Y}}(y|\tilde{y}) f_{\tilde{Y}}(\tilde{y}) d\tilde{y} \quad (1)$$

Estimate extremes corresponding 10^{-2} and 10^{-4} annual exceedance probability, respectively. Compare results with more traditional methods if available.

5. Investigate sensitivity to selected threshold.
6. Investigate the consequences of neglecting directional information in what is done above.
7. If current data is available, indicate effect of including current.

The candidate may of course select another scheme as the preferred approach for solving the requested problem. He may also involve other subjects than those mentioned above if found to be important for answering the overall problem; long term analysis using POT.

The work may be more extensive than anticipated. Some topics may therefore be left out after discussion with the supervisor without any negative influence on the grading.

The candidate should in his report give a personal contribution to the solution of the problem formulated in this text. All assumptions and conclusions must be supported by mathematical models and/or references to physical effects in a logical manner. The candidate should apply all available sources to find relevant literature and information on the actual problem.

The report should be well organized and give a clear presentation of the work and all conclusions. It is important that the text is well written and that tables and figures are used to support the verbal presentation. The report should be complete, but still as short as possible.

The final report must contain this text, an acknowledgment, summary, main body, conclusions, suggestions for further work, symbol list, references and appendices. All figures, tables and equations must be identified by numbers. References should be given by author and year in the text, and presented alphabetically in the reference list. The report must be submitted in two copies unless otherwise has been agreed with the supervisor.

The supervisor may require that the candidate should give a written plan that describes the progress of the work after having received this text. The plan may contain a table of content for the report and also assumed use of computer resources. As an indication such a plan should be available by end of November.

From the report, it should be possible to identify the work carried out by the candidate and what has been found in the available literature. It is important to give references to the original source for theories and experimental results.

The report must be signed by the candidate, include this text, appear as a paperback, and - if needed - have a separate enclosure (binder, diskette or CD-ROM) with additional material.

Supervisor: Sverre K. Haver

Acknowledgement

I would like to express my gratitude to Sverre Haver, my supervisor, for taking great interest in my work and always be available for discussions regarding extreme value statistics. Many thanks go to Kjell Larsen, my co-supervisor, for his teaching of the theoretical background behind SIMO. Statoil is acknowledged through Kjell Larsen for providing the SIMO input files of the semi submersible to be analyzed.

I wish to thank the Norwegian University of Science and Technology for providing the opportunity to take a Master's degree within Marine Technology.

I would like to express my deepest gratitude to my fellow students at the Department of Marine Technology for their unlimited assistance and support throughout all my years at NTNU.

Finally, a special message to my friends at "Grevlatoriet" office; Sigbjørn Rudaa, Einar Biørn-Hansen, Jørgen Holm and Rotem Sharoni - thank you for creating the best final year I could possibly have.

Abstract

The objective of this master's thesis is to perform a long term analysis of a non-linear response problem using the Peak Over Threshold (POT) method. Offset of a semi submersible was selected as suitable response problem to be investigated.

The characteristic responses obtained from the POT analysis is verified and compared to long term responses resulting from an all sea states analysis and original design conditions.

The key idea of the POT method is to establish a long term distribution of the largest response during a random storm. Each storm is modeled as a sequence of stationary 3-hour sea states. The long term distribution of the maximum response is obtained by merging the conditional distribution of the maximum given the most probable maximum with the long term distribution of the most probable maximum. Response contours are created using the Inverse First Order Reliability Method (IFORM), and the largest response on this contour is taken as the q-probability response.

The all sea states approach combines the short term variability of the 3-hour maximum response described conditionally on all realizations of sea states with the long term variability of the weather characteristics under consideration, i.e. significant wave height (H_s), spectral peak period (T_p) and wind velocity (W), to get the long term distribution of the largest response during a random 3-hour sea state. Here, a proper distribution of the weather characteristics is estimated by processing hindcast data for Haltenbanken. The marginal distribution of H_s is established together with the conditional distribution of W given H_s and the conditional distribution of T_p given H_s and W . The q-probability responses are calculated utilizing IFORM.

The traditional design conditions assumed to give a conservative estimate of the 100-year, i.e. ULS, response is taken as the most probable largest response during a storm with 100-year wind speed and 100-year waves. Similarly, the 10,000-year response is taken as the most probable largest response in a sea state modeled with 100-year wind and 10,000-year waves, since waves are proven to be the most important weather characteristic.

This study demonstrates that the POT method is less conservative than the all sea states approach and original design conditions. The practical implication of less conservative q-probability responses obtained from a POT analysis is a more optimized design of offshore structures without compromising the safety aspect.

Sammendrag

Hensikten med denne masteroppgaven er å gjennomføre en langtidsanalyse av et ikke-lineært responsproblem med terskelmetoden (POT-metoden). Forskyvning av en halvt nedsenkbar plattform i Norskehavet ble valgt som et passende responsproblem.

De karakteristiske responsene beregnet med POT-metoden skal verifiseres og sammenlignes med tilsvarende responser utregnet med alle sjøtilstanders metode og tradisjonelle designkriterier.

Hovedidéen bak terskelmetoden er å beregne langtidsfordelingen av den største responsen i en tilfeldig storm. Hver storm er modellert som en serie stasjonære 3-timers sjøtilstander. Man får langtidsfordelingen av den største responsen ved å forene den betingede fordelingen til den største responsen gitt den mest sannsynlige største responsen og langtidsfordelingen av den mest sannsynlige største responsen. Responskonturer etableres med 'First Order Reliability Method' (IFORM), og den største responsen på denne konturlinjen blir valgt som den karakteristiske responsen.

I alle sjøtilstanders metode må korttidfordelingen av 3-timers største respons gitt alle realisasjoner av en sjøtilstand kombineres med langtidsfordelingen av de relevante vær-karakteristikkene (altså H_s , T_p og W) for å få langtidsfordelingen av største respons gitt en tilfeldig 3-timers sjøtilstand. Her vil en langtidsfordeling av vær-karakteristikkene estimeres fra hindcast-data for Haltenbanken. Det betyr at marginalfordelingen til H_s skal etableres sammen med den betingede sannsynlighetsfordelingen av W gitt H_s og den betingende fordelingen av T_p gitt H_s og W . Til slutt estimeres de karakteristiske responsene med IFORM.

Tradisjonelle designkriterier skal gi et konservativt estimat på 100- og 10,00-års respons. For eksempel antas 100-responsen å være lik den mest sannsynlige største responsen i en sjøtilstand med 100-års vindstyrke og verste 100-års bølger. Tilsvarende tar man 10,000-års responsen som den mest sannsynlige største responsen i en sjøtilstand med 100-års vindstyrke og verste 10,000-års bølger, når bølger er antatt å dominere ekstreme responser.

Denne studien viser at POT-metoden gir mindre konservative karakteristiske responser enn alle sjøtilstanders metode og tradisjonelle designkriterier. Den praktiske betydningen av mindre konservatisme i POT metoden er mer optimalisert design av offshore-installasjoner uten å overskride sikkerhetskriterier.

Contents

Acknowledgement	v
Abstract	vi
Sammendrag	viii
1 Introduction	1
1.1 Background	1
1.2 Objective	2
1.3 Thesis outline	2
2 Structure and environment	5
2.1 Description of the structure	5
2.2 Simplified structural model	6
2.3 Environmental data	8
2.3.1 Correction of hindcast data	8
2.4 Defining a storm event	10
3 Theoretical background of simulations in SIMO	13
3.1 Equation of motion	13
3.1.1 Solving the equation of motion	14
3.2 Excitation forces	15
3.2.1 Wind forces	16
3.2.2 Wave forces	18
3.3 Mass, damping and restoring forces	21
3.3.1 Mass forces	21
3.3.2 Damping forces	21

3.3.3	Restoring forces	22
3.4	Dynamic amplification	23
3.5	Generation of time series	24
3.6	Example time series of offset in SIMO	25
4	Introduction to long term analysis	29
4.1	Determine short term variability of the response	31
4.2	Response surfaces for the POT analysis	31
4.2.1	Convergence of the response surfaces	35
4.2.2	Final expression of the response surfaces	39
4.3	Additional response surfaces to be used in the all sea states analysis	41
4.4	Comparing the two sets of response surfaces	44
5	Peak over threshold	47
5.1	Distribution of storm maximum response	48
5.2	Short term variability by $F_{X \tilde{x}}(x \tilde{x})$	49
5.3	Long term variability by $F_{\tilde{X}}(\tilde{x})$	53
5.4	Long term analysis	54
5.4.1	FORM	55
5.4.2	IFORM	57
5.5	ULS and ALS responses	57
5.6	Threshold selection	58
5.6.1	Threshold sensitivity study	59
6	All sea states approach	61
6.1	All sea states to extreme responses	61
6.2	Long term variability of weather	62
6.2.1	Marginal distribution of H_s	62
6.2.2	Conditional distribution of W	65
6.2.3	Conditional distribution of T_p	70
6.2.4	Environmental contour lines of H_s , T_p and W	75

6.3	ULS and ALS responses	77
7	Traditional approach in estimating characteristic responses	81
8	Comparing characteristic responses from POT, all sea states and traditional design conditions	85
9	Conclusion	87
10	Further Work	89
	Bibliography	92
	Appendices	97
A	Response surfaces for the POT analysis	99
A.1	β_G convergence	100
A.2	α_G convergence	101
A.3	β_G dependency on H_s , T_p and W	102
A.4	α_G dependency on H_s , T_p and W	103
A.5	$\beta_G(h, t, w)$ fit to empirical data	104
B	Additional response surfaces for the all sea states analysis	105
B.1	$\beta_G(h, t)$ response surfaces for different W values	106
B.2	$\beta_G(h, t, w)$ fit to empirical data	107
C	Peak Over Threshold	109
C.1	β_v for different thresholds	110
C.2	$F_{\tilde{X}}(\tilde{x})$ for different thresholds	111
C.3	Response contour lines for different threshold	112
D	All sea states approach	113
D.1	Scatter diagram	114
D.2	Conditional distribution of W	115
D.3	Conditional distribution of T_p	120

E	Traditional approach in estimating characteristic responses	127
E.1	Responses along 100-year contour of H_s and T_p in combination with 100-year wind speed	128
E.2	Responses along 10,000-year contour of H_s and T_p in combination with 100-year wind speed	130
E.3	Responses on 100-year contour of H_s and T_p in combination with 10,000-year wind speed	132

List of Figures

2.1	Single degree of freedom system	6
2.2	SIMO model	7
2.3	Correction of T_p	9
2.4	Correction of W	9
2.5	Defining independent storm event	10
3.1	First order wave motion transfer function	18
3.2	Wave drift coefficient	20
3.3	Restoring force of a mooring line	23
3.4	Dynamic amplification	24
3.5	Example time series of offset in SIMO, $H_s = 8.0m$, $T_p = 10.0s$ and $W = 5m/s$	25
3.6	Example time series of offset in SIMO, $H_s = 8.0m$, $T_p = 15.0s$ and $W = 15m/s$	26
4.1	Distribution of 3-hour maximum response	33
4.2	Example α_G response surfaces for different values of W	34
4.3	Example β_G response surfaces for different values of W	34
4.4	α_G convergence for different W sampling points, $H_s = 12m$, $T_p = 14.8s$	36
4.5	β_G convergence for different W sampling points, $H_s = 12m$, $T_p = 14.8s$	36
4.6	β_G dependency on W	38
4.7	α_G dependency on W	38
4.8	β_G response surface for the POT analysis	40
4.9	α_G response surfaces for the POT analysis	40
4.10	Additional β_G response surface to be used in the all sea states analysis	43
4.11	Additional α_G response surfaces to be used in the all sea states analysis	43
4.12	Comparing overlapping region of β_G response surfaces	45

4.13	Comparing overlapping region of α_G response surfaces	46
5.1	Percentil levels of α_s in the exact distribution of storm maximum response	50
5.2	Exact vs. approximate distribution of storm maximum response	51
5.3	Observations of β_v , threshold $H_s = 8m$	53
5.4	Long term distribution of \tilde{x}	54
5.5	Response contours of X and \tilde{X} , threshold $H_s = 8m$	58
6.1	Marginal distribution of H_s	64
6.2	Conditional distribution of W	66
6.3	$\sigma_W(h)$ in conditional distribution of W	67
6.4	$\lambda_W(h)$ in conditional distribution of W	67
6.5	Marginal distribution of W	68
6.6	Contour lines of H_s and W	69
6.7	Difference in empirical σ_{T_p} and $\sigma_{T_p}(h, w)$	71
6.8	Empirical mean T_p given H_s and W	72
6.9	Normalized T_p as a function of normalized W	73
6.10	Parameterized θ	74
6.11	Difference in empirical mean T_p and $\mu_{T_p}(h, w)$	75
6.12	Environmental contour lines, projection onto the H_s - T_p plane	76
6.13	Environmental contour lines, projection onto the H_s - W plane	76
6.14	3-dimensional environmental contour lines	77
7.1	Responses along contours of H_s and T_p	82

List of Tables

2.1	Main particulars of semi submersible	5
3.1	Most important loads	16
4.1	$\beta_G(h, t, w)$ coefficients	39
5.1	β_v variability, threshold $H_s = 8m$	52
5.2	ULS and ALS responses for threshold $H_s = 8m$	58
5.3	Number of observed storms for different thresholds	59
5.4	β_v variability for different thresholds	59
5.5	Parameters in $F_{\bar{X}}(\bar{x})$	60
5.6	ULS and ALS responses for different thresholds	60
6.1	Coefficients in marginal distribution of H_s	63
6.2	ULS and ALS responses from all sea states analysis	79
8.1	Comparing characteristic responses by the three methods	85

Abbreviations

ASS	All sea states
ALS	Accidental limit state, annual exceedance probability of 10^{-4}
cdf	Cumulative density function
HF	High frequency
LF	Low frequency
pdf	Probability density function
POT	Peak over threshold
ULS	Ultimate limit state, annual exceedance probability of 10^{-2}

Nomenclature

A	Cross-sectional area
$A(\omega)$	Frequency dependent added mass
$b_1 - b_3$	Coefficients in $\sigma_W(h)$
C_D	Directional drag coefficient
$C(\omega)$	Frequency dependent potential damping
$c_{wa}(\omega)$	Frequency dependent wave drift coefficient
c_{wind}	Wind force coefficient
D_1	Linear damping matrix
D_2	Quadratic damping matrix
$d_1 - d_3$	Coefficients in $\mu_{Tp}(h)$
$e_1 - e_3$	Coefficients in $\bar{w}(h)$
$F_V(v)$	Normalized distribution of maximum response given the most probable largest maximum
$F_{X H_s, T_p, W}(x h, t, w)$	cdf of 3-hour maximum response given weather characteristics
$F_{X storm}(x storm)$	Distribution of storm maximum response
$F_{X_{3h}}(x)$	Distribution of 3-hour maximum response

$F_X(x)$	Long term distribution of maximum response
$F_{X \tilde{X}}(x \tilde{x})$	cdf of maximum response given the most probable maximum response
$f_1 - f_2$	Coefficients in additional β_G response surface to be used in the all sea states analysis
$f_{H_s, T_p, W}(h, t, w)$	pdf of weather characteristics
$f_{H_s}(h)$	pdf of H_s
$f_{T_p h, w}(t h, w)$	pdf of T_p given H_s and W
$f_{W H_s}(w h)$	pdf of W given H_s
$f_{\tilde{X}}(\tilde{x})$	pdf of most probable largest response
$g()$	Failure boundary
H_s	Significant wave height
$\mathbf{K}(\mathbf{x})$	Stiffness matrix
$k_1 - k_6$	Coefficients in β_G response surface for the POT analysis
M	Number of stationary storm steps
\mathbf{M}	Body mass matrix
N_s	Expected number of storms per year
$p_f(x_{crit})$	Probability of exceeding x_{crit} (critical response)
\bar{q}_{drift}	Mean wave drift force
$\mathbf{q}(\mathbf{t}, \mathbf{x}, \dot{\mathbf{x}})$	Excitation forces
\mathbf{q}_{HF}	High frequency forces
\mathbf{q}_{LF}	Low frequency forces

$\mathbf{q}_{current}$	Current drag forces
\mathbf{q}_{wave}^1	First order wave forces
\mathbf{q}_{wave}^2	Second order wave forces
\mathbf{q}_{wind}	Wind drag forces
$S(\omega)$	Spectrum
T_p	Spectral peak period
$U_1 - U_4$	Standard Gaussian variables
\bar{U}_{wi}	Mean wind velocity
$u(t)$	Fluctuating wind component
$u_1 - u_4$	Points in u-space
ν	Ratio between storm maximum realization and storm most probable maximum
ν_{T_p}	Normalized standard deviation of T_p (σ_{T_p}) with respect to mean T_p (μ_{T_p})
W	Wind speed
\bar{w}	Mean wind speed
w_q	q-probability wind speed
X, x	Response variable and response
X_{3h}	3-hour maximum response
\bar{X}	Mean value of 3-hour maximum response
\mathbf{x}_{HF}	High frequency motions
\mathbf{x}_{LF}	Low frequency motions

\mathbf{x}	Position vector
\tilde{x}	Most probable largest response
x_q	q-probability response
x_{crit}	Critical response
$\Phi(-)$	Standard Gaussian distribution function
α_G	Gumbel location parameter in distribution of 3-hour maximum response
α_{G_i}	Gumbel location parameter in distribution of 3-hour maximum response of sea state i
α_s	Gumbel location parameter in distribution of storm maximum response
α_{H_s}	Weibull location parameter in long term distribution of H_s
$\alpha_{\tilde{x}}$	Weibull location parameter in distribution of most probable largest response
β	Contour radius in Gaussian space
β_G	Gumbel scale parameter in distribution of 3-hour maximum response
β_{G_i}	Gumbel scale parameter in distribution of 3-hour maximum response of sea state i
β_s	Gumbel scale parameter in distribution of storm maximum response
β_v	Normalized β_s with respect to the storm most probable largest response
$\bar{\beta}_v$	Mean β_v
$\beta_{v,2.5\%}$	2.5 percentile level of β_v

$\beta_{v,97.5\%}$	97.5 percentile level of β_v
β_{H_s}	Weibull scale parameter in long term distribution of H_s
$\beta_{\tilde{x}}$	Weibull scale parameter in distribution of most probable largest response
γ	Parameter in expression for $\mu_{T_p}(h, w)$
λ_{H_s}	Weibull shape parameter in long term distribution of H_s
$\lambda_{\tilde{x}}$	Weibull shape parameter in distribution of most probable largest response
μ_{T_p}	Mean T_p
$\mu_{\ln(T_p)}$	Mean of $\ln(T_p)$
ω	Angular frequency
ω_0	Natural frequency
ϕ	Variable to create hypersphere in u-space
ψ	Variable to create hypersphere in u-space
ρ_{air}	Air density
σ_X	Standard deviation of the 3-hour maximum response
σ_{T_p}	Standard deviation of T_p
$\sigma_{\ln(T_p)}$	Standard deviation of $\ln(T_p)$
θ	Parameter in expression for $\mu_{T_p}(h, w)$
ε	Phase shift
φ	Variable to create hypersphere in u-space
$\xi(t)$	Time dependent wave elevation

$h(\tau)$

Retardation function

Chapter 1

Introduction

1.1 Background

Characteristic loads and responses of offshore structures are defined by an annual probability of exceedance. In design of offshore structures, the characteristic loads and responses need to be controlled to ensure adequate robustness against overload and failure. Two limit states, ULS (ultimate limit state) and ALS (accidental limit state), are therefore established and defined from the annual probability, q -probability, of exceedance. ULS corresponds to an annual exceedance probability of 10^{-2} , while ALS defines an annual exceedance probability of 10^{-4} . To estimate ULS and ALS characteristics, all sources of inherent randomness must be taken into account. This means that some kind of long term analysis is required to obtain a reliable estimate of the characteristic responses.

ULS and ALS responses are in some cases not defined in terms of annual exceedance probabilities. Traditionally, the characteristic offset is taken as the most probable largest offset during a storm with prescribed design conditions. For example, the ULS response of a moored semi submersible is taken as the most probable largest response in a storm with 100-year waves and wind. It may be of interest to find the level of conservatism for this characteristic offset, and this would again require a full long term analysis.

1.2 Objective

The q-probability offset of a typical large semi submersible will be investigated using the peak over threshold (POT) method and the all sea states approach. The q-probability responses from the two long term analyses will then be compared to the traditional approach in estimating characteristic responses.

The selected problem is of non-linear nature and requires a suitable number of time domain simulations to identify the short term variability of the response given any weather condition. All forces act in surge direction, i.e. directional variability of the weather is neglected. Current forces are also neglected. SIMO is used for the time domain simulations and Matlab is used for post processing of the results. Weather data for Haltenbanken area will be used in the analysis.

1.3 Thesis outline

Chapter 2 provides the reader with an introduction to the thesis. The actual structure to be investigated will be introduced together with the simplified computer model in SIMO. Environmental data required for the long term analyses will be reviewed briefly, and a storm event for the POT method will be defined.

Chapter 3 is devoted entirely to the theoretical background of time domain simulations in SIMO. This chapter will explain the interaction between the structure and environmental forces that is important for evaluating the results.

Chapter 4 gives a brief introduction to long term analysis. In this chapter, two sets of response surfaces to be used in the POT and all sea states analysis are established. The first set of response surfaces includes all observed weather conditions and will be used in the POT method and for calculating the all sea states 100-year response. The second set of response surfaces are established to include non-observed sea states that will be used for calculating the all sea states 10,000-year response.

Chapter 5 is where the POT analysis is explained step by step. Threshold selection for the POT analysis will be discussed. The IFORM approach will also be reviewed before it is used in estimating the q-probability responses.

Chapter 6 includes the all sea states approach. The main focus will be to establish a long term distribution of the weather characteristics, since the response surfaces is already established in Chapter 4.

Chapter 7 covers the traditional approach in estimating q-probability offset.

Chapter 8 is devoted to compare the results of the POT method, all sea states approach and traditional design conditions.

Chapter 9 & 10 will give some concluding remarks together with suggestions for further work.

Chapter 2

Structure and environment

In this chapter, the main particulars of the semi submersible used in the analysis will be reviewed together with a brief description of the simplified computer model of the structure that is used in SIMO. In addition, the selected threshold for the POT analysis and correction of hind-cast data will be discussed.

2.1 Description of the structure

The structure is a typical spread-moored production semi submersible that comprises of a ring pontoon with six columns that supports the topside, and the hull is symmetric about the x-axis.

The semi submersible's main particulars are summarized in Table 2.1.

Table 2.1: Main particulars of semi submersible

Hull length/width	102.4/96.0m
Deck length/width	114.0/96.0m
Operational displacement	84848mt
Operational draught	25m
Air gap	20m

The mooring system consists of 4x4 catenary lines that are connected to each corner of the semi.

The catenary lines are made of chains together with a wire segment of 180m for 12 lines, and 280m for the remaining 4 lines. The diameter of the chains and wires is 142mm and 136mm, respectively. There are 16 suction anchors, that are 5m in diameter and 10.5m in height, connecting the chains to the sea floor.

2.2 Simplified structural model

Since it is assumed that all forces are acting in surge direction, one may better understand the vessel surge motions by considering the platform model as a single degree of freedom system with stiffness, damping, mass and force excitation terms as depicted in Figure 2.1. The mass terms consists of body mass and added mass. The damping terms mainly arise from hydrostatic damping and the stiffness term are caused by the mooring lines (and risers).

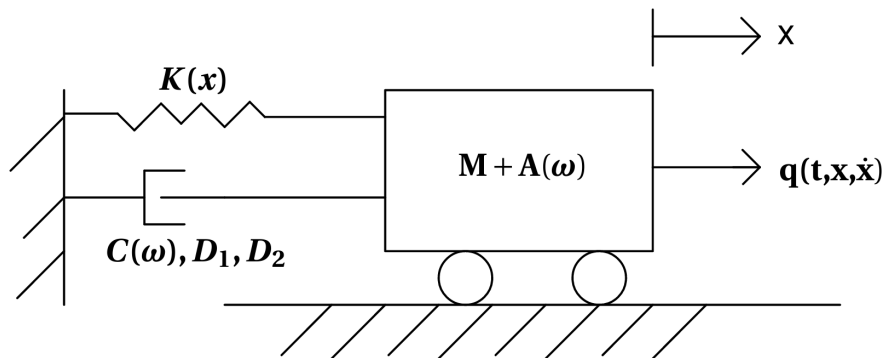


Figure 2.1: Simplified single degree of freedom system

Here $M + A(\omega)$ is total mass, $C(\omega)$, D_1 and D_2 are damping terms, $K(x)$ provides stiffness and $q(t, x, \dot{x})$ are the environmental excitation forces.

A time series of offset is calculated by establishing all terms in the equation of motion in all six degrees of freedom, and solving the equation of motion in the time domain. This procedure will be explained in Chapter 3. The catenary system and semi submersible are treated as de-coupled. Hence, the mooring lines provide the main restoring forces, and the dynamic effects from the mooring lines and risers are neglected. Further, only static (mean) forces, wave frequency forces

and low frequency forces are considered because these forces are the largest contributors to the platform's response in surge, sway and yaw. Low frequency forces are usually not large, but significant amplifications might occur since their frequency can be close to the natural period in surge, sway and yaw, Faltinsen (1990).

Each time domain analysis will simulate a 3-hour sea state. The analysis begins from a stationary static configuration. When dynamic loads are applied, changes from static to dynamic motions introduce transients, and the results should be interpreted after these transients have dissipated. Consequently, each analysis simulates 12000 seconds, whereas the first 1200 seconds is assumed part of the transient face. The remaining 10800 seconds (equivalent to 3-hours) are considered for the post processing of the results.

A complete SIMO model of the typical large semi submersible used in the analysis was provided by Larsen (2016). A picture of the vessel as it appears in SIMO is presented in Figure 2.2. All environmental forces act in surge direction and the vessel is free to move in all six degrees of freedom. Risers are included in the analysis even though they will have little effect on the results.

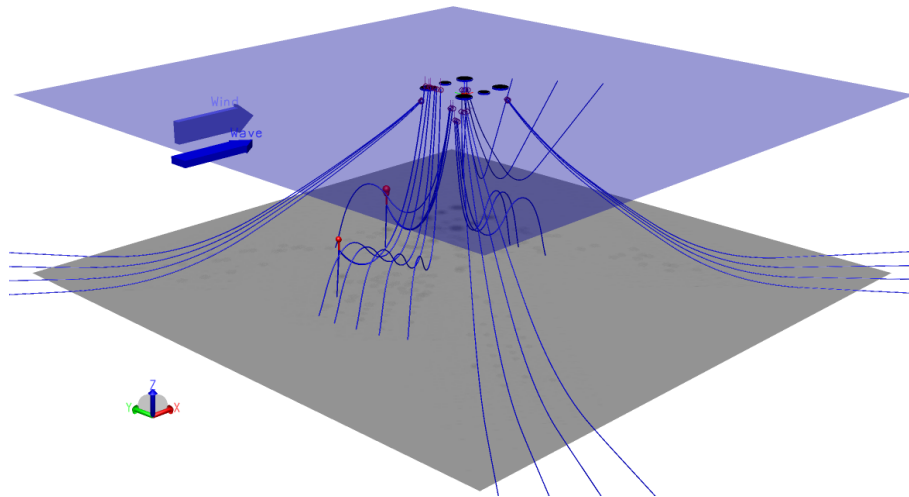


Figure 2.2: SIMO model

In SIMO, waves are modeled with a Jonswap double peaked spectrum and wind with a NPD spectrum.

2.3 Environmental data

Reliable historical data of wind and waves are important in design of offshore structures. Often a proper sample of environmental data is lacking. Therefore, environmental hindcast data is produced by running numerical models based on historical data that is available, such as wind data. For example, in the first extensive hindcast survey at the Norwegian Meteorological Institute, wind and wave data were generated from an air pressure field using a wave generation model, Haug and Guddal (1981).

The hindcast data used in this study is from Haltenbanken area (WAM10) and was provided by Haver (2016). WAM10 contains weather characteristics every third hour from 1957-2014, equivalent to 166,053 observed 3-hour sea states.

2.3.1 Correction of hindcast data

An examination of the hindcast data reveals that T_p values are discrete with logarithmic spacing. The discrete values of observed T_p when $H_s \geq 8m$ are 10.2, 11.2, 12.3, 13.5, 14.9, 16.4, 18, 19.8s. To better replicate a real ocean environment, the spectral peak periods are scattered randomly about these discrete values, Haver (2015a). Correction of T_p values are only carried out once, since the correction is random in nature.

In addition, the largest wind speeds in the hindcast data are slightly too small. The fraction of wind speeds above $15m/s$ are therefore increased by 20%. The corrected weather data for $H_s \geq 8m$ are compared to the original hindcast data in Figure 2.3 and 2.4. The corrected environmental data will be used in the analysis.

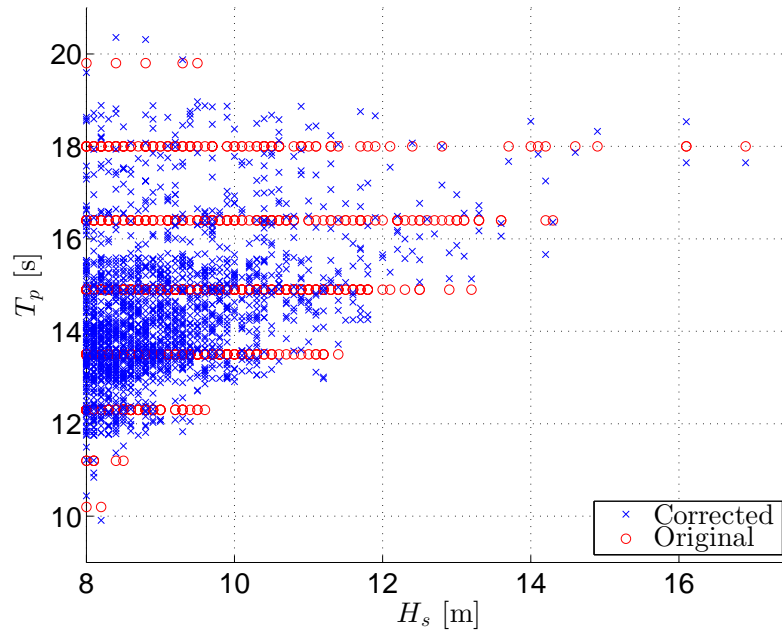


Figure 2.3: Correction of T_p . The original hindcast data are scattered randomly about the discrete T_p values.

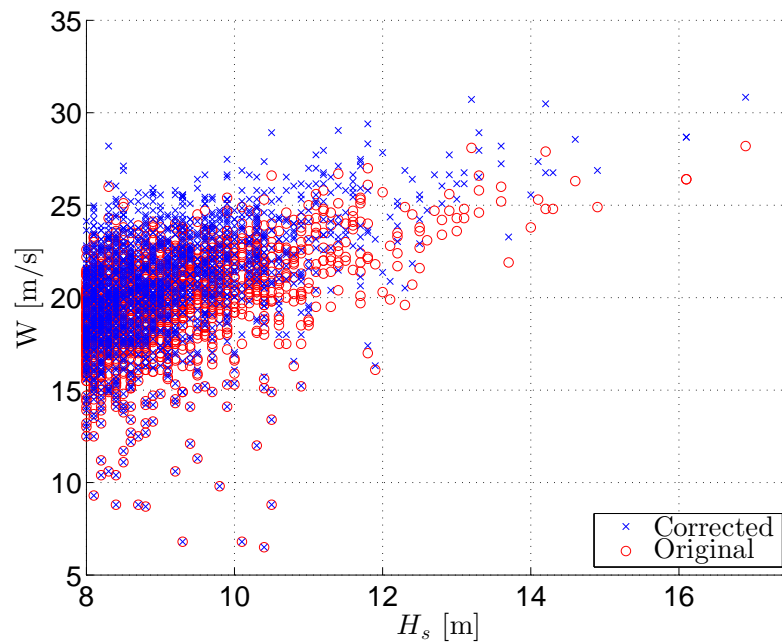


Figure 2.4: Correction of W . The fraction of wind speed above 15 m/s is increased by 20%.

2.4 Defining a storm event

The POT method requires that a storm event is defined. In this context, a storm is initiated as the most the important weather characteristic increases above some threshold. Here it is assumed that H_s is the most important weather characteristic and a storm event will be build up by consecutive sea states as long as H_s is above the selected threshold. Each storm is assumed to be statistically independent. Therefore, correlation between adjacent storms is reduced by merging two consecutive storms when the time window between the two storms is less than or equal 24 hours. The storms will be merged by merely including the sea states *above* the selected threshold as indicated in Figure 2.5. This is because sea states with less severity than the threshold are expected to give a negligible contribution to extreme responses.

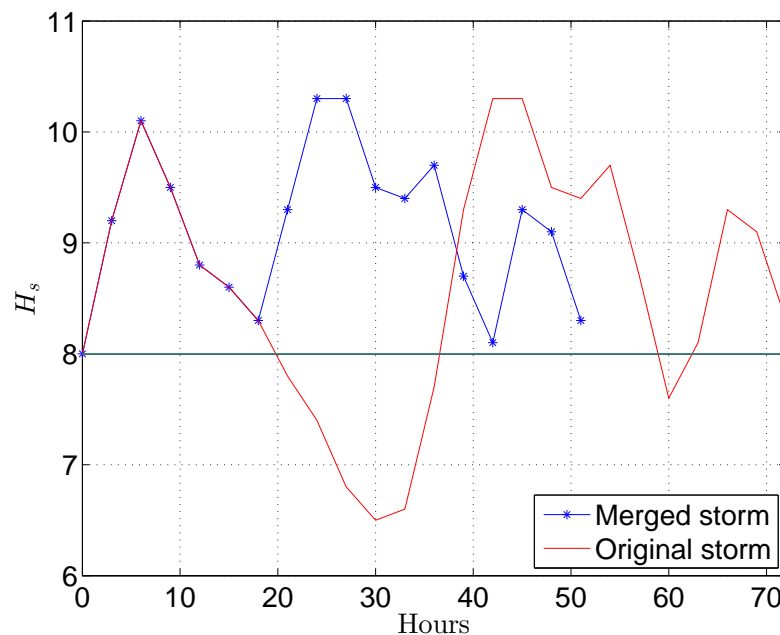


Figure 2.5: Example of three storms merged to one for threshold $H_s = 8m$. The original storm was observed 14-17.02.1959.

For the Hindcast data at Haltenbanken, there are 446 observed storms for threshold $H_s = 8m$. The number of storms is reduced to 398 as correlated storms are counted as one. These 398 independent storm events will be used in the POT analysis for threshold $H_s = 8m$.

The number of independent storm events is further reduced to 360 if the time window between

correlated storms is increased to 48 hours. This might indicate that the selected criteria for correlated storms need further verification. An alternative approach, as suggested by Tromans and Vandersohuren (1995), is to consider the through in H_s between two storms. If this through is less than 80% of the lowest peak, the storms are broken at the through to form two independent events.

Chapter 3

Theoretical background of simulations in SIMO

It is important to know the theory behind SIMO for better understanding and evaluation of the results. In this chapter, the theoretical background of SIMO will be explained in view of the response problem.

3.1 Equation of motion

Time domain simulations are necessary to establish a distribution function of the semi submersible's maximum offset since the problem is of non-linear nature. SIMO performs time domain simulations by solving the equation of motion, i.e. Eq. 3.1, in six degrees of freedom, SIM (2013).

$$[\mathbf{M} + \mathbf{A}(\omega)]\ddot{\mathbf{x}} + \mathbf{C}(\omega)\dot{\mathbf{x}} + \mathbf{D}_1\dot{\mathbf{x}} + \mathbf{D}_2\dot{\mathbf{x}}|\dot{\mathbf{x}}| + \mathbf{K}(\mathbf{x})\mathbf{x} = \mathbf{q}(\mathbf{t}, \mathbf{x}, \dot{\mathbf{x}}) \quad (3.1)$$

Where \mathbf{M} is the body mass matrix, $\mathbf{A}(\omega)$ is frequency dependent added mass matrix, $\mathbf{C}(\omega)$ is frequency dependent potential damping matrix, \mathbf{D}_1 is the linear damping matrix, \mathbf{D}_2 is the

quadratic damping matrix, $\mathbf{K}(\mathbf{x})$ is the displacement dependent stiffness matrix and $\mathbf{q}(\mathbf{t}, \mathbf{x}, \dot{\mathbf{x}})$ is the excitation forces given by time and space, SIM (2013). All terms in Eq. 3.1 will be explained later in this chapter.

3.1.1 Solving the equation of motion

Two different solution methods to solve Eq. 3.1 are available in SIMO. The next two subsections will introduce these methods.

Retardation function

Eq. 3.1 shall be evaluated in the time domain for non-linear problems. It may be convenient to rewrite the frequency dependent term in Eq. 3.1 to a convolution integral.

$$[\mathbf{M} + \mathbf{A}(\omega = \infty)]\ddot{\mathbf{x}} + \mathbf{D}_1\dot{\mathbf{x}} + \mathbf{D}_2\dot{\mathbf{x}}|\dot{\mathbf{x}}| + \mathbf{K}(\mathbf{x})\mathbf{x} + \int_0^t \mathbf{h}(t - \tau)\dot{\mathbf{x}}(\tau) d\tau = \mathbf{q}(\mathbf{t}, \mathbf{x}, \dot{\mathbf{x}}) \quad (3.2)$$

Where $\mathbf{h}(\tau)$ is the retardation function.

$$\mathbf{h}(\tau) = \frac{1}{2\pi} \int_{-\infty}^{\infty} \mathbf{C}(\omega) + i\omega(\mathbf{A}(\omega) - \mathbf{A}(\omega = \infty))e^{i\omega\tau} d\omega = \frac{1}{2\pi} \int_{-\infty}^{\infty} \mathbf{H}(\omega) d\omega \quad (3.3)$$

The complete derivation of Eq. 3.2 and 3.3 can be found in SIM (2013).

Separation of motions

Instead of solving Eq. 3.1 in the time domain by use of the retardation function, the motions may be separated into a low-frequency and a high-frequency part. It follows that the excitation forces are categorized into low frequency forces, \mathbf{q}_{LF} , and high frequency forces, \mathbf{q}_{HF} . The position vector of the system is defined as the sum of the displacements caused by the high and low

frequency excitation forces, SIM (2013).

$$\mathbf{x} = \mathbf{x}_{LF} + \mathbf{x}_{HF} \quad (3.4)$$

The high frequency motions can be solved in the frequency domain, which requires that the assumptions of a linear system are fulfilled. Subsequently, the quadratic damping matrix is set to zero and the stiffness matrix is kept constant. The high frequency response is then calculated by solving Eq. 3.5 in the frequency domain.

$$[\mathbf{M} + \mathbf{A}(\omega)]\ddot{\mathbf{x}}_{HF} + [\mathbf{C}(\omega) + \mathbf{D}_1]\dot{\mathbf{x}}_{HF} + \mathbf{K}\mathbf{x}_{HF} = \mathbf{q}_{HF} \quad (3.5)$$

The low frequency motions are found by solving the dynamic equilibrium equation of the system as per Eq. 3.6.

$$[\mathbf{M} + \mathbf{A}(\omega = 0)]\ddot{\mathbf{x}}_{LF} + \mathbf{D}_1\dot{\mathbf{x}}_{LF} + \mathbf{D}_2\dot{\mathbf{x}}_{LF}|\dot{\mathbf{x}}_{LF}| + \mathbf{K}\mathbf{x}_{LF} = \mathbf{q}_{LF} \quad (3.6)$$

There will be no radiation damping resulting from low frequency motions. Hence, the potential damping matrix, i.e. $\mathbf{C}(\omega)$, is equal to zero.

3.2 Excitation forces

The excitation forces are the sum of environmental forces included in the analysis.

$$\mathbf{q}(t, \mathbf{x}, \dot{\mathbf{x}}) = \mathbf{q}_{wind} + \mathbf{q}_{wave}^1 + \mathbf{q}_{wave}^2 + \mathbf{q}_{current} \quad (3.7)$$

Where \mathbf{q}_{wind} is the wind drag forces, \mathbf{q}_{wave}^1 are the first order wave forces, \mathbf{q}_{wave}^2 are the second order wave forces and $\mathbf{q}_{current}$ are the current drag force. Current forces will not be discussed

since it is omitted in the analysis.

These forces are separated into three categories; (1) mean forces, (2) wave frequency forces and (3) low frequency forces. The different force contributions are summarized in Table 3.1.

Table 3.1: Most important loads for this response problem

Excitation	Mean	Wave frequency	Low frequency
Waves	2 nd order mean drift	1 st order	2 nd order diff. freq. drift
Wind	Mean wind		Wind gust
Current	Mean current		

The wind, current and second order drift forces cause a static displacement on the platform. The first order wave forces are proportional to the wave amplitude and excite the platform with the same frequencies as the incoming waves. The natural periods of the semi submersibles in surge, sway and yaw are usually above 100 seconds. Hence, these modes are excited by the low frequency forces caused by slowly varying second order difference frequency drift forces and wind gusts. The magnitude of the low frequency forces is usually not large, but when the mean period is close to the natural period in surge, sway and yaw, significant amplifications might occur.

3.2.1 Wind forces

Wind forces are characterized by a mean value excited by the mean wind velocity and low frequency forces due to wind gusts. The mean wind velocity will give a mean offset, while the wind gusts will produce slowly varying motions of the vessel, Faltinsen (1990). In SIMO, the wind gusts are assumed to follow a Gaussian stochastic process, SIM (2013). Variations in the mean wind speed with height can be accounted for by assuming a predetermined idealized wind profile, DNV (2014).

A typical description of the wind force acting orthogonal on a structural member is given by Eq.

3.8, N-0 (2007).

$$q_{wind}(t) = \frac{1}{2} \rho_{air} C_D A [\bar{U}_{wi} + u(t)]^2 \quad (3.8)$$

Where ρ_{air} is the air density, C_D is the directional drag coefficient of the body, A is the cross-sectional area in the wind direction, \bar{U}_{wi} is the mean wind velocity and $u(t)$ represents the fluctuating wind component.

Introducing $c_{wind} = \frac{1}{2} \rho_{air} C_D A$ and letting the wind forces be calculated from the instantaneous wind and body velocities gives Eq. 3.9.

$$q_{wind}(t) = c_{wind} [\bar{U}_{wi} + u(t) - \dot{x}(t)]^2 \quad (3.9)$$

For illustrative purposes, higher order terms of $u(t)$ and $\dot{x}(t)$ can be neglected when it is assumed that $\bar{U}_{wi} \gg u(t) + \dot{x}(t)$. Low frequency motions, \dot{x}_{LF} , are also introduced since wind gusts are characterized as low frequency forces. This means that Eq. 3.9 simplifies to Eq. 3.10.

$$q_{wind}(t) \approx c_{wind} \bar{U}_{wi}^2 + 2c_{wind} \bar{U}_{wi} u(t) - 2c_{wind} \bar{U}_{wi} \dot{x}(t)_{LF} \quad (3.10)$$

The first and second term in Eq. 3.10 represents a static force and a low frequency excitation force, respectively. The third term represents linear damping, Larsen (2015).

The wind forces are in SIMO based on the instantaneous wind and body velocities. In addition, variations in the wind velocity with height can be accounted for by selecting a wind profile. For this system, the wind time series is generated from a NPD spectrum. Generation of time series is later explained in Sec. 3.5.

3.2.2 Wave forces

Wave forces causing surge, sway and yaw motions are characterized by first order forces that are proportional with the wave height, mean drift forces due to second order effects and slowly varying drift motions due to difference frequency second order effects, Greco (2012).

First order wave forces

Fluid particles in linear theory move in circular orbits and remains in the same position after one period, Newman (1977). This means that there is no net mass transport of the fluid in a potential flow field. It further implies that first order forces in surge, sway and yaw is connected to the structure's ability to generate waves, Faltinsen (1990). These forces are linear and proportional to the wave amplitude. Consequently, the response due to first order wave forces are solved in the frequency domain.

In SIMO, the first order wave forces and motions are calculated using transfer functions that are computed with diffraction theory programs, such as WAMIT or WADAM, SIM (2013). The first order wave motion transfer function in surge is depicted in Figure 3.1.

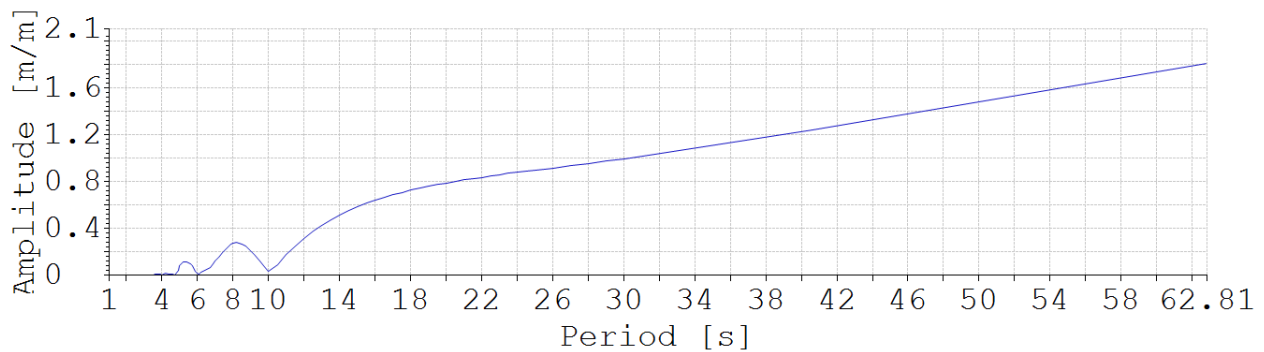


Figure 3.1: First order wave motion transfer function

The transfer function experience some cancellation effects around periods close to 10 seconds. For higher periods, the transfer function increases strictly. Hence, it is expected that sea states modeled with spectral peak periods close to 10s will have less pronounced wave frequency forces than for higher T_p values.

Second order wave forces

The horizontal wave particle velocity is positive beneath the crest. Below the mean free surface, the fluid particle velocity component is equal in magnitude and opposite in sign beneath the crest and through. Since the crest is always higher than the through, a net non-linear transportation of fluid must exist, Newman (1977), and a floating body will experience drift forces. One may also understand the wave drift force by considering incident waves that are reflected from the structure. Due to conservation of momentum, the reflected waves must cause a force acting on the body in the wave propagation direction. Consequently, the wave drift force are connected to the body's ability the reflect waves, Faltinsen (1990).

The drift forces can be divided into a second order mean drift force and a second order slowly varying force proportional to the wave height squared.

The mean drift force can be calculated by integration of the wave pressure field to the exact surface and then taking time average or by demanding conservation of momentum for the wave system in the far field. In SIMO, the mean drift force is calculated by solving $\bar{q}_{drift} = 2 \int_0^{\infty} c_{wa}(\omega) S_{\eta}(\omega) d\omega$, where c_{wa} is the wave drift coefficient, SIM (2013). The wave drift coefficient for different periods is given in Figure 3.2.

The slowly varying drift force exists due to difference frequency effects that arise from different portions of the wave spectrum, Newman (1974). The magnitude of the slowly varying drift load is not large, but if the mean period is close to the natural period in surge, sway or yaw, a significant amplification might occur because of little damping in the system, Faltinsen and Løken (1980). There are several options to calculate the slowly varying drift forces in SIMO. Newman's approximation, as outlined in Newman (1974) and in Faltinsen (1990), are most commonly used.

The irregular variations in the wave drift coefficient for smaller periods than 8 seconds are probably caused by numerical noise. It is noticed that there is a local peak in the drift coefficient around periods 10 – 11 seconds. It follows that slowly varying drift forces and mean drift forces are expected to be more important for sea states modeled with T_p around 10 – 11 seconds.

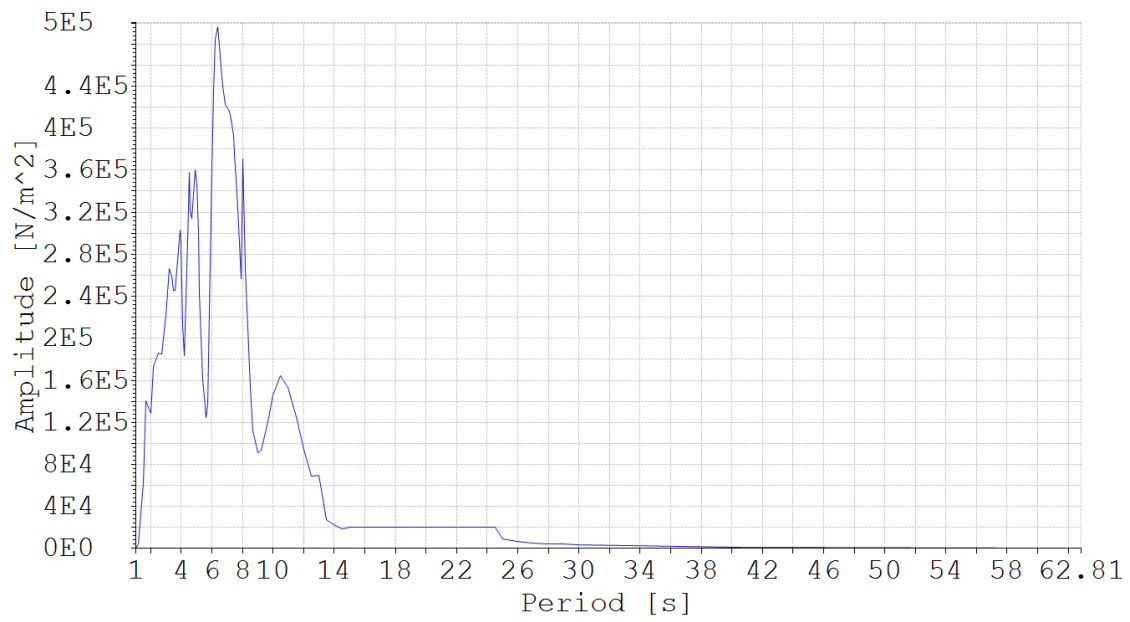


Figure 3.2: Wave drift coefficient in surge

3.3 Mass, damping and restoring forces

3.3.1 Mass forces

Mass forces are proportional to acceleration. It consists of physical mass and frequency dependent added mass. Physical mass is constant and equals the platform weight. Frequency dependent added mass are additional mass felt by the floating body when subject to forced oscillations, and is caused by fluid that must be pushed around the moving body.

The added mass is indirectly implemented in SIMO since it is maintained within the retardation function and/or the transfer functions.

3.3.2 Damping forces

The damping force of the system can be divided into three groups as in Eq. 3.1. $\mathbf{C}(\omega)$ represents the frequency dependent potential damping, \mathbf{D}_1 is the linear damping matrix and \mathbf{D}_2 is the quadratic damping matrix.

Potential damping

$\mathbf{C}(\omega)$ describes the potential damping that arises from the generation of waves on the free surface, causing energy to dissipate away from the moving body. Potential damping is only applicable for wave frequency motions since $\mathbf{C}(\omega) \approx \mathbf{0}$ when the structure is oscillating with low frequencies.

Potential damping is linear and can be estimated using diffraction theory programs. Typically, $\mathbf{C}(\omega)$ is estimated using WADAM or WAMIT and imported to SIMO. $\mathbf{C}(\omega)$ affects the high frequency motions that are solved in the frequency domain and can therefore be included in the retardation function as explained in Sec. 3.1.1.

Linear damping matrix

Linear damping matrix is expressed by \mathbf{D}_1 and is in this context used to calibrate the SIMO model with model tests. Drag damping from the mooring lines is the most important damping term contained within the linear damping matrix.

Other linear damping terms such as wind damping, current damping and slow drift damping are calculated from the instantaneous relative velocities, and are not included in \mathbf{D}_1 .

Quadratic damping matrix

\mathbf{D}_2 expresses the quadratic damping matrix and is used to calibrate the SIMO model with model tests.

3.3.3 Restoring forces

$\mathbf{K}(\mathbf{x})$ contain the restoring forces in surge, sway and yaw caused by the mooring system and risers. The properties of the mooring lines in SIMO are based on the mooring analysis program MIMOSA, SIM (2013). It is assumed that the mooring lines can be treated as quasi-static, implying that the transverse drag forces on the line are neglected. Hence, the shape of the cable will be a function of the top end motion, MIM (2003). The mooring lines form catenaries that are modeled with the catenary equations. Transverse bottom friction is neglected so the lines are free to rotate about the anchor points.

Total horizontal stiffness of one mooring line can be separated into geometric and elastic stiffness. Geometric stiffness results from the weight of the chain, while elastic stiffness results from elongation of the line. Geometric and elastic stiffness acts like two springs in series.

The horizontal restoring force of a mooring line is plotted against the top end displacement in Figure 3.3. For small displacements, the restoring force is close to linear dependent on the top end displacement. The restoring force becomes more non-linear as the offset increases.

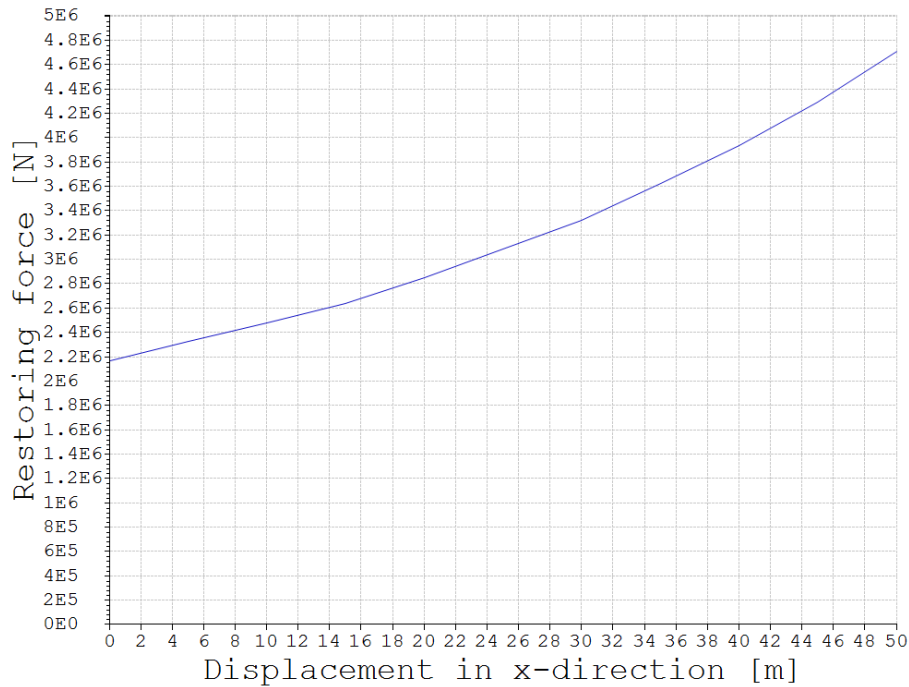


Figure 3.3: Horizontal restoring force of one mooring line as a function of displacement.

3.4 Dynamic amplification

Structures exposed to dynamic loads will experience some kind of dynamic amplification. The ratio between the load frequency and the natural frequency, i.e. $\frac{\omega}{\omega_0}$, of the structure governs the magnitude of this dynamic amplification. The dynamic amplification felt by the structure for different damping levels are plotted in Figure 3.4.

One may categorize dynamic systems into stiffness dominated, resonance dominated and inertia dominated. Each system is balanced by different force components. For instance, excitations forces of inertia-dominated structures are balanced out by mass forces and resonance dominated systems are balanced out by the damping forces.

When offset is considered, the governing excitation forces are categorized into static forces, wave forces and low frequency forces. If wave frequency forces are isolated, the system may be categorized as an inertia dominated system. Similarly, the system can be categorized as a

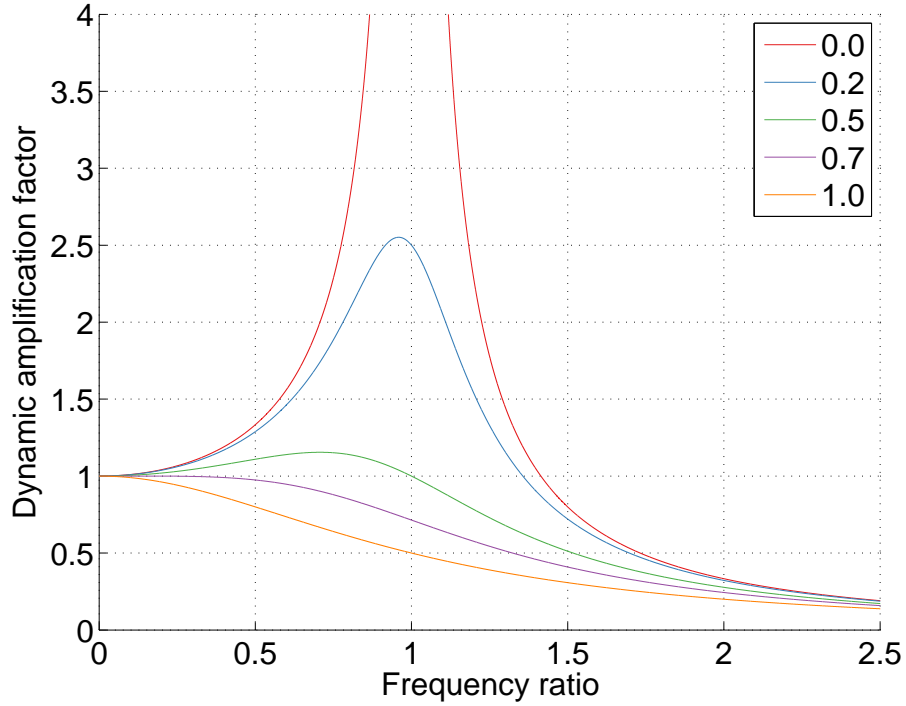


Figure 3.4: Dynamic amplification factor as a function of frequency ratio for different damping levels.

resonance dominated system when the low frequency forces (wind gust and slowly varying drift forces) are isolated. Low frequency forces are important since the system will experience large amplifications when the low frequencies are close to the natural frequency of the system.

3.5 Generation of time series

Time series are created by summing up harmonic components from a discretized spectrum, where sampled pseudo-random phase shifts (ε) uniformly distributed over $[0, 2\pi]$ are added to each harmonic component. For example, the generation of a wave elevation time series, $\xi(t)$, will be given by Eq. 3.11 (Myrhaug, 2009).

$$\xi(t) = \sum_{i=1}^N \sqrt{2S(\omega_i)\Delta\omega} \cos(\omega_i t + \varepsilon_i) \quad (3.11)$$

Time series that are generated according to Eq. 3.11 will repeat themselves with a period $T = \frac{2\pi}{\Delta\omega_{i,min}}$, where $\Delta\omega_{i,min}$ is the smallest frequency increment.

SIMO normally uses Fast Fourier transform (FFT) to generate time series. This procedure requires equal frequency increment and that $N = 2^i$, where i is an integer, SIM (2013).

3.6 Example time series of offset in SIMO

It is of interest to identify the most important excitation forces in this problem, and qualitatively discuss the relative importance of these excitation forces for different weather conditions. Hence, an example time series of the response (offset in surge) are given in Figure 3.5 for a sea state modeled with $H_s = 8m$, $T_p = 10s$ and $W = 5m/s$.

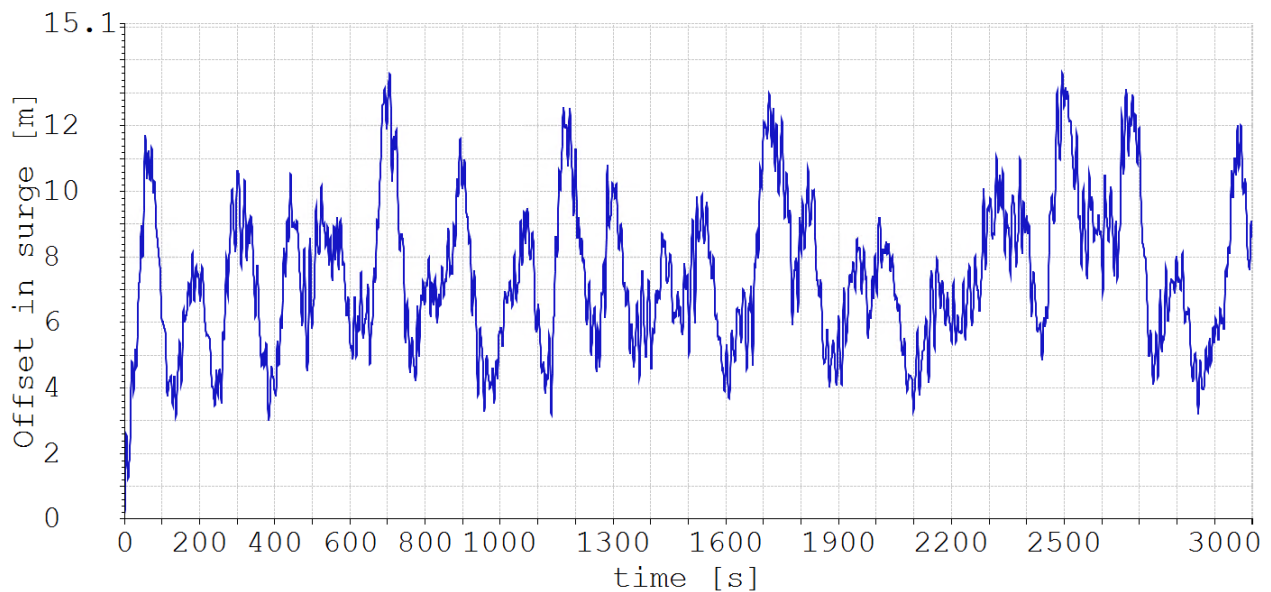


Figure 3.5: Time series of offset calculated in SIMO when $H_s = 8.0m$, $T_p = 10.0s$ and $W = 5m/s$

In Figure 3.5, the transient face where the semi submersible goes from a static position to oscillate about a mean offset is evident for the first -say- 200 seconds of the simulation. In this sea state, the platform is oscillating about a mean offset of 7.4m with a period of more than 100 seconds. The mean offset is here caused by wind forces and wave drift forces. Current gives no contribution to the static displacement since it is excluded from the analysis. The slowly

variations about the mean offset is caused by the slowly varying environmental forces, i.e. difference frequency effects from waves and wind gusts, that becomes important when they excite the structure around its natural frequency. Further, the oscillations with higher frequencies are caused by first order wave frequency forces.

Another time series was generated for a sea state modeled with $H_s = 8m$, $T_p = 15s$ and $W = 15m/s$ and is depicted in Figure 3.6.

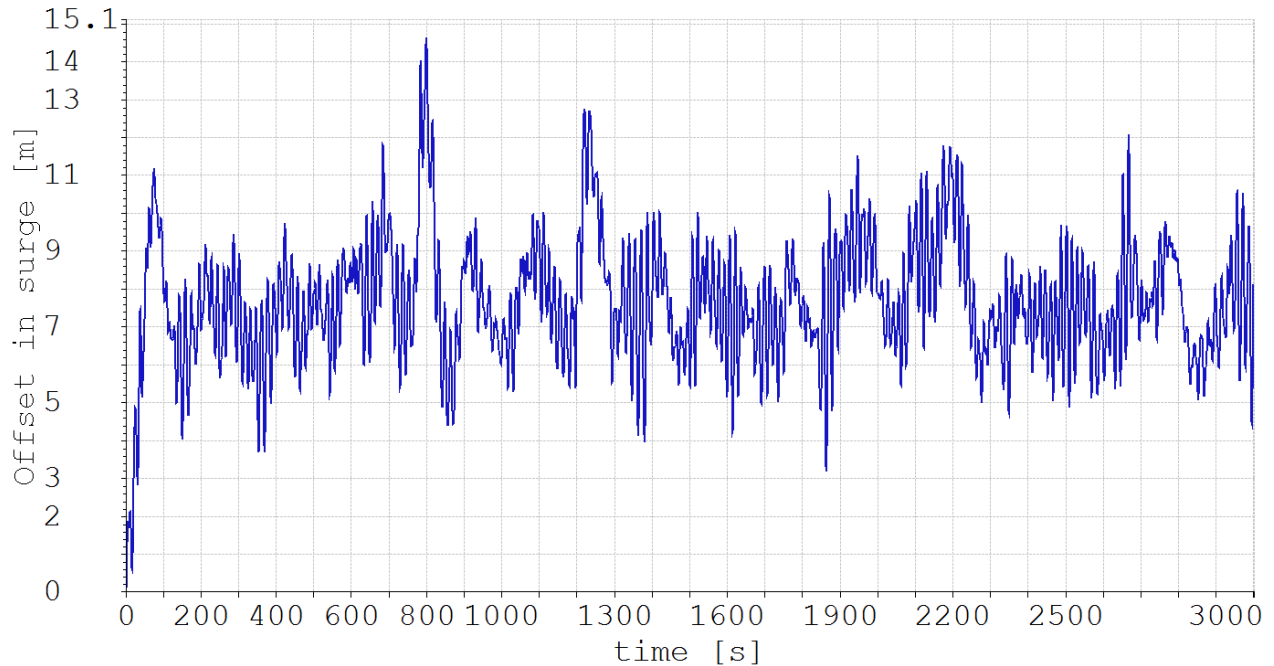


Figure 3.6: Time series of offset calculated in SIMO when $H_s = 8.0m$, $T_p = 15.0s$ and $W = 15m/s$

The mean offset in Figure 3.6 ($H_s = 8m$, $T_p = 15s$ and $W = 15m/s$) is 7.7m. This is slightly larger than the mean offset in Figure 3.5 ($H_s = 8m$, $T_p = 10s$ and $W = 5m/s$). This effect is caused by larger wind forces resulting from increasing the wind velocity, DNV (2010). Some of the gain in mean offset are counterweighted against a smaller mean drift force as the wave drift coefficient, given in Figure 3.2, is reduced when the spectral peak period is increased from $T_p = 10s$ to $T_p = 15s$.

Further, the relative importance of the wave frequency motions and the slowly varying motions are different in Figure 3.5 and Figure 3.6. This effect can be explained by investigating the first order wave motion transfer function in surge, Figure 3.1, and the wave drift force coefficient,

Figure 3.2. The transfer function experience some cancellation effects when T_p is around 10 seconds, and increases strictly for larger periods. Hence, it is expected that the wave frequency motions are more important as T_p is increased from 10s to 15s. The wave drift coefficient experience a local maximum for T_p around 10 – 11s and decreases for higher T_p values. As a consequence, the relative importance of the slowly varying motions will be reduced as T_p is increased from 10s to 15s.

Chapter 4

Introduction to long term analysis

Offset of a semi submersible are caused by environmental forces. These environmental forces are of concern in severe sea states with a corresponding rare probability of occurrence. Imagine a time series of the offset for one of these severe sea states given by some weather characteristics (H_s , T_p and W). The response time series will be different when the same sea state, i.e. the same H_s , T_p and W , is observed twice. It follows that the observed maximum response is different every time the same sea state is observed. Hence, it is possible to create a distribution of the maximum response given some weather characteristics.

The q-probability response can only be estimated if all sources of inherent randomness are taken into account. There are two distinct sources of randomness: (1) long term variability and (2) short term variability. The long term variability is typically the most important source of randomness, since it is likely that the q-probability response occurs in a severe sea state with a small probability of occurrence. Despite this, the short term variability, i.e. the response given some sea state, cannot be neglected since an extreme response can occur in an ordinary sea state, but in combination with a rare short term realization of the response quantity.

To perform reliable estimates of the q-probability response, some sort of long term analysis must be carried out. The full long term distribution of the maximum response can only be calculated if the short term and long term variability of the responses and loads are known. There

are two methods for long term analysis that will be discussed herein; the peak over threshold method and the all sea states approach.

In a POT analysis, the most probable largest maximum offset, denoted \tilde{x} , within an arbitrary storm is treated as the independent stochastic variable. Different interpretations of the method have been presented in detail by Jahns and Wheeler (1973), Haring (1978) and Tromans and Vandersohuren (1995). The short term variability is made conditional on \tilde{x} . The long term variability of \tilde{x} is found by fitting a proper probabilistic model to observations of \tilde{x} . The full long term distribution is found by convolution of the short term and long term variability as per Eq. 4.1.

$$F_X(x) = \int_{\tilde{x}} F_{X|\tilde{x}}(x|\tilde{x}) f_{\tilde{x}}(\tilde{x}) d\tilde{x} \quad (4.1)$$

Where $F_{X|\tilde{x}}(x|\tilde{x})$ is considered as the short term variability and $f_{\tilde{x}}(\tilde{x})$ is the long term variability. X is the storm maximum response.

In the all sea states approach, Battjes (1972) and Nordenstrøm (1971), the short term variability is made conditionally on the most important sea state characteristics. Waves and winds are important for offset of semi submersibles and the short term variability is therefore made conditionally on H_s , T_p and W . The long term variability of H_s , T_p and W can be estimated from hindcast data. It follows that the long term distribution of the maximum response is given by Eq. 4.2.

$$F_X(x) = \iiint_{H_s, T_p, W} F_{X|H_s, T_p, W}(x|h, t, w) f_{H_s, T_p, W}(h, t, w) dh dt dw \quad (4.2)$$

Where $F_{X|H_s, T_p, W}(x|h, t, w)$ is considered as the short term variability and $f_{H_s, T_p, W}(h, t, w)$ is the long term variability. X is the 3-hour maximum response.

4.1 Determine short term variability of the response

A reasonable number of time domain simulations must be performed to determine the short term variability of the response, i.e. $F_{X|\tilde{X}}(x|\tilde{x})$ and $F_{X|H_s, T_p, W}(x|h, t, w)$.

A possible cost efficient approach is to perform a number of 3-hour simulations of sea states given by H_s , T_p and W with reasonable resolution covering the actual sample space. For each of the simulation points it is assumed that the maximum response is Gumbel distributed. Consequently, the Gumbel parameters, α_G and β_G , are determined for each simulation point using method of moments and continuous functions (response surfaces) can be fitted to the point estimates. Hence, the distribution of the maximum response given H_s , T_p and W within the sample space is found using the generated response surfaces.

The short term variability in the all sea states, i.e. $F_{X|H_s, T_p, W}(x|h, t, w)$, is known once the response surfaces are established. Further, the analysis of each storm step in the POT method will be performed using these response surfaces.

In this thesis, there are two sets of response surfaces within two sample spaces. First, response surfaces for the POT analysis that include all observed sea states above threshold $H_s = 8m$ is created. These response surfaces are also used to calculate the 100-year response in the all sea states analysis. Later, when estimating the all sea states 10,000-year response, it becomes evident that another set of response surfaces is required to include non-observed sea states not covered by the response surfaces for the POT analysis. Hence, another set of response surfaces is created to account for these non-observed sea states.

4.2 Response surfaces for the POT analysis

In the POT analysis, the sample space of H_s , T_p and W is selected to include all observed sea states given threshold $H_s = 8m$. The sample space varies as follows:

H_s : 8-18m, with an increment of 2m

T_p : 10-22s, with an increment of 1.2s

W : 5-35m/s, with an increment of 6m/s

Some of these sea states are unrealistic, but they will work as outer boundaries for the response surfaces. Initially, 20 time domain simulations were conducted for each of the sea states within the sample space. This was later extended to 40 simulations per sea state to reduce the statistical uncertainties in the results, resulting in 40 observed maximum responses for $6 \cdot 11 \cdot 6 = 396$ different sea states. The Gumbel distribution was fitted to the observed maximums for each sea state using method of moments with the relationship given in Eq. 4.3.

$$\beta_G = \frac{\sqrt{6}}{\pi} \sigma_X \quad (4.3)$$

$$\alpha_G = \bar{X} - 0.5772\beta_G$$

Where \bar{X} and σ_X is the mean and standard deviation of the 40 observed maximum offsets of the given sea state. The adequacy of the Gumbel distribution is considered by plotting the cumulative distribution of the maximum response for a randomly selected sea state together with the observed maximum responses. This is done for some selected storms in Figure 4.1. The Gumbel distribution is considered suitable since the observations follow a straight line.

Figure 4.1 indicates that the Gumbel distributions seem to follow the observed maximum responses with reasonable accuracy. With the obtained Gumbel parameters for all sea states, the short term variability of the maximum response for each simulation point given by H_s , T_p and W are defined by α_G and β_G . Subsequently, one may use some kind of interpolation technique between the simulation points to describe the short term variability of the maximum response for all sea states within the predefined sample space.

The challenge is to establish response surfaces of α_G and β_G as a function of H_s , W and T_p . An example of the response surfaces $\alpha_G(h, t)$ and $\beta_G(h, t)$ for each of the six sampled W values can be reviewed in Figure 4.2 and 4.3. Please notice that the lower layer of $\alpha_G(h, t)$ in Figure 4.2 is for

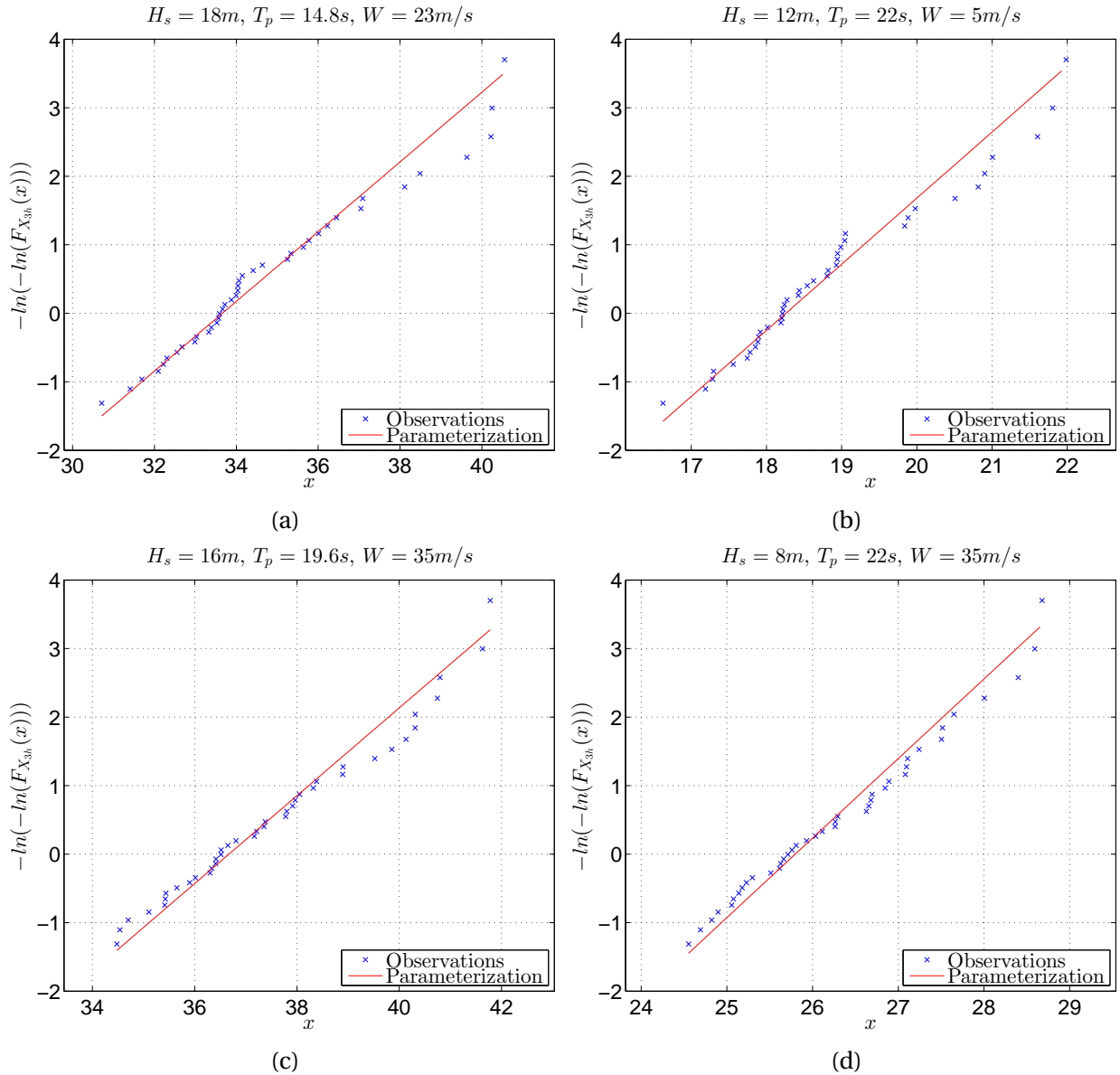


Figure 4.1: Distribution of 3-hour maximum response in some selected sea states

a sea states with $W = 5\text{ m/s}$, increasing with a 6 m/s increment to $W = 35\text{ m/s}$ for the top layer.

Some interesting features of the platform response are observed from Figure 4.2. It looks like the most probable largest response, i.e. α_G , increases linearly with H_s and follows some kind of sine curve with T_p . Similarly, the distance between two layers of $\alpha_G(h, t)$ increases non-linearly with W .

An important contributor to the maximum response is the wave frequency forces. These forces

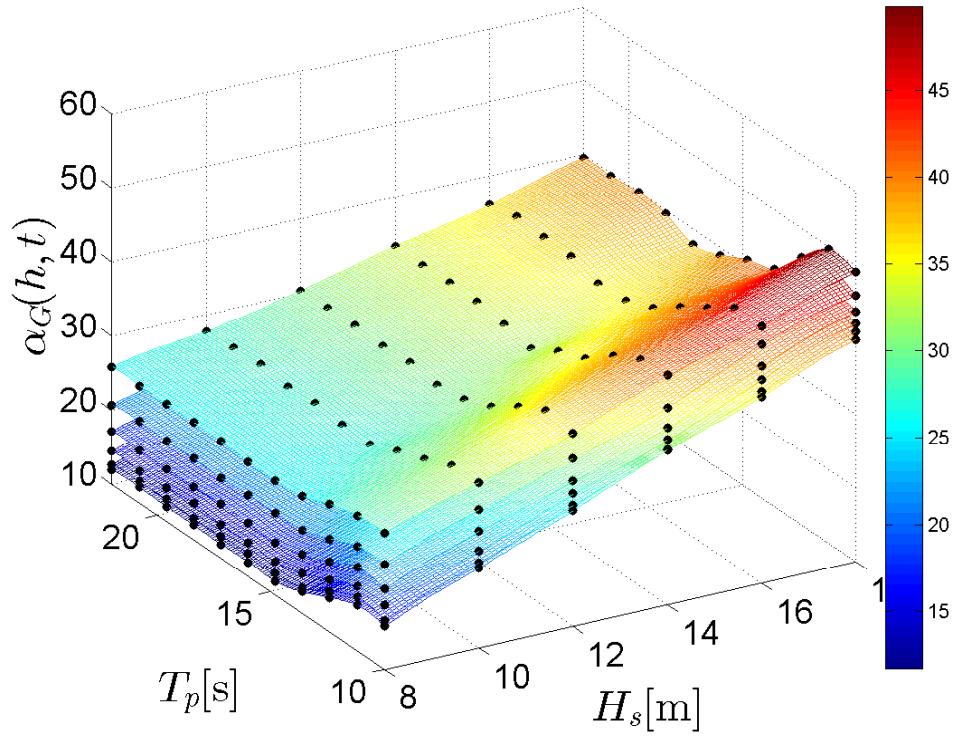


Figure 4.2: $\alpha_G(h, t)$ for different W values. Each layer represent one sampled W value.

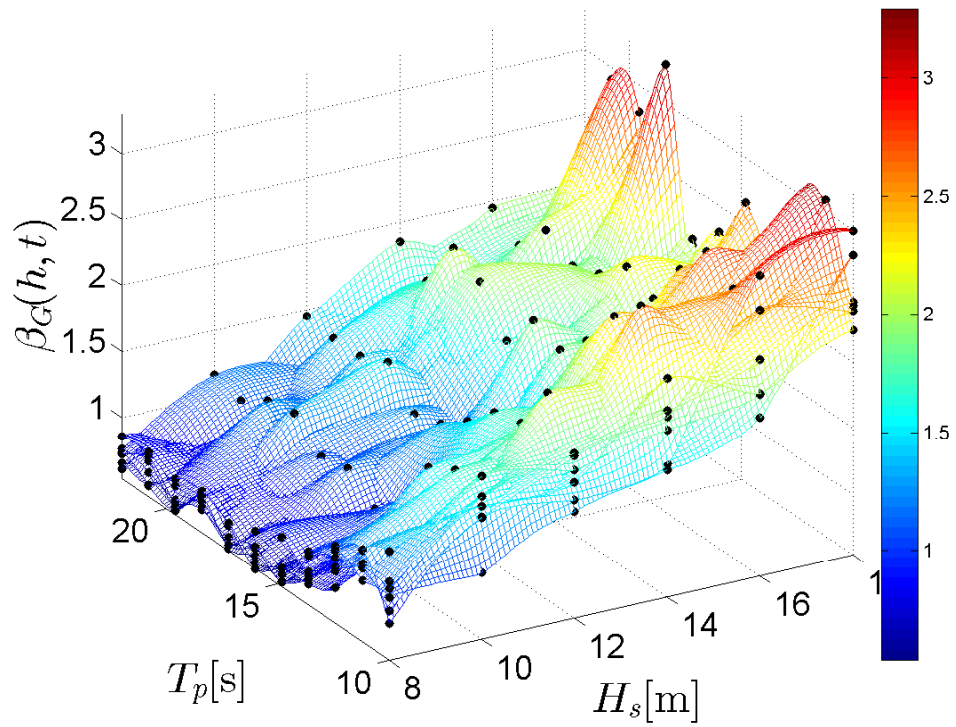


Figure 4.3: $\beta_G(h, t)$ for different W values. Each layer represent one sampled W value.

are linear dependent on H_s and can explain α_G linear dependency on H_s . It should, however, be noted that increasing H_s will also give larger mean drift and slowly varying drift forces because of more energy in the wave spectrum.

Also, recall that the drift coefficient experiences a local maximum for periods around 10–11 seconds, see Figure 3.2. This is the main contributor to the rapid increase in α_G as T_p approaches 10–11 seconds, since a larger wave drift coefficient creates more pronounced slowly varying drift forces in this area. The mean drift forces also increase as T_p approaches 10–11 seconds, but this effect is assumed to be less important.

Wind forces are quadratic dependent on the wind velocity as given by Eq. 3.8. The wind excites the platform with a mean wind force and a slowly varying wind force. The mean force will be quadratic dependent on the wind speed and the wind gusts follow a Gaussian stochastic process. Subsequently, it comes as no surprise that α_G is non-linearly dependent on W .

According to Figure 4.3, it might look like β_G increases linearly with H_s , but β_G dependency on T_p and W is uncertain because of the irregular variations of $\beta_G(h, t)$. A too small data set (40 simulations) per sea state might cause the irregular variations in β_G response surfaces since the β_G values have yet to converge.

4.2.1 Convergence of the response surfaces

More accurate β_G values should be found before the response surfaces of the Gumbel parameters can be used in the analysis. A possible approach is to find the approximate number of simulations required to obtain convergence. Therefore, 250 simulations were performed for some selected sea states, and the resulting α_G and β_G values are plotted against increasing number of simulations. An example plot that displays the convergence rate of α_G and β_G when $H_s = 12m$ and $T_p = 14.8s$ are presented in Figure 4.4 and 4.5. Similar convergence plots for some other sea states can be reviewed in Appendix A.1 and A.2.

The study reveals that the convergence of α_G is faster than for β_G . It seems like α_G is reliable

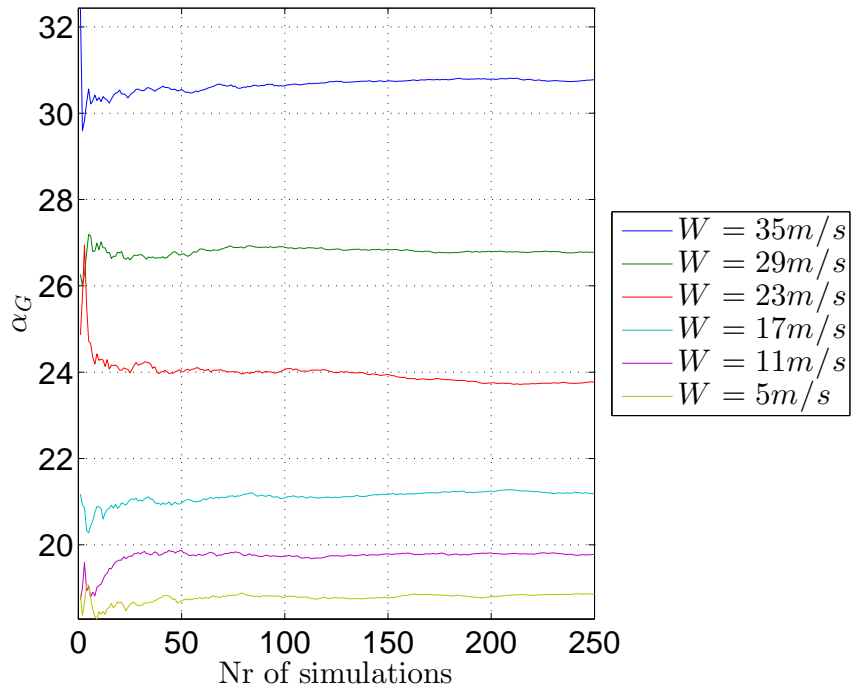


Figure 4.4: α_G convergence for different W sampling points, $H_s = 12m$, $T_p = 14.8s$

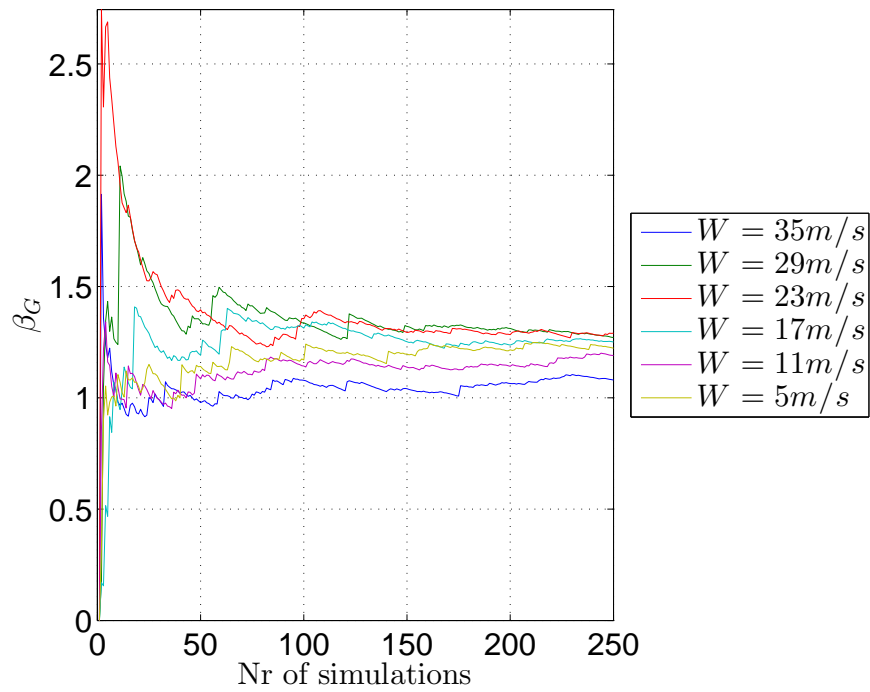


Figure 4.5: β_G convergence for different W sampling points, $H_s = 12m$, $T_p = 14.8s$

after -say- 40 simulations, but Figure 4.5 indicates that 40 simulations would yield inaccurate estimates of β_G . Hence, a far larger amount of simulations must be performed before β_G converges, maybe up to 150 simulations per sea state, indicating that it would be too computational demanding to calculate β_G with brute force.

An alternative solution is to assume that β_G is a function of H_s , T_p and W , and determine $\beta_G(h, t, w)$ by least square fitting to the data.

β_G dependency on H_s is revealed by keeping T_p and W constant and run many simulations for increasing numbers of H_s , and subsequently plot β_G as a function of H_s . The same can be done for T_p and W . Using the simulations from the convergence study, there are 250 observations of the maximum response for some selected sea states. These 250 simulations yield 10 observations of α_G and β_G when each observation of the Gumbel parameters are calculated from 25 realizations of the maximum response using method of moments. In Figure 4.6, β_G is plotted as a spline function fitted to the average of these 10 β_G values for increasing W values ($H_s = 12$ and $T_p = 14.8s$). For each respective sea state, the error bars indicate one standard deviation of the 10 β_G values and are included to give an idea of the uncertainty level. Similar plots of α_G were also generated and an example plot is given in Figure 4.7. All plots resulting from this study are presented in Appendix A.3 and A.4.

The figures in Appendix A.3 indicates that β_G is close to linear dependent on H_s and increases around $T_p = 10 - 11s$. In Figure 4.6 it is noticed that β_G can be considered constant for different W values, alternatively decreasing for extreme W values. β_G being constant for different W values is a useful approximation since the response surfaces can be fitted in 2D instead of 3D for the existing data sample. In the following it will therefore be assumed that β_G are constant for different W values.

Figure 4.7 reveals that α_G calculated from 25 simulation has a relative small standard deviation compared to β_G . Hence, α_G for each simulation point is calculated according to Eq. 4.3 once a proper model for $\beta_G(h, t, w)$ is established.

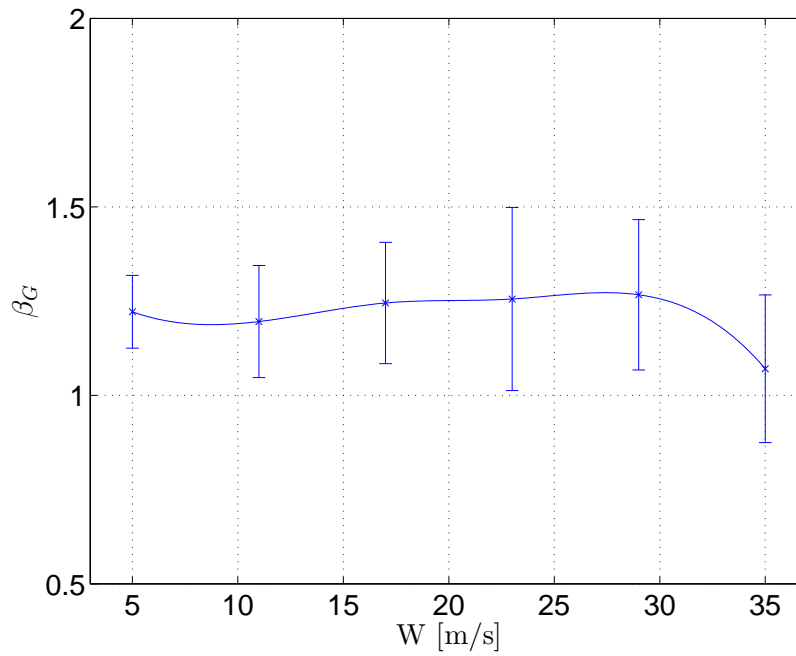


Figure 4.6: Spline function fitted to mean β_G for increasing W , $H_s = 12m$ and $T_p = 14.8s$. The error bars equals one standard deviation of the β_G sample.

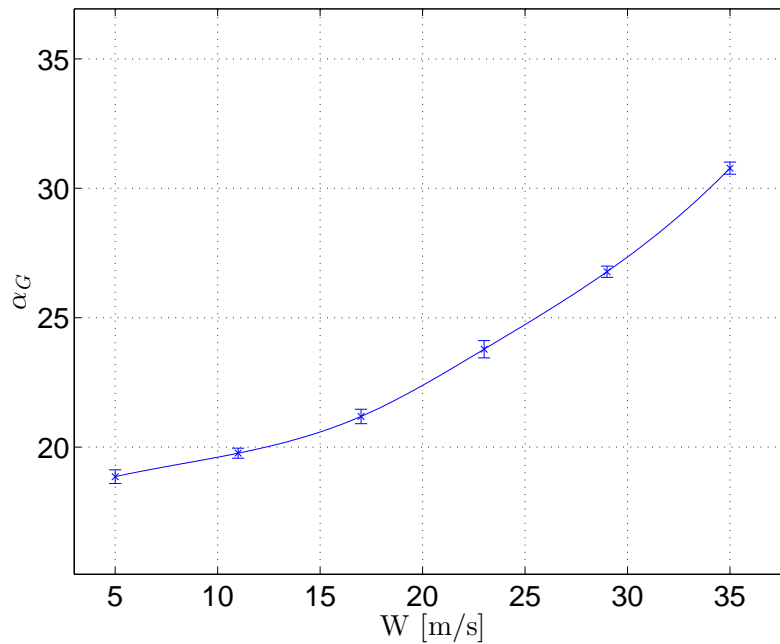


Figure 4.7: Spline function fitted to mean α_G for increasing W , $H_s = 12m$ and $T_p = 14.8s$. The error bars equals one standard deviation of the α_G sample.

4.2.2 Final expression of the response surfaces

To determine the β_G response surface it is assumed that β_G is constant for all values of W . This assumption enables a least square fit to six values of β_G for each sampled sea state given by H_s and T_p within the condition space. Non-linear least square fit is performed using Matlab's curve fitting toolbox and a proposed function for the β_G response surface is given in Eq. 4.4.

$$\beta_G(h, t, w) \approx \beta_G(h, t) = k_1 h + k_2 t + k_3 \cos\left(\frac{t + k_4}{k_5}\right) + k_6 \quad (4.4)$$

Coefficient $k_1 - k_6$ is given in Table 4.1.

Table 4.1: $\beta_G(h, t, w)$ coefficients

Coefficients	Best fit	95% confidence bounds
k_1	0.14	(0.13, 0.15)
k_2	-0.047	(-0.053, -0.041)
k_3	0.19	(0.15, 0.22)
k_4	7.20	(5.36, 9.04)
k_5	1.48	(1.36, 1.59)
k_6	0.39	(0.25, 0.53)

The proposed β_G model and its confidence bounds are plotted in 2D together with empirical β_G values at different wind speeds in Appendix A.5 for verification purposes. A similar plot in 3D are given below in Figure 4.8, where the model is given as a surface and empirical β_G values are given as blue dots.

Figure 4.8 proves that the proposed β_G model fits the data well. Subsequently, new α_G values for each simulation point must be recalculated according to Eq. 4.3 from the mean of the observed maximums and the proposed model for $\beta_G(h, t, w)$. The resulting response surfaces of these α_G values will be used in the analysis and is depicted in Figure 4.9 below. It is noticed that there are little difference between the α_G response surfaces that will be used in the analysis, i.e. Figure 4.9, compared to the initial response surfaces in Figure 4.2.

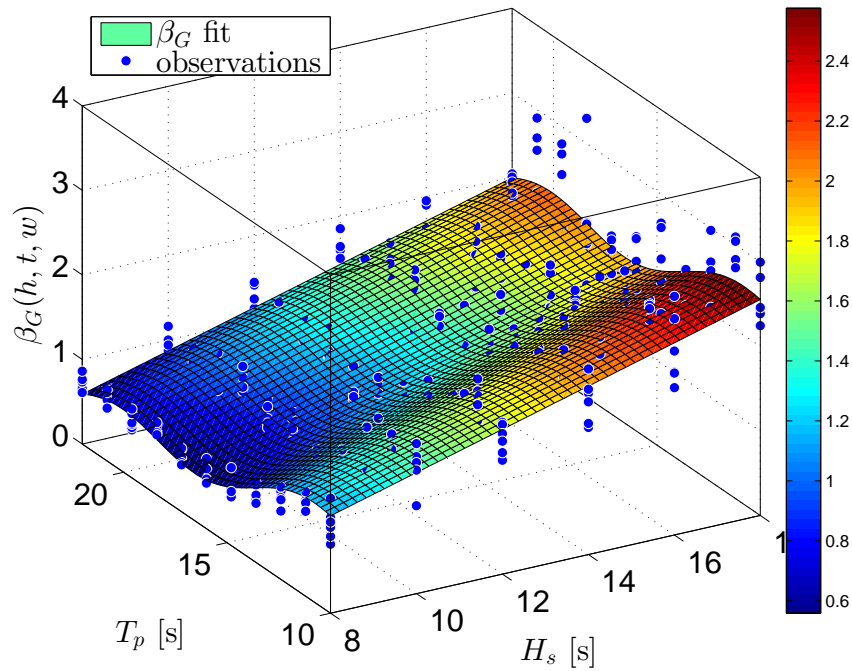


Figure 4.8: Proposed $\beta_G(h, t, w)$ compared to observed β_G for different H_s and T_p combinations. Since β_G is assumed to be independent of W , there are six observations per H_s and T_p combination.

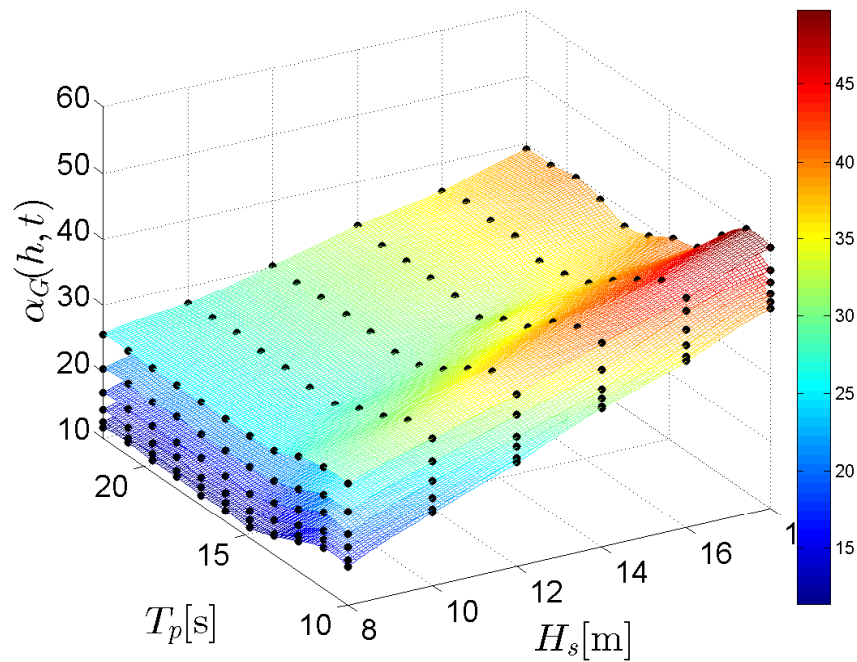


Figure 4.9: $\alpha_G(h, t)$ for different wind classes. The lowest layer of α_G corresponds to wind speed 5 m/s , increasing with a 6 m/s increment to 35 m/s for the top layer. Each black dot represent a simulation point with the resulting α_G value.

A bi-harmonic spline technique is used to describe the α_G response surfaces given any combination of H_s and T_p , i.e. $\alpha_G(h, t)$, for each of the six sampled wind speeds. This results in six response surfaces of α_G as depicted in Figure 4.9. It follows that linear interpolation between the sampled wind speeds gives α_G for any H_s , T_p and W combination, i.e. $\alpha_G(h, t, w)$. In Matlab the bi-harmonic interpolation between H_s and T_p values was conducted using the built in function 'griddata(..., method)', where the method is denoted 'v4'. The 'v4' spline interpolation technique is described by Sandwell (1987).

4.3 Additional response surfaces to be used in the all sea states analysis

The IFORM analysis in the all sea states approach requires that the short term response characteristics are available for a reasonable area surrounding the critical part of the environmental surface. Later it becomes evident that the critical part of the 10,000-year environmental contour surface of wind and waves lies outside the response surfaces obtained in Section 4.2. Hence, a second sample space is created to include these non-observed sea states. This sample space runs from:

H_s : 14-22.1m, with an increment of 2m (last increment of 2.1m)

T_p : 14.8-25.6s, with an increment of 1.2s

W : 17-41m/s, with an increment of 6m/s

Both sample spaces, i.e. the sample space created in Section 4.2 and the sample space created in this section, are cubic since it simplifies the post-processing in Matlab. As a result, many of the simulation points are overlapping for the two sample spaces. It should be noted that the ULS design point in the all sea states analysis is covered by the response surfaces created in Section 4.2. To preserve consistency between the two long term analyses, the ULS response in the all sea states analysis will be calculated using the response surfaces for the POT analysis. Only the ALS

response in the all sea states analysis will be calculated using the response surfaces obtained in this section.

The procedure for establishing response surfaces of the Gumbel parameters remains the same as in Section 4.2, but a less extensive investigation of β_G response surfaces are carried out. Also here, 40 simulations are performed for each simulation point resulting in 40 observations of the maximum response for each sea state. Afterwards, the Gumbel parameters are calculated from the mean and variance of the observed maximums using method of moments.

β_G response surfaces as a function of H_s and T_p , i.e. $\beta_G(h, t)$, are plotted for each of the five sampled wind speeds and given in Appendix B.1. Also now, β_G response surfaces have yet to converge, and once again it is assumed that β_G is independent of W and a function is fitted to the sample data. The proposed model for β_G is given in Eq. 4.5.

$$\beta_G(h, t, w) = f_1 + f_2 h = -0.592 + 0.146h \quad (4.5)$$

The proposed β_G model is plotted in 2-dimensions together with observations at different wind speeds in Appendix B.2 for verification purposes. In Figure 4.10, the $\beta_G(h, w, t)$ model is plotted in 3D together with observations. Finally, α_G is calculated as $\alpha_G = \bar{X} - 0.5772 \cdot \beta_G(h, t, w)$, where \bar{X} is the mean value of the maximum response for each sea state. The resulting α_G response surface is depicted as bi-harmonic spline functions of H_s and T_p for each sampled W value and given in Figure 4.11.

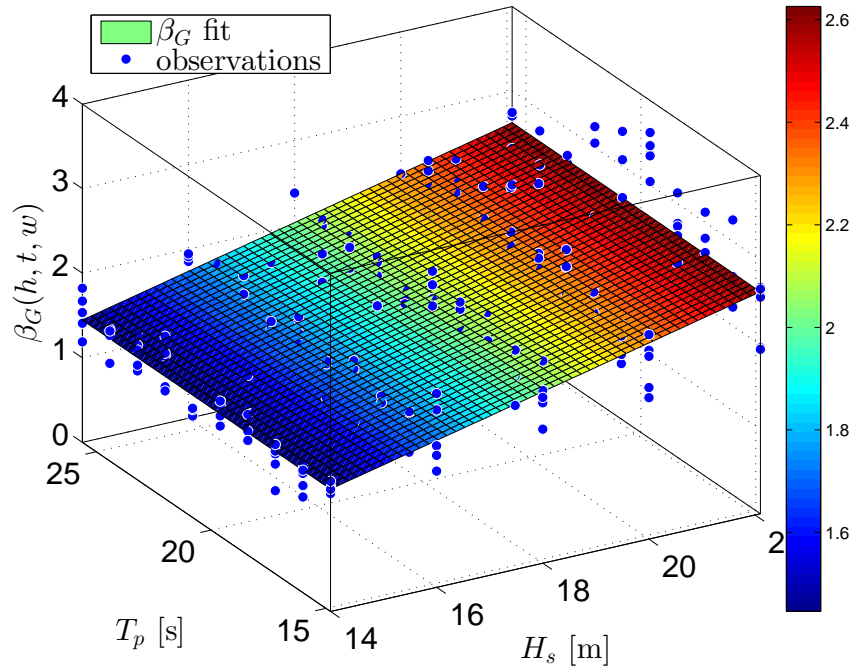


Figure 4.10: Proposed $\beta_G(h, t, w)$ compared to observed β_G for different H_s and T_p combinations. Since β_G is assumed to be independent of W , there are five observations per H_s and T_p combination.

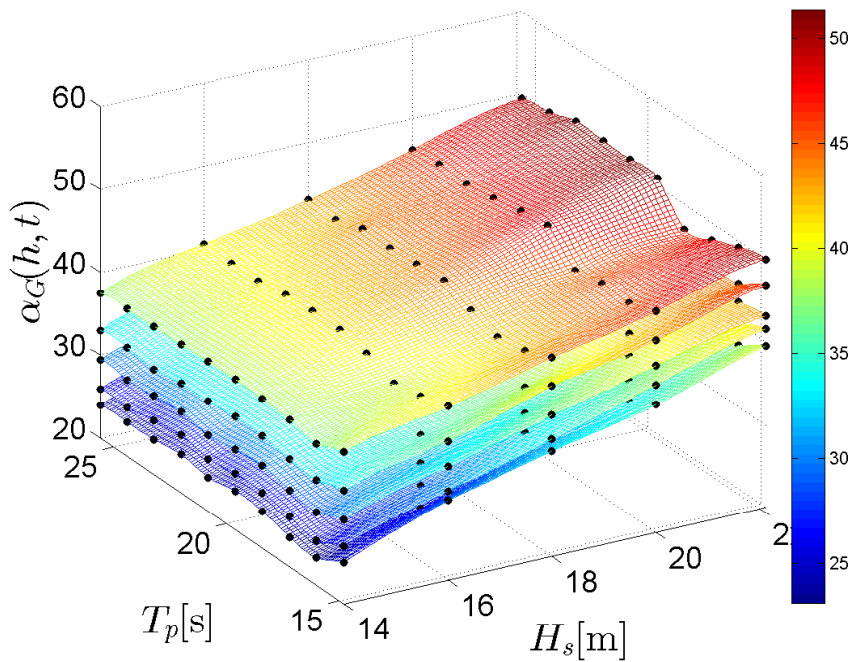


Figure 4.11: $\alpha_G(h, t)$ for different wind classes. The lowest layer of α_G corresponds to wind speed 17 m/s , increasing with a 6 m/s increment to 41 m/s for the top layer. Each black dot represent a simulation point with the resulting α_G value.

4.4 Comparing the two sets of response surfaces

The first set of response surfaces was designed to only capture observed sea states to perform a proper POT analysis. This set of response surfaces is also used to calculate the ULS response in the all sea states analysis. Later when the 10,000-year environmental surface was created for the all sea states analysis, it was clear that the first set of response surfaces did not enclose important non-observed sea states. Hence, another set of response surfaces were created to estimate the all sea states 10,000-year response.

It is of interest to study the difference in the two response surfaces at their overlapping regions. The difference in β_G response surfaces are visualized by plotting the proposed models in 2D for overlapping H_s values as in Figure 4.12. Figure 4.12 indicates that the difference in $\beta_G(h, w, t)$ in the overlapping region is not large.

Similar 2D plots are created to illustrate the difference in α_G response surfaces. These plots are given in Figure 4.13. It is seen that the difference between α_G response surfaces in the overlapping region is relatively small.

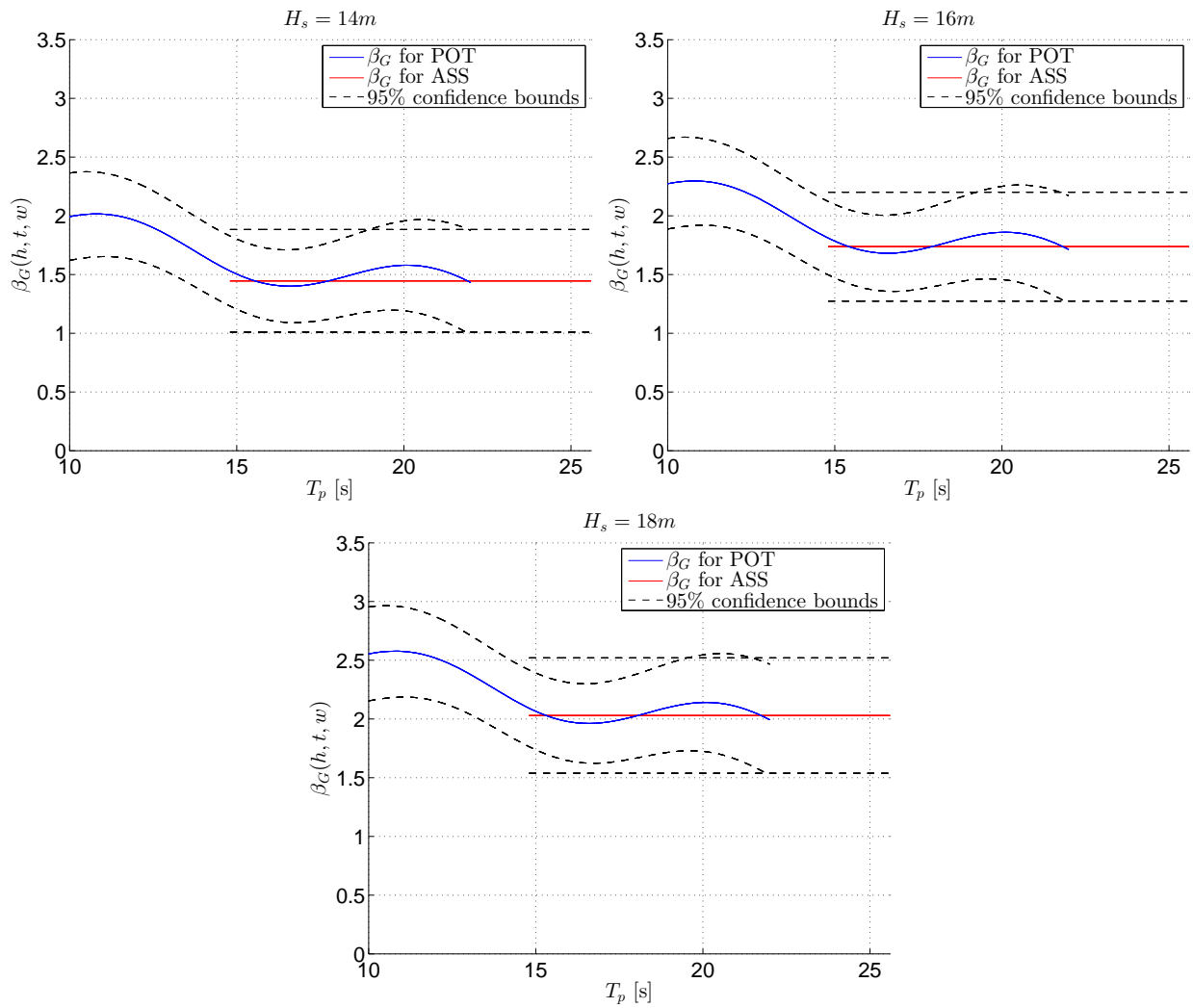


Figure 4.12: Comparing overlapping region of β_G response surfaces.

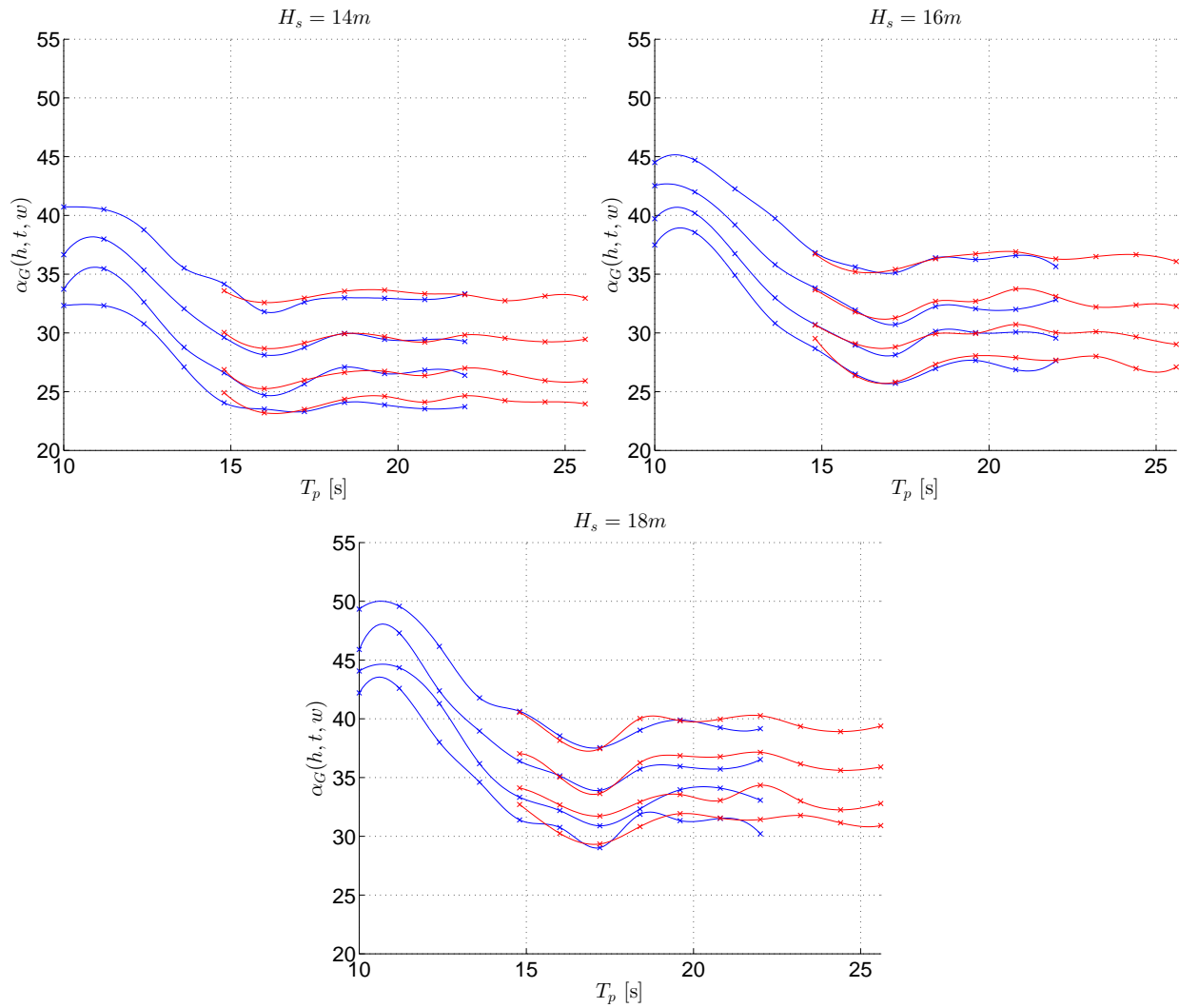


Figure 4.13: Comparing overlapping region of α_G response surfaces for different H_s values. The lower α_G lines are for $W = 17 m/s$, increasing with a $6 m/s$ increment to $35 m/s$ for the top line.

Chapter 5

Peak over threshold

The peak over threshold method only includes sea states above a certain threshold. Different interpretation of the method has been presented in detail by Jahns and Wheeler (1973), Haring (1978), Tromans and Vandersohuren (1995) and Haver (2013). The POT method as outlined by Haver (2013) is used in this thesis.

The POT method is applicable when the extreme responses are governed by the occurrences of some few extreme weather conditions, like e.g. hurricanes. The POT method is therefore, traditionally, more frequently in use abroad than within Norway. The key idea of the POT method is to establish a long term distribution of the largest response during a random storm (Haver, 2004). The long term distribution of the maximum response is obtained by convolution of the conditional distribution of the maximum given the most probable maximum (i.e. the short term variability) with the long term distribution of the most probable maximum as in Eq. 5.1.

$$F_X(x) = \int_{\tilde{x}} F_{X|\tilde{X}}(x|\tilde{x}) f_{\tilde{X}}(\tilde{x}) d\tilde{x} \quad (5.1)$$

Here, $F_{X|\tilde{X}}(x|\tilde{x})$ represents the short term variability of the response given the most probable maximum response and $f_{\tilde{X}}(\tilde{x})$ represents the long term variability of the most probable largest response.

$F_{X|\tilde{X}}(x|\tilde{x})$ and $f_{\tilde{X}}(\tilde{x})$ in Eq. 5.1 can be estimated when the distribution of the storm maximum response, denoted $F_{X|storm}(x|storm)$, is known for all observed storms. Subsequently, the POT analysis should be initiated by determining reliable $F_{X|storm}(x|storm)$ for all observed storms.

5.1 Distribution of storm maximum response

The distribution of the storm maximum response may be simplified as a sequence of stationary sea states with a corresponding 3-hour duration. When the distribution of the maximum response during a random 3-hour sea state is Gumbel distributed, with parameters denoted α_{G_i} and β_{G_i} , the probability of all responses being smaller than or equal than a randomly selected response during an entire storm cycle can be written as, (Jahns and Wheeler, 1973):

$$\begin{aligned} F_{X|storm}(x|storm) &= \prod_{i=1}^M \exp\left(-\exp\left(-\frac{x - \alpha_{G_i}}{\beta_{G_i}}\right)\right) \\ &= \exp\left(-\sum_{i=1}^M \exp\left(-\frac{x - \alpha_{G_i}}{\beta_{G_i}}\right)\right) \end{aligned} \quad (5.2)$$

where M is the number of stationary 3-hour sea states the storm is divided into. Eq. 5.2 assumes that all storm steps are statistical independent. This assumption is not exactly fulfilled since the slowly varying environmental characteristics are correlated to some degree. This effect is, however, rather minor.

α_{G_i} and β_{G_i} is calculated for any sea state within the prescribed sample space by using the proposed response surfaces in Section 4.2. Hence, α_{G_i} is found by the response surfaces depicted in Figure 4.9 in combination with linear interpolation between sampled W values, and β_{G_i} is calculated using the proposed expression in Eq. 4.4.

5.2 Short term variability by $F_{X|\tilde{X}}(x|\tilde{x})$

It is convenient to rewrite the exact distribution of the storm maximum response as a Gumbel distribution, as stated in Eq. 5.3.

$$F_{X|storm}(x|storm) \approx \exp(-\exp(-\frac{x - \alpha_s}{\beta_s})) \quad (5.3)$$

The storm Gumbel parameters, i.e. α_s and β_s , are found from the exact distribution, i.e. $F_{X|storm}(x|storm)$. Recall that $F_{X|storm}(x|storm)$ was calculated for all observed storms according to Eq. 5.2. α_s is equal to the most probable largest value of the exact distribution, i.e. $\alpha_s = \tilde{x}$. Here, α_s is calculated by solving $\frac{d^2 F_{X|storm}(x|storm)}{dx^2} = 0$ with respect to x numerically in Matlab because the most probable largest value occurs as the pdf reaches its maximum. However, as long as $F_{X|storm}(x|storm)$ is close to Gumbel distributed, α_s may be approximated by solving $\alpha_s \approx F_{X|storm}^{-1}(e^{-1})$. It follows that the calculated values of α_s are verified by plotting the percentile level of α_s in $F_{X|storm}(x|storm)$ for all storms as in Figure 5.1.

Notice that the percentile level of storms modeled with one stationary sea state are always equal to e^{-1} , since these storms are exactly replicated by the Gumbel distribution. The percentile levels are always smaller than e^{-1} for storms modeled with more than one sea state, even though the difference is rather minor.

β_s can be estimated by considering the slope of the curve in the origin as the storm distribution is plotted in Gumbel probability paper.

The difference between the exact, i.e. $F_{X|storm}(x|storm)$, and the approximated distribution, i.e. Gumbel distribution with parameters α_s and β_s , for some selected storms is plotted in Gumbel probability paper in Figure 5.2. The function of the exact distribution will for some storms be somewhat concave when plotted in Gumbel probability paper, i.e. the function will be curved on the non-conservative side compared to the approximated distribution. However, this effect is assumed to be negligible.

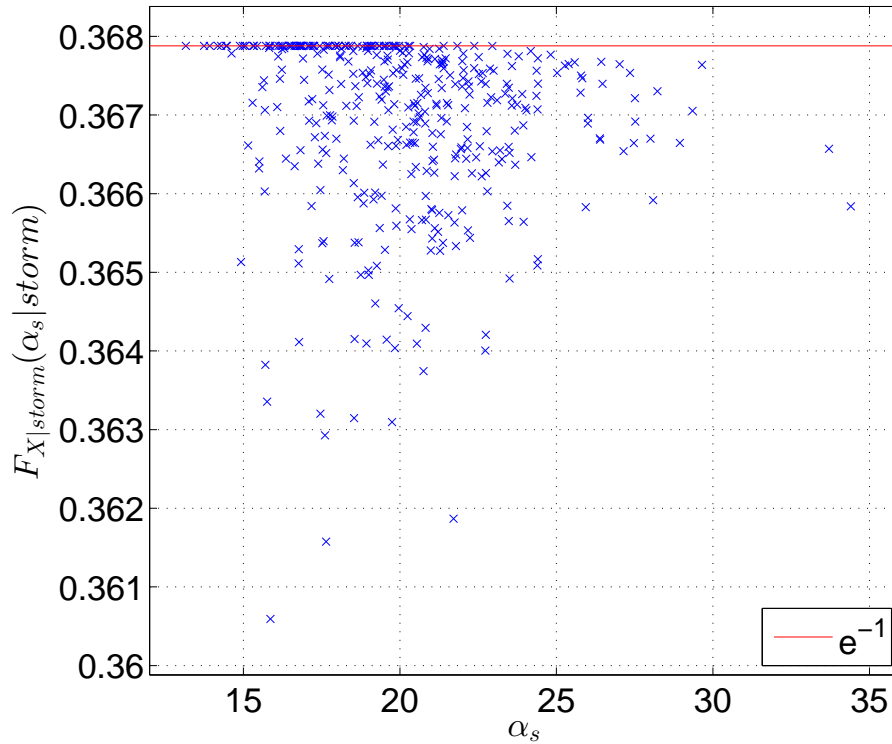


Figure 5.1: Percentile levels of α_s in the exact distribution of storm maximum response.

From Figure 5.2 it is clear that there are small differences between the exact and approximated distributions of the storm maximum response. It seems like the largest error is connected to the curvature of the exact distribution that is not replicated by the approximated distribution, but this effect is only evident for very small probabilities of exceedance and can therefore be neglected. Further, storm (b) is exactly reproduced by the approximated distribution since this storm is modeled as one stationary sea state. Storm (c) is the most severe storm that was observed for these hindcast data. This storm has a duration of 72 hours, but are only modeled with 15 stationary storm steps since sea states below the threshold ($H_s = 8m$) is filtered out as explained in Section 2.4.

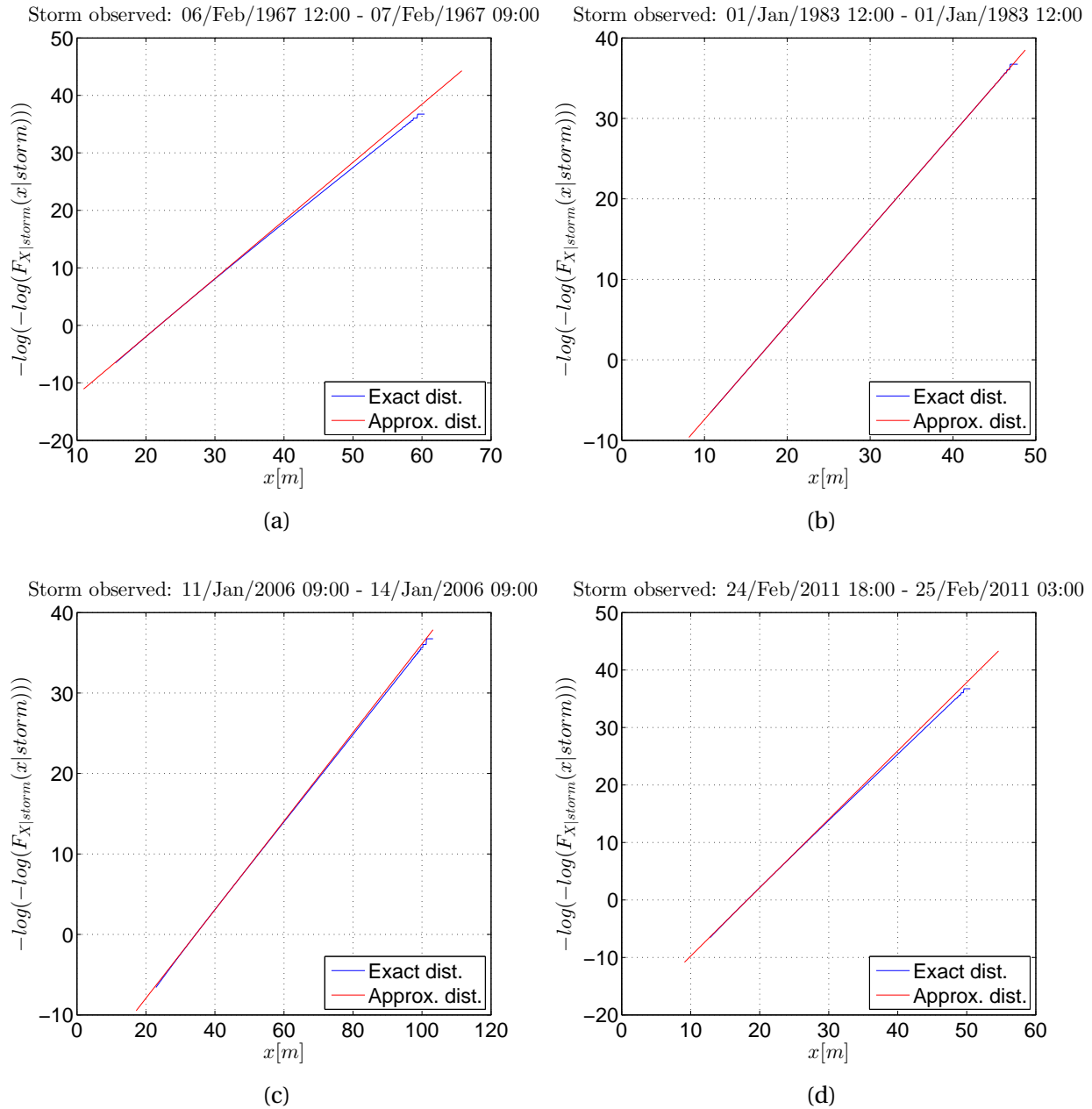


Figure 5.2: Comparing the exact storm distribution of $F_{X|storm}(x|storm)$ with the approximated distribution

Next, the distribution function of the storm maximum response given the most probable maximum response, $F_{X|\tilde{x}}(x|\tilde{x})$, must be estimated to capture the effect of the short term variability of x around \tilde{x} . Introducing the ratio $\nu = \frac{x}{\tilde{x}}$ under the hypothesis that all extreme responses follow the Gumbel distribution, with location parameter $\alpha_\nu = 1$ and constant scale parameter denoted β_ν , gives the following distribution of V , Haver (2013).

$$F_V(\nu) = \exp[-\exp[-\frac{\nu-1}{\beta_\nu}]] \quad (5.4)$$

The basic idea is to assume that the location parameter β_ν is constant for all storms. This results in a conditional distribution of the maximum response given the most probable largest response.

$$F_{X|\tilde{x}}(x|\tilde{x}) = \exp[-\exp[-\frac{x-\tilde{x}}{\beta_\nu\tilde{x}}]] \quad (5.5)$$

α_s and β_s have already been calculated for each storm. Using that $\tilde{x} = \alpha_s$, a proper sample of β_ν is easily calculated by $\beta_\nu = \frac{\beta_s}{\tilde{x}}$. The calculated β_ν values are then plotted against \tilde{x} for all storms and depicted in Figure 5.3.

Figure 5.3 indicates that the scatter in β_ν for a random storm is large. In this context it is assumed that the mean β_ν for all storms given the selected threshold can be used in the further analysis. In Table 5.1, the mean and the 95% probability band of β_ν is listed.

Table 5.1: β_ν variability, threshold $H_s = 8m$

	Value
$\bar{\beta}_\nu$	0.0501
$\beta_{\nu,97.5\%}$	0.0578
$\beta_{\nu,2.5\%}$	0.0406

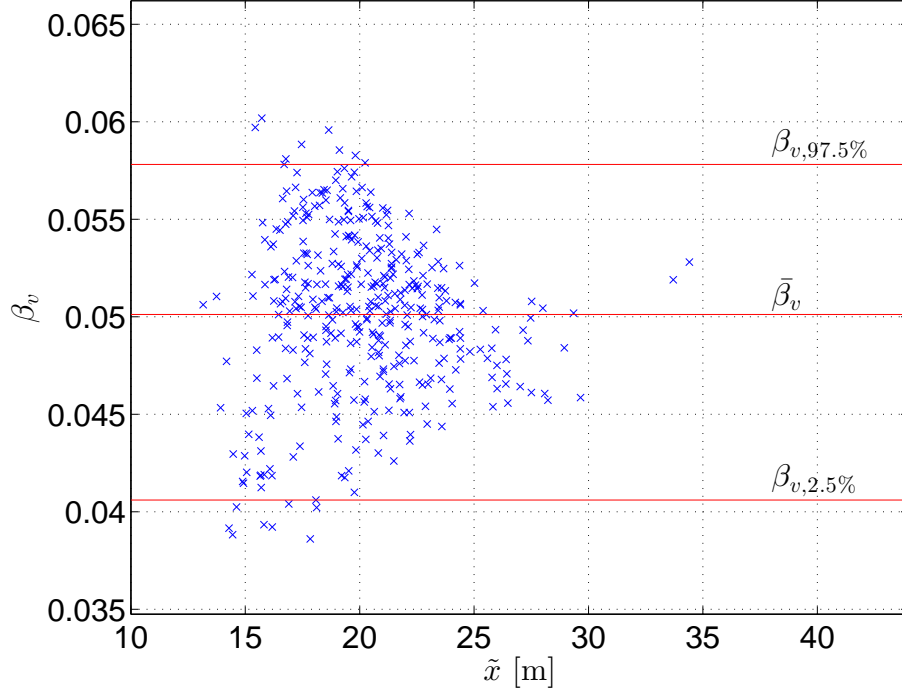


Figure 5.3: Observations of β_v . There are one observation of β_v for each storm, threshold $H_s = 8m$.

5.3 Long term variability by $F_{\tilde{X}}(\tilde{x})$

In Section 5.2, the distribution function of the storm maximum response was found for all storms. α_s corresponds to the most probable largest response, i.e. \tilde{x} , for each storm. A proper probabilistic model can then be fitted to the sample of most probable largest responses to obtain the long term distribution of the storm most probable maximum, i.e. $F_{\tilde{X}}(\tilde{x})$. A 3-parameter Weibull distribution seems to be a reasonable model for the observed \tilde{x} values. The method of moments was used to fit the probability distribution to the observed data by estimating the distribution parameters from the mean, variance and skewness of the data. Hence, the following model for $F_{\tilde{X}}(\tilde{x})$ is proposed:

$$F_{\tilde{X}}(\tilde{x}) = 1 - \exp\left(-\left(\frac{\tilde{x} - \alpha_{\tilde{x}}}{\beta_{\tilde{x}}}\right)^{\lambda_{\tilde{x}}}\right) = 1 - \exp\left(-\left(\frac{\tilde{x} - 14.5}{6.37}\right)^{1.84}\right) \quad (5.6)$$

The adequacy of the selected model is verified by plotting the model and observed values in Weibull probability paper as in Figure 5.4.

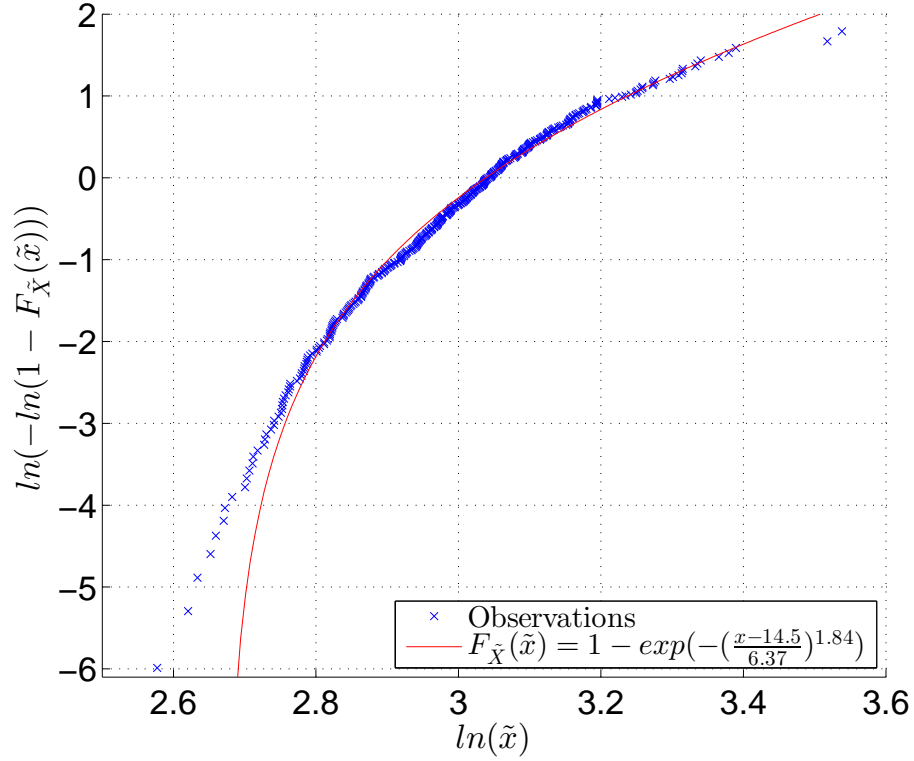


Figure 5.4: Long term distribution of most probable largest response, i.e. $F_{\tilde{X}}(\tilde{x})$.

The distribution of the storm most probable maximum response represents the long term variability of the storm extremity as felt by the response under consideration, Haver (2013). Figure 5.4 illustrates that the proposed distribution represents a suitable fit for higher \tilde{x} values. Since extreme responses are of concern, the distribution represents a suitable model for $F_{\tilde{X}}(\tilde{x})$.

5.4 Long term analysis

Finally, the distribution of the maximum response in a random storm, i.e. $F_X(x)$ is found by solving Eq. 5.1. Accounting for the average number of observed storms per year, the q-probability maximum response value reads

$$1 - F_X(x_q) = \frac{q}{N_s} \quad (5.7)$$

where N_s is the expected number of storms above the selected threshold per year.

A convenient way of calculating Eq. 5.1 is to use the Inverse First Order Reliability Method (IFORM). The IFORM approach is an extension of the First Order Reliability Method (FORM). These two approaches will be explained in the next sections.

5.4.1 FORM

The First Order Reliability Method (FORM) is used when the integral in Eq. 5.1 is difficult to solve numerically. FORM provides an efficient approach of predicting the response with small exceedance probabilities.

Assume that the aim is to find the probability of exceeding a critical response, denoted x_{crit} . A typical limit state function for this purpose is given by Eq. 5.8 (Haver and Winterstein, 2008).

$$g(X, \tilde{X}; x_{crit}) = x_{crit} - X(\tilde{X}) \quad (5.8)$$

Where X is the 3-hour maximum response. The failure boundary is defined as the event of x_{crit} being exceeded and occurs when Eq. 5.8 becomes negative. This further implies that the failure boundary are given by $g() = 0$. Now the probability of exceeding x_{crit} are estimated by solving Eq. 5.9.

$$p_f(x_{crit}) = \iint_{g() < 0} f_{X|\tilde{X}}(x|\tilde{x}) f_{\tilde{X}}(\tilde{x}) dx d\tilde{x} \quad (5.9)$$

The integral in Eq. 5.9 can be calculated numerically or estimated without explicit integration by utilizing the FORM approach. The integral needs to be transformed to the Gaussian space (u-space) that consists of independent, standard Gaussian variables denoted U_1, U_2, U_3 and U_4 , see e.g. Madsen et al. (1986).

$$\begin{aligned}
F_{\tilde{X}}(\tilde{x}) &= \Phi(u_1) \Leftrightarrow u_1 = \Phi^{-1}[F_{\tilde{X}}(\tilde{x})] \\
F_{X|\tilde{X}}(x|\tilde{x}) &= \Phi(u_2) \Leftrightarrow u_2 = \Phi^{-1}[F_{X|\tilde{X}}(x|\tilde{x})]
\end{aligned}
\tag{5.10}$$

Where $F_{\tilde{X}}(\tilde{x})$ is given by Eq 5.6 and $F_{X|\tilde{X}}(x|\tilde{x})$ is given by Eq. 5.5.

This transformation conserves probability at all points. It is a unique one-to-one mapping of points in the physical parameter space to the u-space since all the involved functions increases monotonically. Because of the transformation given by Eq. 5.10, all points in the u-space with a constant probability density will form a circle. A larger circle radius indicates a smaller probability density. The failure surface can be mapped in the Gaussian space by utilizing Rosenblatt transformation. The point in u-space closest to the origin is referred to as the design point. This point is the most probable combination of X and \tilde{X} as the critical response is exceeded. For very small probabilities, one may expect that the probability contribution rapidly decays moving away from origin and further into the failure boundary. Utilizing this feature, the failure boundary can be linearized in the design point. This linearization of the failure boundary in u-space is referred to as the First Order Reliability Method. With this assumption, the probability of exceeding the critical response, x_{crit} corresponds to the probability of exceeding a tangent line along the contour going through the design point. Hence, the failure probability is constant and given by Eq. 5.11.

$$p_f(x_{crit}) = \Phi(-\beta) \tag{5.11}$$

Now the upper tail of the target distribution, $F_X(x)$, can be estimated by repeating the procedure above for various x_{crit} . In this way, extreme responses corresponding to some target percentile can be estimated by interpolation or by a suitable iterative procedure.

5.4.2 IFORM

The Inverse First Order Reliability Method (IFORM) represents an alternative and, in this case, a faster approach than FORM to estimate response values corresponding to a given q-probability of exceedance. The main idea is that the annual target percentile level is known and that the corresponding response level is to be determined. This means that the radius of the circle with constant probability in u-space is known, and the target q-probability response variable exists on this circle.

In this study there are 56.8 years of hindcast data (166,053 recorded 3-hour sea states) and 398 independent storms for threshold $H_s = 8m$. The resulting average number of storms per year is 7.0. This means that the ALS circle radius in u-space is equivalent to $-\Phi^{-1}(\frac{10^{-4}}{7.0}) = 4.185$, and the 10,000-year event exists on this u-space circle. The circle can be transformed back to the physical parameter space, representing all combinations of X and \tilde{X} with an annual return period of 10^{-4} . The largest of these responses is taken as the target 10,000-year response.

5.5 ULS and ALS responses

Utilizing the IFORM approach to solve Eq. 5.1, response contours with return period of 10^{-2} and 10^{-4} per year is created and depicted in Figure 5.5. The contour lines of x and \tilde{x} are calculated with $\bar{\beta}_v$ in Table 5.1. Sensitivity to β_v is indicated by calculating response contour lines using the 95% confidence bounds of β_v .

The largest value of x on the q-probability response contour is taken as the x_q response. The q-probability responses for threshold $H_s = 8m$ with corresponding sensitivity to β_v is given in Table 5.2.

Table 5.2 indicates that the q-probability responses are not very sensitive to the selected β_v values. Further, the ALS response seems to be somewhat more sensitive to β_v than the ULS response.

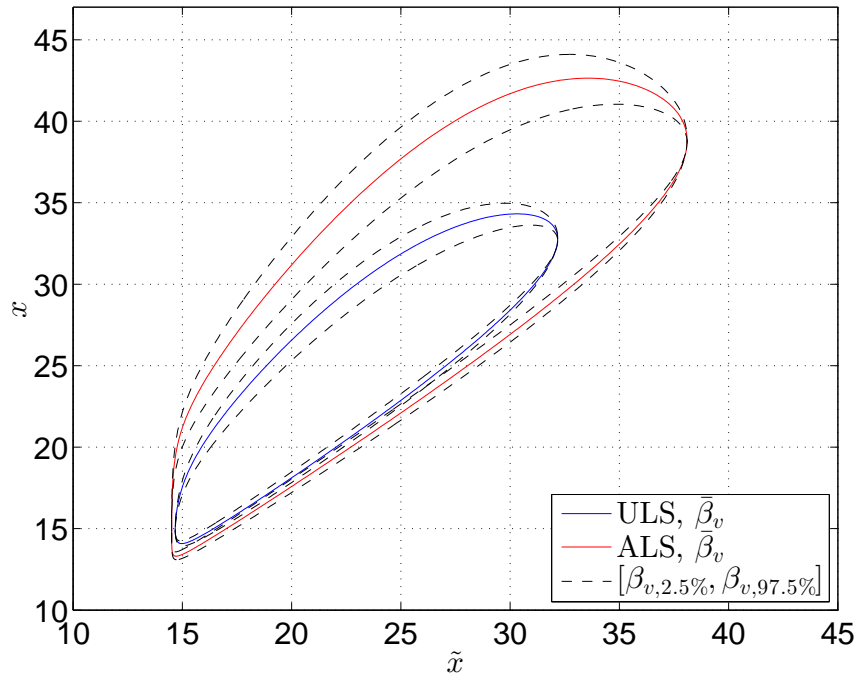


Figure 5.5: ULS and ALS response contours. Sensitivity to β_v is indicated with dotted lines

Table 5.2: ULS and ALS responses

	$\bar{\beta}_v$	$[\beta_{v,2.5\%}, \beta_{v,97.5\%}]$
ULS	34.3m	[33.6m, 35.0m]
ALS	42.6m	[41.0m, 44.1m]

5.6 Threshold selection

Threshold selection is a crucial part of most POT analyses. A proper threshold should be selected to describe the tail of the long term response distribution. A too low threshold is likely to violate the asymptotic behavior of the model, leading to bias. Similarly, a too high threshold will generate few observed extremes that the model can be estimated from, which will again lead to high variance of the results. Hence, balancing bias and variance is an important part of selecting

an appropriate threshold (Coles, 2001).

5.6.1 Threshold sensitivity study

It is of interest to study the effect of the selected threshold on the predicted q-probability responses. Hence, additional POT analyses were performed with threshold $H_s = 9m$ and $H_s = 10m$. The methodology of merging correlated storms as explained in Section 2.4 was adopted. The number of observed and merged (independent) storms for different H_s thresholds are listed in Table 5.3. The independent storm events are used in the analysis.

Table 5.3: Number of observed and independent storms for different thresholds

Threshold	Observed storms	Independent storms
$H_s = 8m$	446	398
$H_s = 9m$	226	207
$H_s = 10m$	109	103

The distribution of the maximum response for all independent storms given threshold $H_s = 9m$ and $H_s = 10m$ is calculated using the response surfaces of α_G and β_G obtained in Section 4.2. The resulting β_v values are plotted against \bar{x} for different thresholds and given in Appendix C.1.

Table 5.4: β_v variability for different thresholds

Threshold	$\bar{\beta}_v$	$[\beta_{v,2.5\%}, \beta_{v,97.5\%}]$
$H_s = 8m$	0.0501	[0.0406, 0.0578]
$H_s = 9m$	0.0488	[0.0416, 0.0556]
$H_s = 10m$	0.0485	[0.0437, 0.0568]

The long term distribution of \tilde{x} is assumed to follow a 3-parameter Weibull distribution for all

thresholds. The parameters are calculated using method of moments and are listed in Table 5.5 for different thresholds. The adequacy of the proposed models for $F_{\bar{X}}(\bar{x})$ is verified in Appendix C.2.

Table 5.5: Parameters in $F_{\bar{X}}(\bar{x})$ for different thresholds

Threshold	$\alpha_{\bar{x}}$	$\beta_{\bar{x}}$	$\lambda_{\bar{x}}$
$H_s = 8m$	14.50	6.37	1.84
$H_s = 9m$	16.85	5.34	1.59
$H_s = 10m$	17.67	6.12	1.75

Finally, the q-probability responses are determined utilizing IFORM for various thresholds and β_v values. These results are listed in Table 5.6. The 100-year (ULS) and 10,000-year (ALS) response contour lines for different β_v values and threshold are given in Appendix C.3.

Table 5.6: ULS and ALS responses for different thresholds

Threshold	ULS, $\bar{\beta}_v$	ULS, [$\beta_{v,2.5\%}$, $\beta_{v,97.5\%}$]	ALS, $\bar{\beta}_v$	ALS, [$\beta_{v,2.5\%}$, $\beta_{v,97.5\%}$]
$H_s = 8m$	34.3	[33.6, 35.0]	42.6	[41.0, 44.1]
$H_s = 9m$	34.9	[34.5, 35.4]	44.0	[42.9, 45.2]
$H_s = 10m$	35.2	[34.9, 35.7]	44.2	[43.5, 45.5]

If the characteristic responses do not change much for different thresholds, it is appropriate to select the lowest threshold giving the same longterm responses. In this case, the characteristic responses increase for higher thresholds. Threshold $H_s = 10m$ has too few observations leading to a high variance in the result. Threshold $H_s = 9m$ seems to be a proper choice with twice as many observations and almost the same characteristic responses than threshold $H_s = 10m$. Hence, the ULS and ALS response resulting from the POT analysis is taken as 34.9m and 44.0m, respectively.

Chapter 6

All sea states approach

The all sea state approach assumes that each 3-hour event is statistically independent. This assumption is not fulfilled because of the inherent correlation between adjacent sea states. Consequently, it is expected that the q-probability responses will be slightly on the safe side, Haver (2013). It follows that the all sea states approach is expected to yield more conservative q-probability responses than the POT method.

6.1 All sea states to extreme responses

A full long term analysis of the response is possible by combining the short term variability of the 3-hour maximum response described conditionally on all possible realizations of sea states with the long term probability distribution of the weather characteristics under consideration. The long term distribution of the 3-hour maximum response is then given by Eq. 6.1.

$$F_X(x) = \iiint_{H_s, T_p, W} F_{X|H_s, T_p, W}(x|h, t, w) f_{H_s, T_p, W}(h, t, w) dh dt dw \quad (6.1)$$

Here, the weather characteristics are taken as significant wave height (H_s), spectral peak period

(T_p) and wind speed (W) because these parameters are the most important contributors to the maximum response.

The short term variability of the response given some weather characteristics is already known since the responses surfaces of α_G and β_G are known for all relevant combinations of H_s , T_p and W , see Chapter 4.

The long term probability distribution of the weather characteristics are estimated from the given hindcast data and will be explained in the next section.

6.2 Long term variability of weather

The long term variability of the weather conditions can be found by fitting a joint probability model to simultaneous observations of H_s , T_p and W . The joint distribution can conveniently be written as Eq. 6.2.

$$f_{H_s, T_p, W}(h, t, w) = f_{H_s}(h) f_{W|H_s}(w|h) f_{T_p|H_s, W}(t|h, w) \quad (6.2)$$

Eq. 6.2 can be rewritten in different ways, but it is appropriate to determine the marginal distribution of the most important weather characteristic for the maximum response. Then a larger data sample is available to determine the parameters in the marginal distribution. Here it is assumed that H_s is the most important weather characteristic.

6.2.1 Marginal distribution of H_s

The upper tail of H_s is adequately modeled using a 3-parameter Weibull model given by Eq. 6.3.

$$F_{H_s}(h) = 1 - \exp\left(-\left(\frac{x - \alpha_{H_s}}{\beta_{H_s}}\right)^{\lambda_{H_s}}\right) \quad (6.3)$$

α_{H_s} , β_{H_s} and λ_{H_s} are determined using method of moments following the procedure outlined in Haver (2015b). Subsequently, α_{H_s} , β_{H_s} and λ_{H_s} were determined from the mean, standard deviation, and skewness, of the sample data by solving the equations in Eq. 6.4.

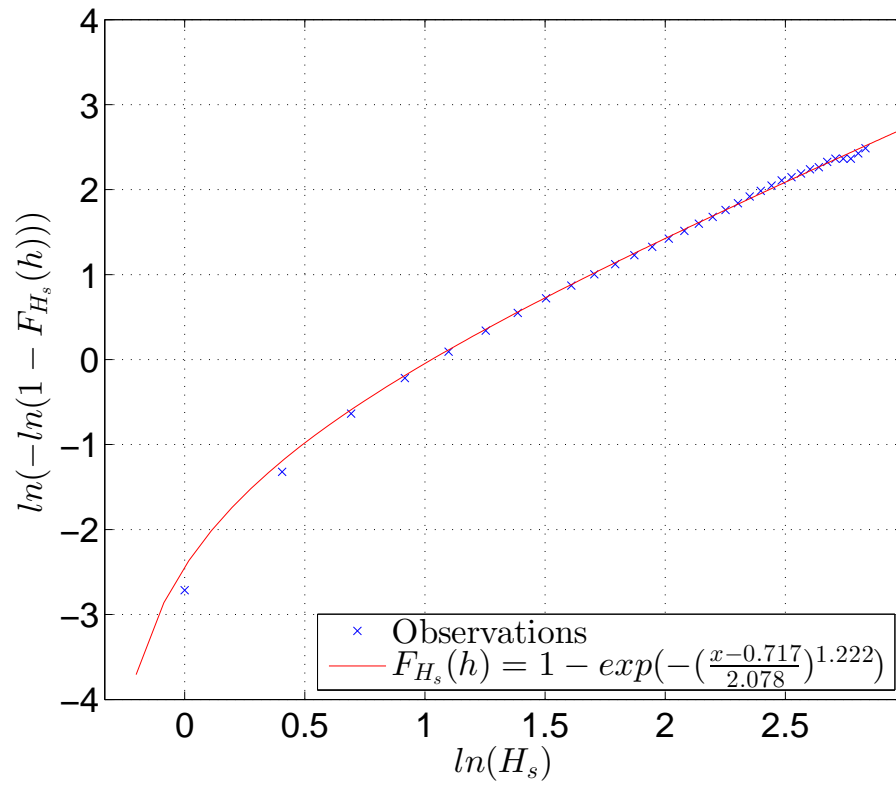
$$\begin{aligned}\gamma_{H_s} &= \frac{\Gamma(1 + \frac{3}{\lambda_{H_s}}) - 3\Gamma(1 + \frac{1}{\lambda_{H_s}})\Gamma(1 + \frac{2}{\lambda_{H_s}}) + 2\Gamma^3(1 + \frac{1}{\lambda_{H_s}})}{(\Gamma(1 + \frac{2}{\lambda_{H_s}}) - \Gamma^2(1 + \frac{1}{\lambda_{H_s}}))^{\frac{3}{2}}} \\ \beta_{H_s} &= \frac{\sigma_{H_s}}{\sqrt{(\Gamma(1 + \frac{2}{\lambda_{H_s}}) - \Gamma^2(1 + \frac{1}{\lambda_{H_s}}))}} \\ \alpha_{H_s} &= \bar{H}_s - \beta_{H_s}\Gamma(1 + \frac{1}{\lambda_{H_s}})\end{aligned}\tag{6.4}$$

Where γ_{H_s} is the wave heights coefficient of skewness, σ_{H_s} is the wave heights standard deviation and \bar{H}_s is the mean wave height. The calculated parameters are listed in Table 6.1.

Table 6.1: Coefficients in marginal distribution of H_s

Coefficients	Value
α_{H_s}	0.717
β_{H_s}	2.078
λ_{H_s}	1.222

The fitted model is verified by plotting the distribution and hindcast sample data in Weibull probability paper as depicted in Figure 6.1.

Figure 6.1: Marginal distribution of H_s

6.2.2 Conditional distribution of W

Wind speed is commonly modeled with the Weibull distribution, Morgan et al. (2011). Hence, an expression for $F_{W|H_s}(w|h)$ is proposed in Eq. 6.5.

$$F_{W|H_s}(w|h) = 1 - \exp\left(-\left(\frac{w}{\sigma_W(h)}\right)^{\lambda_W(h)}\right) \quad (6.5)$$

The Weibull parameters, σ_W and λ_W , are determined from observed W values within different classes of H_s using method of moments. The classes of H_s are seen as rows in the omnidirectional scatter diagram displayed in Appendix D.1. There are for instance 179 observed wind speeds in the first class defined by $0 \leq H_s \leq 0.5$, and the Weibull parameters are determined for these observed values. The adequacy of the proposed model can be verified by plotting the distribution within each H_s class in Weibull probability paper. The Weibull distribution was considered suitable since the curves were close to linear as can be seen for some selected H_s classes in Figure 6.2. The fitted distributions to data for other sea states can be reviewed in Appendix D.2.

Subsequently, the Weibull parameters have been determined for each H_s class and proper functions are fitted to the data points. The proposed model for $\sigma_W(h)$ is given and verified in Figure 6.3. The fitting was conducted using Matlab curve fitting tool together with the bi-square robust fitting option.

However, two different models for the shape parameter, $\lambda_W(h)$, will be investigated. Both models are given as spline functions to better replicate empirical observations for smaller H_s classes and they are depicted in Figure 6.4. The empirical values of λ_W increase rapidly for higher H_s classes. The models for $\lambda_W(h)$ will be assumed to converge towards some value when $H_s > 15m$. For this problem, the ‘best fit’ represent a good fit to empirical values and is assumed to converge towards 12.5. The ‘constrained model’ seems to be a poor fit for higher H_s values, but is created for the 100 and 10,000-year wind speeds (denoted $W_{10^{-2}}$ and $W_{10^{-4}}$, respectively) to be consistent with extreme wind speeds predicted by the marginal distribution of W .

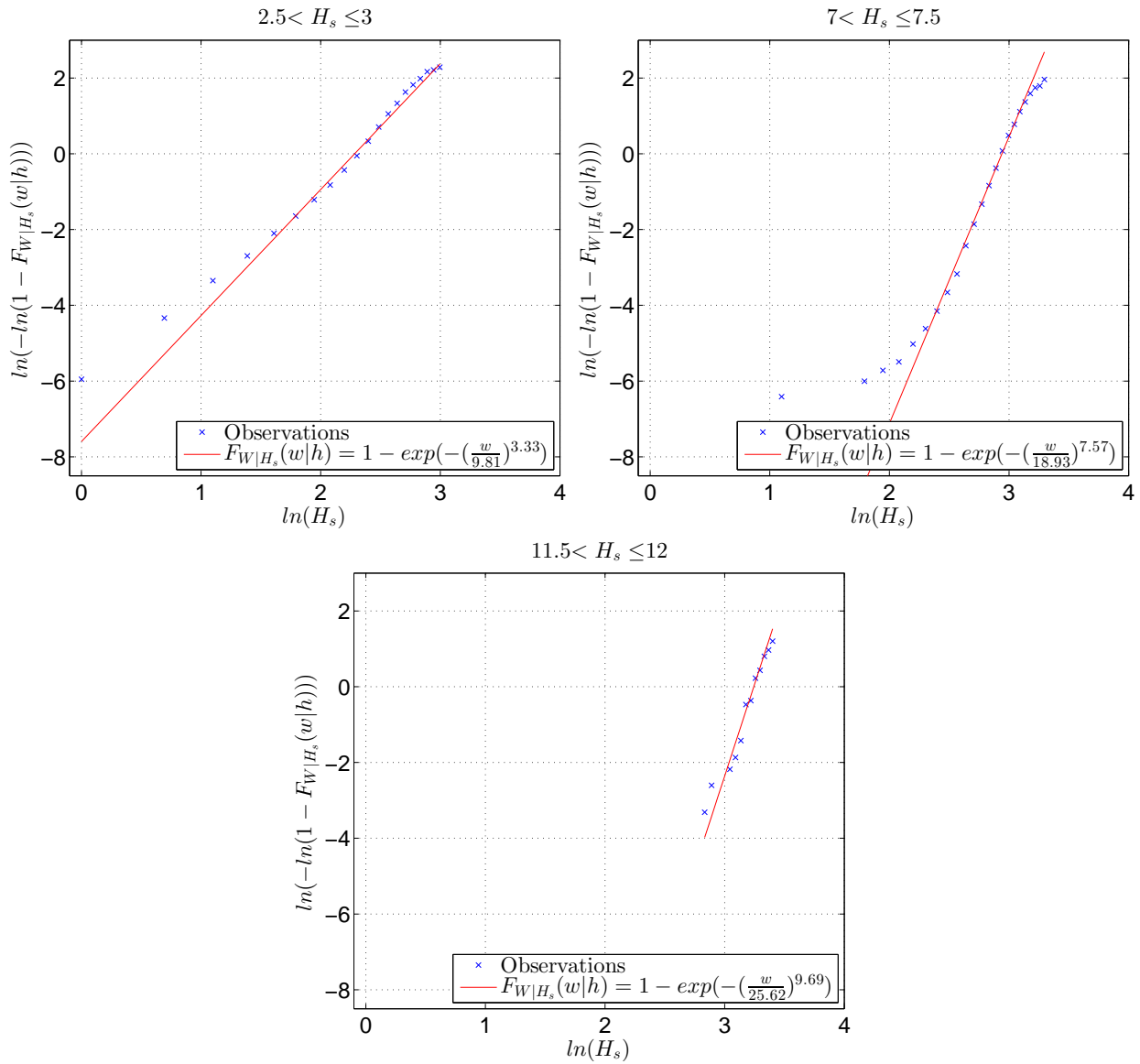


Figure 6.2: Cumulative distribution of W within different classes of H_s . The empirical observations are given together with the fitted 2-parameter Weibull distribution.

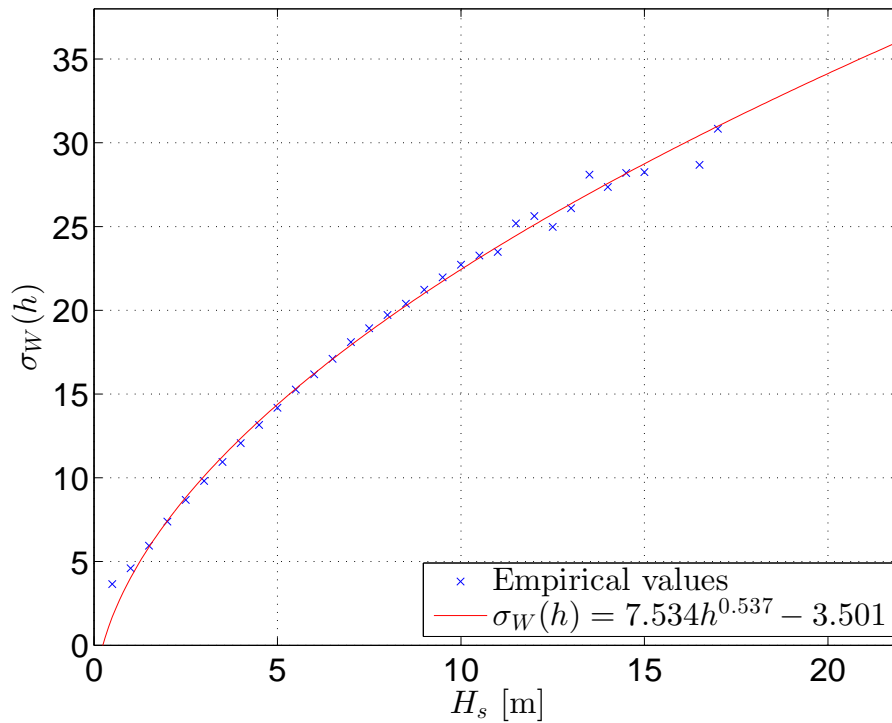


Figure 6.3: Proposed model for $\sigma_W(h)$ together with observed σ_W for different H_s classes.

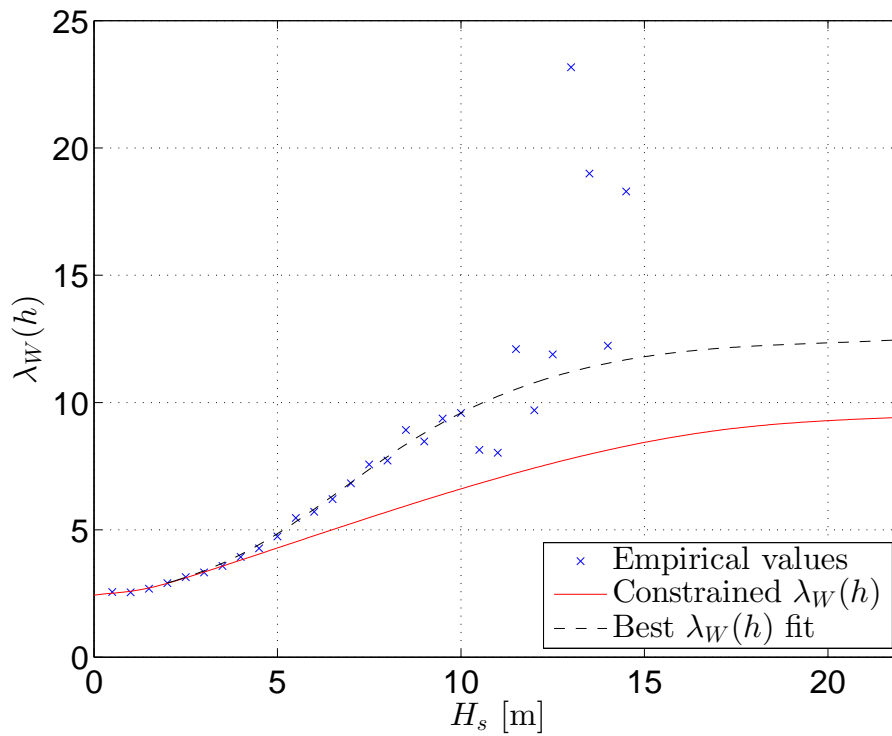


Figure 6.4: Two models for $\lambda_W(h)$ to be investigated. The models are given as spline functions and compared to empirical observations.

The joint model should predict the same extreme weather conditions as the marginal distributions. Consequently, it is of interest to find the 100 and 10,000-year wind speeds predicted by the marginal distribution of W , i.e. $F_W(w)$. A 3-parameter Weibull model seems to be a suitable model and the distribution parameters were estimated using method of moments. The model is plotted with observed wind speeds and is given in Figure 6.5. Accounting for the number of sea states per year, the q -probability wind speeds are determined by solving $F_W(w_q) = 1 - \frac{q}{2920}$. From Figure 6.5 it is noticed that the target 100 year and 10,000-year wind speeds for the joint model are $W_{10^{-2}} = 33.6\text{m/s}$ and $W_{10^{-4}} = 39.3\text{m/s}$.

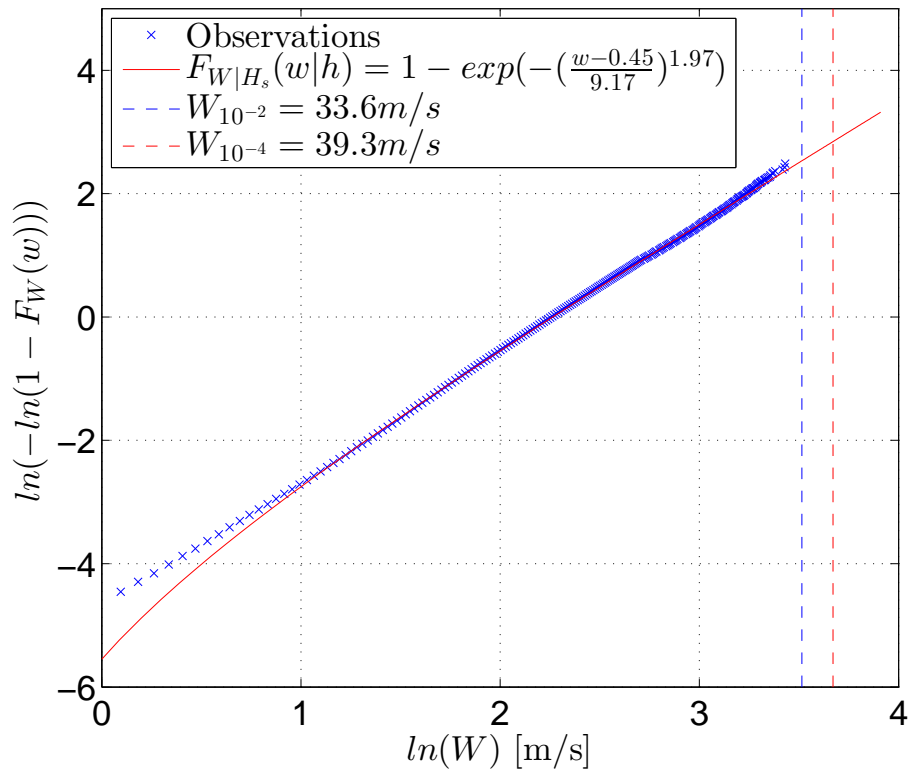


Figure 6.5: Marginal distribution of W compared to empirical observations.

The resulting contour lines of H_s and W are found using IFORM with the relations given by Eq. 6.6. The ULS circle radius in u -space is equal to $-\Phi^{-1}\left(\frac{10^{-2}}{2920}\right) = 4.5$.

$$\begin{aligned}
 F_{H_s}(h) &= \Phi(u_1) \Leftrightarrow u_1 = \Phi^{-1}[F_{H_s}(h)] \\
 F_{W|H_s}(w|h) &= \Phi(u_2) \Leftrightarrow u_2 = \Phi^{-1}[F_{W|H_s}(w|h)]
 \end{aligned}
 \tag{6.6}$$

In addition, the resulting combinations of H_s and W with a return period of 100-years (ULS) and 10,000-years (ALS) are given in Figure 6.6. The 100-year wind speed corresponds to the largest value of W on the ULS contour.

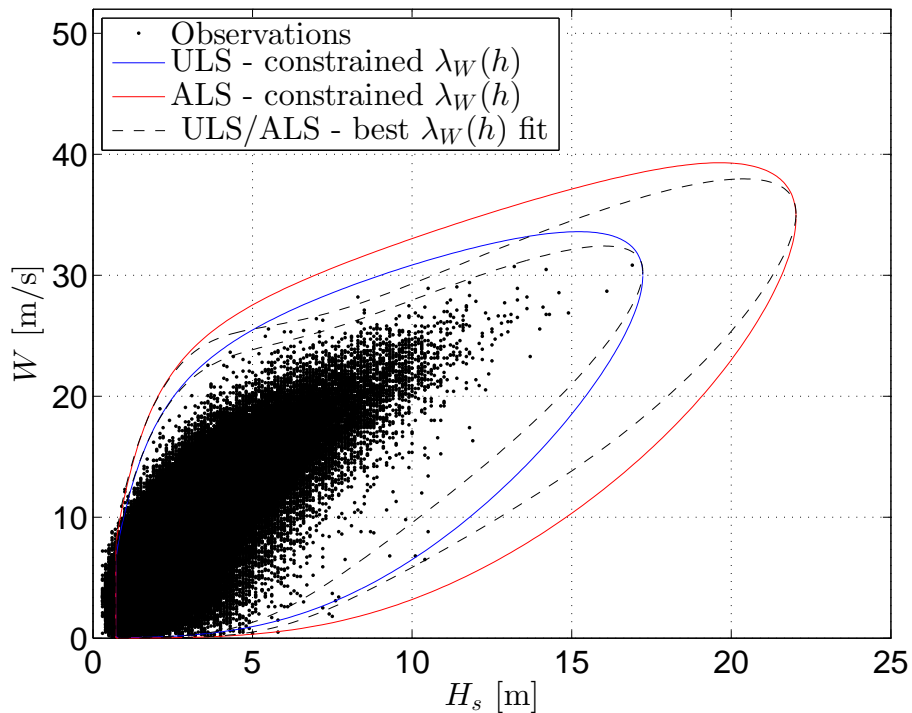


Figure 6.6: Contour lines of H_s and W . The constrained model of $\lambda_W(h)$ is used for the ULS (blue) and ALS (red) lines. The black dotted lines indicates contours calculated with the ‘best $\lambda_W(h)$ fit’.

Here it will be assumed that the joint model for H_s and W is sufficiently accurate once the q -probability wind speeds resulting from the contour matches the q -probability wind speeds of the marginal distribution of W . The contour lines illustrates that using the ‘best $\lambda_W(h)$ fit’ will result in too small q -probability wind speeds. Decreasing $\lambda_W(h)$ will give thicker contours of H_s and W with a corresponding increase in extreme wind speeds for the joint model. Therefore, the constrained model for $\lambda_W(h)$ will be used since it provides the same q -probability wind speeds as predicted by $F_W(w)$.

6.2.3 Conditional distribution of T_p

Based on experience, $f_{T_p|H_s, W}(t|h, w)$ is satisfactory modeled by the lognormal distribution, Johannessen et al. (2002).

$$f_{T_p|H_s}(t|h) = \frac{1}{\sqrt{2\pi}t\sigma_{\ln(T_p)}(h, w)} \exp\left[-\frac{1}{2}\left(\frac{\ln(t) - \mu_{\ln(T_p)}(h, w)}{\sigma_{\ln(T_p)}(h, w)}\right)^2\right] \quad (6.7)$$

Where $\mu_{\ln(T_p)}(h, w)$ and $\sigma_{\ln(T_p)}(h, w)$ are the mean and standard deviation of $\ln(T_p)$, respectively. For each class of H_s and W in the scatter diagram in Appendix D.1, the mean, μ_{T_p} , and standard deviation, σ_{T_p} , of the observed spectral peak periods are used to calculate $\mu_{\ln(T_p)}$ and $\sigma_{\ln(T_p)}$ according to Eq. 6.8.

$$\begin{aligned} \mu_{\ln(T_p)} &= \ln\left[\frac{\mu_{T_p}}{\sqrt{1 + v_{T_p}^2}}\right] \\ \sigma_{\ln(T_p)}^2 &= \ln[v_{T_p}^2 + 1] \end{aligned} \quad (6.8)$$

Where,

$$v_{T_p} = \frac{\sigma_{T_p}}{\mu_{T_p}} \quad (6.9)$$

Based on experience, the standard deviation can be expressed as a function of the wave height and mean wave period given by Eq. 6.10, Johannessen et al. (2002).

$$\sigma_{T_p}(h, w) = [-0.0017 + 0.259e^{-0.113h}] \mu_{T_p}(h, w) \quad (6.10)$$

The proposed model for $\sigma_{T_p}(h, w)$ are verified by plotting the difference between observed standard deviations of T_p and $\sigma_{T_p}(h, w)$ in Figure 6.7. $\mu_{T_p}(h, w)$ in Eq. 6.10 is then substituted with

observed values of the mean spectral peak period for each class of H_s and W .

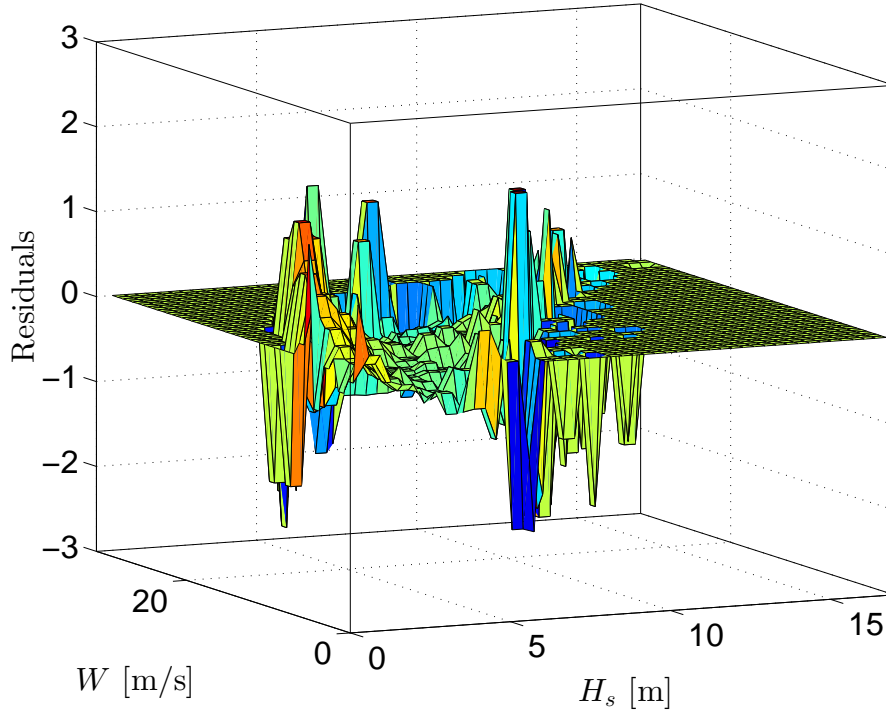


Figure 6.7: Difference in standard deviation of empirical T_p and model. The empirical mean T_p for different H_s and W classes is used instead of $\mu_{T_p}(h, w)$ in the model. Positive residuals means that the observed T_p standard deviation is larger than suggested by the model.

The challenge is then to determine $\mu_{T_p}(h, w)$, i.e. the mean spectral peak period given by H_s and W . Hence, observed μ_{T_p} for different H_s and W values were plotted in 3D and depicted in Figure 6.8.

Figure 6.8 shows that for constant H_s values, T_p decreases for increasing W . Further, for constant wind speeds the period increases with H_s . This behavior can be described with Eq. 6.11.

$$\mu_{T_p}(h, w) = \mu_{T_p}(h) \left[1 + \theta \left(\frac{w - \bar{w}(h)}{\bar{w}(h)} \right)^\gamma \right] \quad (6.11)$$

Where $\mu_{T_p}(h)$ is the mean peak period for a given value of H_s and $\bar{w}(h)$ is the mean wind speed for any given H_s . The idea is that the term $[1 + \theta(\frac{w - \bar{w}(h)}{\bar{w}(h)})^\gamma]$ will adjust T_p when the wind speed is below or above the expected wind speed for each particular wave height, (Johannessen et al., 2002). It follows that θ and γ will determine T_p dependency on the wind speed for different H_s .

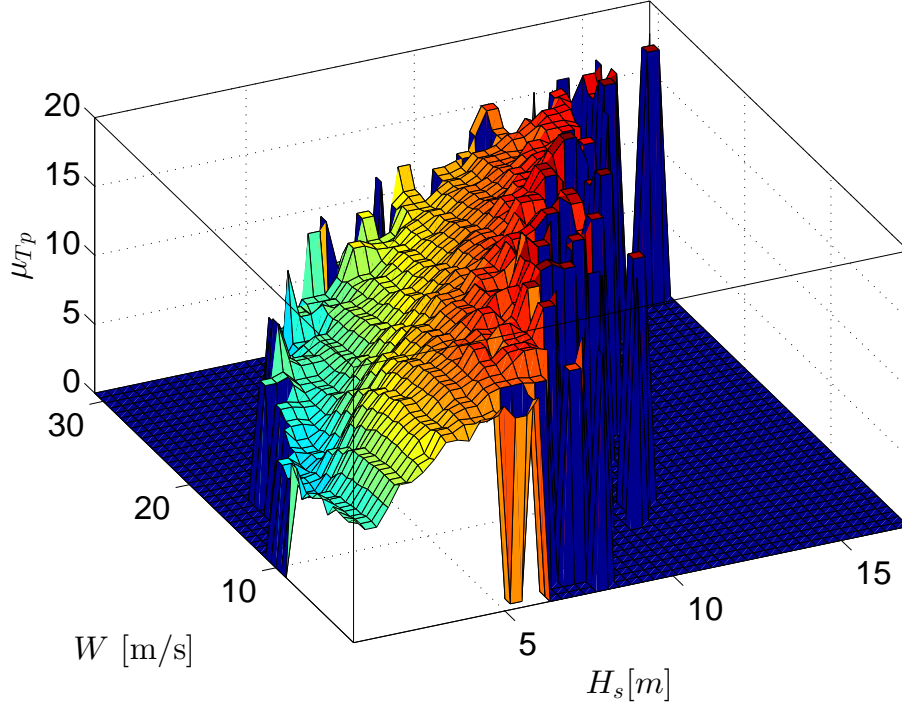


Figure 6.8: Empirical mean T_p in different classes of H_s and W .

values.

μ_{T_p} and \bar{w} were plotted for different H_s classes and the following parameterizations are proposed in Eq. 6.12.

$$\begin{aligned}\mu_{T_p}(h) &= d_1 + d_2 h^{d_3} = 6.004 + 2.146h^{0.612} \\ \bar{w}(h) &= e_1 + e_2 h^{e_3} = -0.620 + 4.727h^{0.665}\end{aligned}\tag{6.12}$$

These parameterizations are verified in Appendix D.3. Subsequently, θ and γ can be determined by rewriting Eq. 6.13 as:

$$\frac{\mu_{T_p}(h, w)}{\mu_{T_p}(h)} - 1 = \theta \left(\frac{w - \bar{w}(h)}{\bar{w}(h)} \right)^\gamma\tag{6.13}$$

Now the normalized period, i.e. $\frac{\mu_{T_p}(h, w)}{\mu_{T_p}(h)} - 1$, can be plotted against the normalized wind speed,

i.e. $\theta(\frac{w-\bar{w}(h)}{\bar{w}(h)})^\gamma$ to give an idea of suitable θ and γ values. A selection of these plots for different H_s classes are displayed in Figure 6.9. The fitted distributions of other H_s classes are given in Appendix D.3.

As can be seen from Figure 6.9, the trend follows some kind of sine function for small H_s values and is almost linear for higher wave heights. Since extreme wave heights is of concern, it will be assumed that there is a linear relationship between the normalized T_p and the normalized wind speed. Following this approximation, γ is equal to 1.

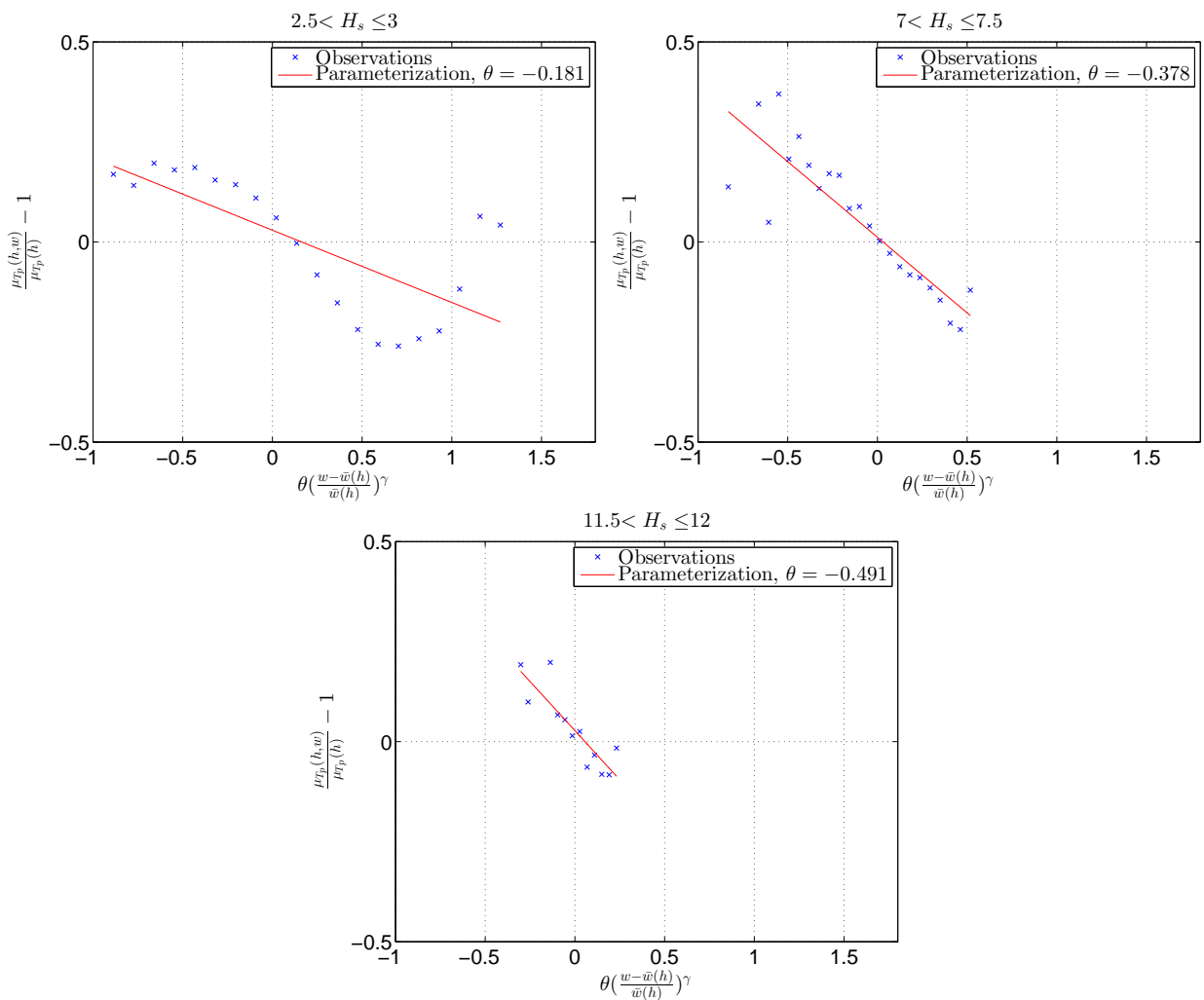


Figure 6.9: Normalized T_p as a function of normalized W

The slopes, i.e. θ , of the normalized functions seem to increase for higher H_s classes. A proper function of $\theta(h)$ can thus be selected by plotting θ as a function of H_s as in Figure 6.10.

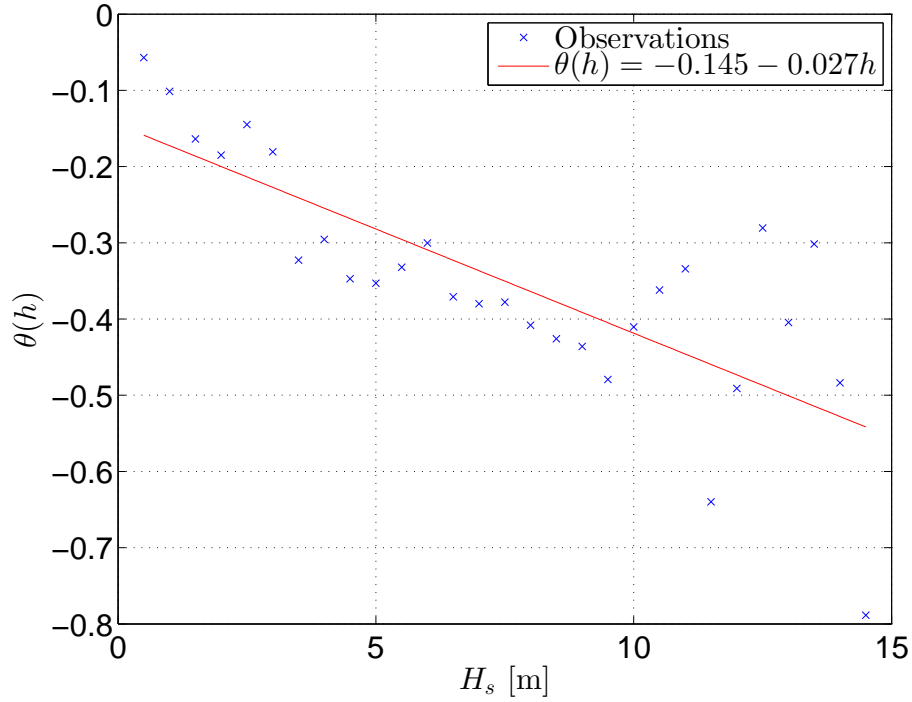


Figure 6.10: The slope between the normalized T_p and normalized wind speed, i.e. θ , as a function of the significant wave height.

In Figure 6.10 a suitable regression line of $\theta(h)$ is proposed. Finally, a model for the mean spectral peak period given H_s and W , i.e. $\mu_{T_p}(h, w)$, is given by inserting $\theta(h)$, $\mu_{T_p}(h)$, $\bar{w}(h)$ and $\gamma = 1$ into Eq. 6.11. Hence, the final expression for $\mu_{T_p}(h, w)$ is given by Eq. 6.14.

$$\mu_{T_p}(h, w) = (6.004 + 2.146h^{0.612}) \cdot [1 + (-0.145 - 0.027) \left(\frac{w + 0.620 - 4.727h^{0.665}}{-0.620 + 4.727h^{0.665}} \right)] \quad (6.14)$$

To verify the proposed model of $\mu_{T_p}(h, w)$, residuals between observed mean peak periods and the model are plotted for all sea states and can be investigated in Figure 6.11. A positive residual means that the empirical mean T_p is larger than indicated by the model.

The residual plot clearly illustrate that the proposed models for $\sigma_{T_p}(h, w)$ and $\mu_{T_p}(h, w)$ is adequate for high H_s and W values, and can therefore be used in the further analysis. There are some deviations between observed values and the model for lower H_s and W classes, but this is of little concern since extreme weather conditions are of interest when aiming for q-probability responses.

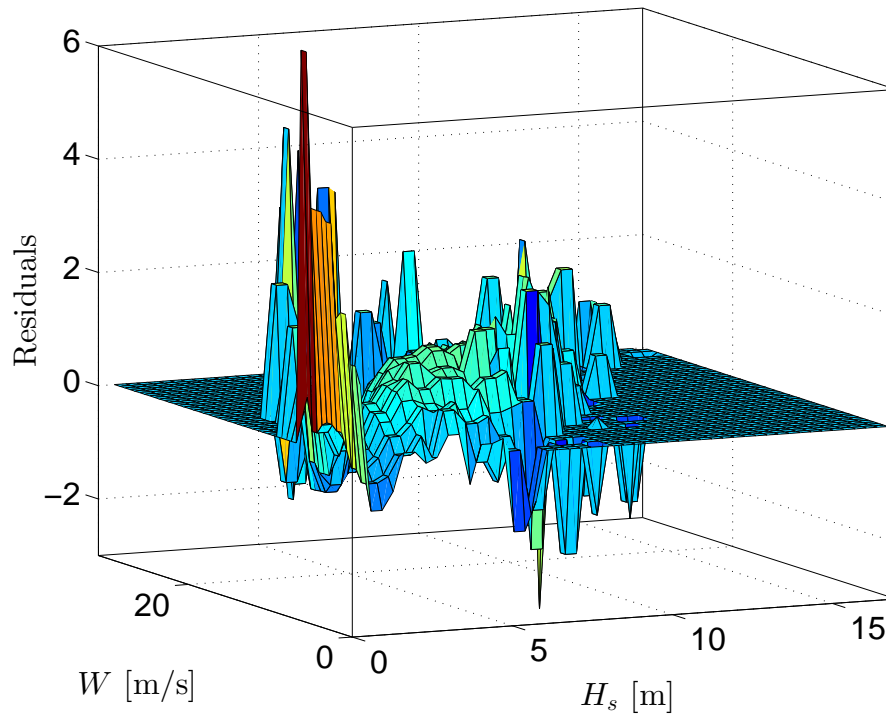


Figure 6.11: Difference in empirical mean T_p and proposed model, i.e. $\mu_{T_p}(h, w)$ for all combinations of H_s and W . Positive residuals means that the empirical mean T_p is larger than predicted by the model.

The final expression for the parameters in the conditional log-normal distribution is found by inserting the proposed models of $\sigma_{T_p}(h, w)$, i.e. Eq. 6.10, and $\mu_{T_p}(h, w)$, i.e. Eq. 6.14, into Eq. 6.8.

6.2.4 Environmental contour lines of H_s , T_p and W

Contour lines of H_s , T_p and W are obtained from the joint distribution of H_s , W and T_p using IFORM. These contour lines are plotted in Figure 6.12-6.14 together with the ‘first’ sample space (defined in Sec. 4.2) that merely includes observed sea states and the ‘second’ sample space (defined in Section 4.3) that shall include non-observed sea states. The outer boundaries of the first sample space are given by the lower left rectangular in Figure 6.12 and Figure 6.13, and by the lower left cube in Figure 6.14.

From Figure 6.12-6.14 it becomes evident why the second sample space is needed. Some sea

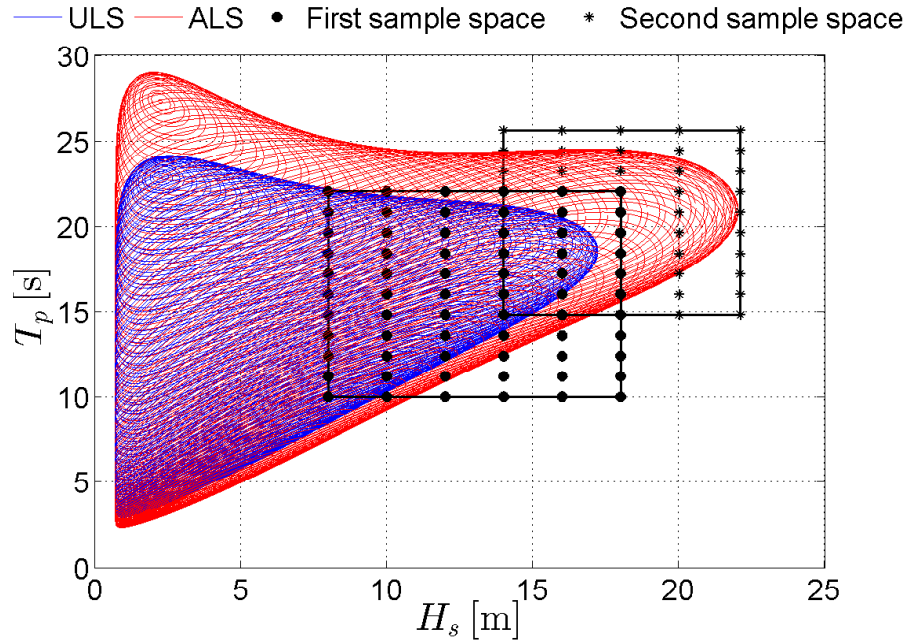


Figure 6.12: Environmental contour lines projected onto the H_s - T_p plane. Simulation points within the first and second sample space are given as black dots and asterisks, respectively. The second sample space was created to include sea states within the ALS environmental contour that lies outside the first sample space.

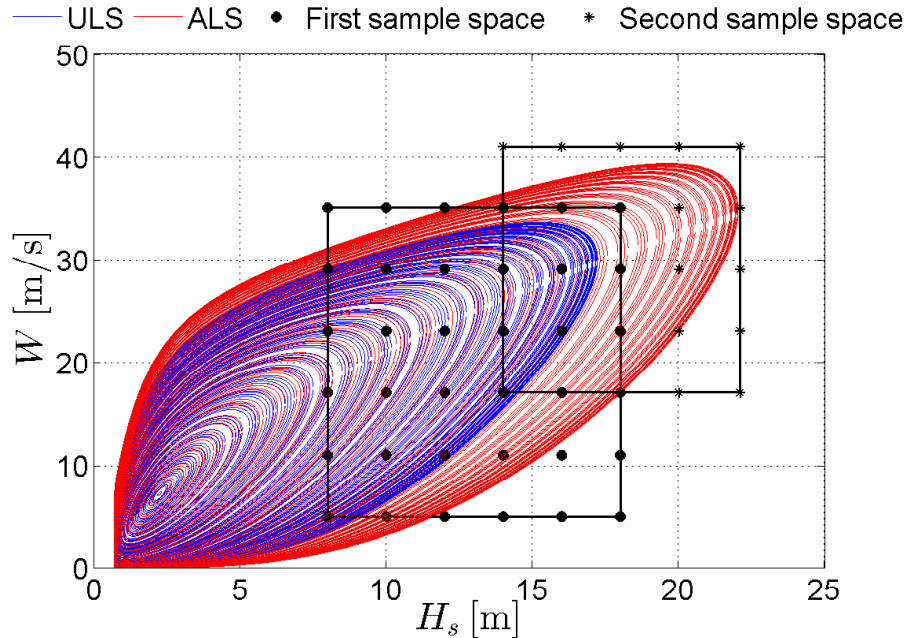


Figure 6.13: Environmental contour lines projected onto the H_s - W plane with simulation points defining the sample spaces.

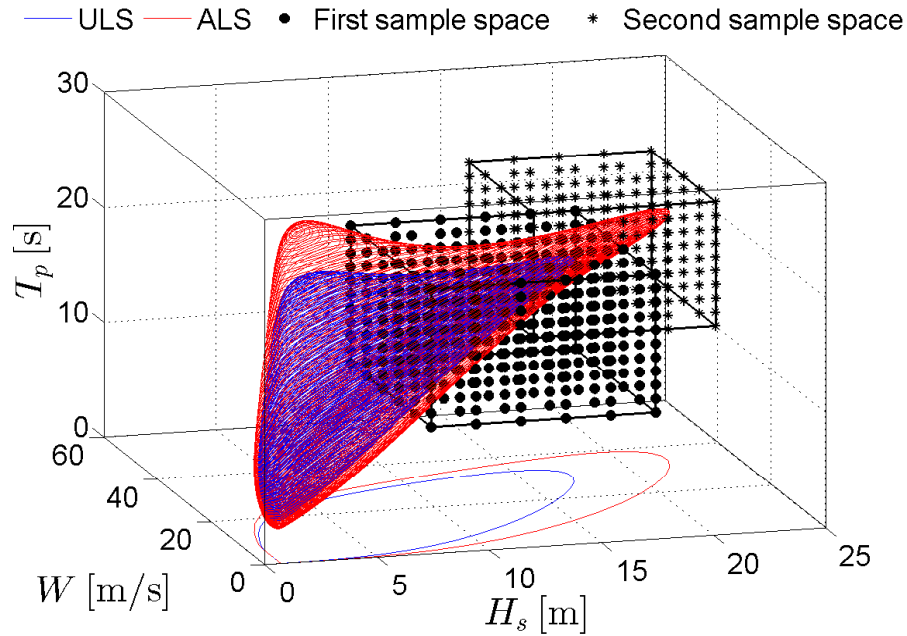


Figure 6.14: 3-dimensional environmental contour lines with simulation points defining the sample spaces.

states inside the 10,000-year weather contour are not included by the first sample space. The second sample space is designed to include the ALS design point and will therefore be used when calculating the all sea states ALS response using IFORM. The all sea states ULS response will be calculated with the first sample space, i.e. the sample space used for the POT analysis, to preserve consistency between the POT and all sea states analyses.

6.3 ULS and ALS responses

In the all sea states approach, $F_{X|H_s, T_p}(x|h, t)$ is known once the response surfaces are established.

The ULS and ALS responses are now estimated using IFORM, Meling et al. (2000). For this 4-parameter problem, the 4-dimensional surface in the Gaussian u-space with constant q-probability is modeled as a hypersphere with radius, β , defined by Eq. 6.15, WolframMathWorld (2016)

$$\begin{aligned}
u_1 &= \beta \cdot \sin(\psi) \sin(\varphi) \sin(\phi) \\
u_2 &= \beta \cdot \sin(\psi) \sin(\varphi) \cos(\phi) \\
u_3 &= \beta \cdot \sin(\psi) \cos(\varphi) \\
u_4 &= \beta \cdot \cos(\psi)
\end{aligned} \tag{6.15}$$

Where ψ and φ run over the range 0 to π , while ϕ runs over 0 to 2π .

To perform the IFORM analysis, one need to transform the integral to the Gaussian space (u-space) that consists of independent, standard Gaussian variables denoted U_1 , U_2 , U_3 and U_4 . In this transformed space, points of constant probability density define a 4-dimensional hypersphere. Taking the number of 3-hour sea states during a year into account, the ULS hypersphere radius is $\beta = 4.5$. Similarly, the ALS hypersphere radius is $\beta = 5.4$

$$\begin{aligned}
F_{H_s}(h) &= \Phi(u_1) \Leftrightarrow u_1 = \Phi^{-1}[F_{H_s}(h)] \\
F_{W|H_s}(w|h) &= \Phi(u_2) \Leftrightarrow u_2 = \Phi^{-1}[F_{W|H_s}(w|h)] \\
F_{T_p|H_s,W}(t|h, w) &= \Phi(u_3) \Leftrightarrow u_3 = \Phi^{-1}[F_{T_p|H_s,W}(t|h, w)] \\
F_{X|H_s,W,T_p}(x|h, w, t) &= \Phi(u_4) \Leftrightarrow u_4 = \Phi^{-1}[F_{X|H_s,W,T_p}(x|h, w, t)]
\end{aligned} \tag{6.16}$$

The hypersphere can then be transformed back to the physical parameter space to form a 4-dimensional contour of H_s , T_p , W and X with a constant probability of exceedance. This requires that the Gumbel parameters for the actual combination of H_s , T_p and W are known. It would not be efficient to perform SIMO simulations for each realization of X given the weather characteristics H_s , T_p and W . Hence, the response surfaces are used for this purpose. The response surfaces for the POT analysis will be used to calculate the ULS response to preserve consistency between the two long term analyses. The response surfaces from the POT analysis do not include the ALS design point. Thus, the additional response surfaces created in Sec. 4.3 will be used to calculate the 10,000-year response. The largest responses on the ULS and ALS contour are taken as the characteristic values. The result of this IFORM analysis are summarized in Table 6.2.

Table 6.2: ULS and ALS responses

	Response [m]
ULS	36.7
ALS	52.1

$F_{X|H_s, T_p, W}(x|h, t, w)$ is independent of H_s , T_p and W if the short term variability of the response problem can be neglected. Consequently, one may produce a design contour from the slowly varying environmental characteristics and the design contour can be visualized as environmental contours in 3D as in Figure 6.12-6.14. If the variability of the response given the environmental characteristics is important, and in this case it is, the 10^{-2} design point will be located inside the 10^{-2} environmental contour sphere. Hence, the 10^{-2} design point will be the most likely combination of H_s , T_p , W and X as failure takes place and corresponds to a sea state with exceedance probability larger than 10^{-2} , but in combination with a rather rare short term realization of the response quantity. It follows that an increasingly important short term variability of the response will increase the exceedance probability of the weather characteristic, Haver and Winterstein (2008). In this case the ULS response occurs in combination with $H_s = 16.8m$, $T_p = 18.2s$ and $W = 30.5m/s$, and is referred to as the design point. In the (U_1, U_2, U_3) -space, this design point is located on a sphere with radius $\beta = 4.43$, which approximately corresponds to the 72-year environmental contour surface. The ALS design point is $H_s = 20.8m$, $T_p = 19.9s$ and $W = 34.9m/s$. Similarly, this sea state is located on a sphere in (U_1, U_2, U_3) -space with radius $\beta = 5.19$ and corresponds to the $3.3 \cdot 10^3$ -year environmental contour surface.

Chapter 7

Traditional approach in estimating characteristic responses

In design of semi submersibles, the original design conditions assumed to give a conservative estimate of the 100-year, i.e. ULS, response is taken as the most probable largest response during a storm with 100-year wind speed and 100-year waves. Similarly, the 10,000-year design loads is taken as the most probable largest response in a sea state modeled with 100-year wind speed and 10,000-year waves, if waves are the most important weather characteristics. Otherwise, the ALS response will be taken as the most probable largest response during a storm with 10,000-year wind speed and 100-year waves. Directional variability of wind and waves is neglected together with current forces since the results shall be comparable with the q-probability responses from the long term analyses. The effect of line failure will not be considered even though it is an important design criterion.

The joint model for wind and waves created in Chapter 6 is used to obtain the q-probability contour of the weather characteristics. Hence, the 100-year and 10,000-year wind speed corresponds to 33.6 m/s and 39.3 m/s (see Figure 6.5), respectively. 100 and 10,000-year waves are taken as the worst combination along the contour of H_s and T_p . In this problem, waves are the most important weather characteristic. The characteristic responses are then taken as the most probable largest response during a storm with 100-year wind speed and worst combination of

H_s and T_p along the q-probability contour.

Hence, 50 simulations were performed for some few selected sea states along the ULS and ALS contours of H_s and T_p combined with 100-year wind speed. Hence, 50 absolute maximum responses were used to determine the Gumbel parameters in the distribution of the maximum response for a given sea state. The Gumbel parameters are determined using method of moments. The fit of the Gumbel distribution to the maximum responses is given in Appendix E.1 and E.2. Notice that α_G represent the most probable largest response for the given sea state. The result of the analysis is depicted in Figure 7.1.

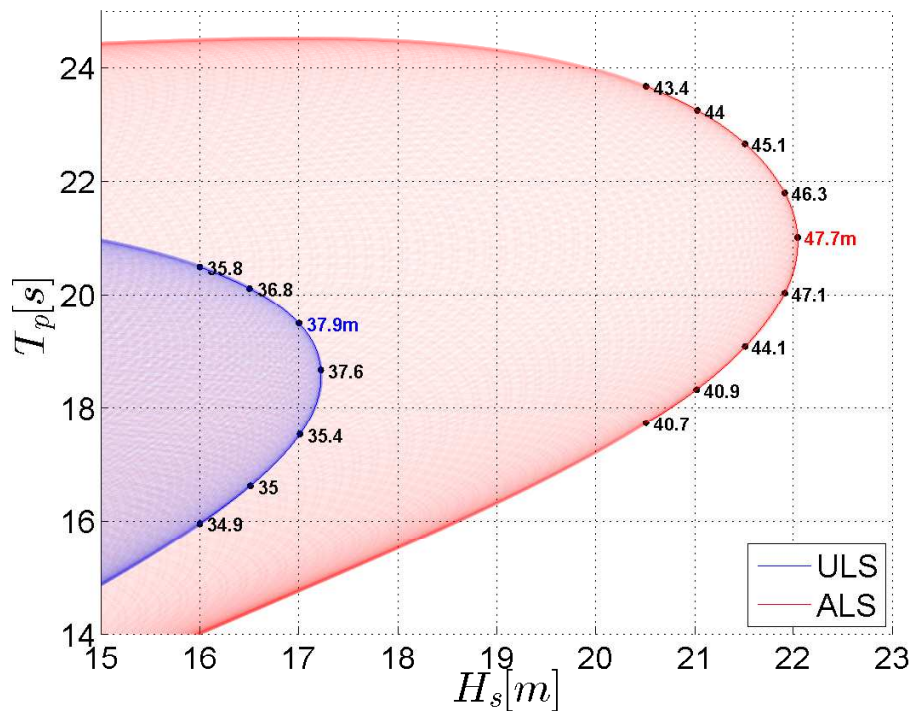


Figure 7.1: Responses along contours combined with 100 year wind speed, i.e. $W = 33.6\text{m/s}$. Simulation points are given as black dots together with its respective most probable largest response.

Figure 7.1 indicates that the ULS offset occurs for a significant wave height smaller than the 100-year H_s . The ULS offset is 37.9m and occurs in combination $H_s = 17.0\text{m}$ and $T_p = 19.5\text{s}$. The ALS offset is 47.7m in a storm modeled with $H_s = 22.0\text{m}$ and $T_p = 21.0\text{s}$ and 100-year wind.

It should be mentioned that the most probable largest response during a storm with 10,000-

year wind speed, i.e. $W_{10^{-4}y} = 39.3m/s$, and 10^{-2} year waves, i.e. $H_s = 17.0m$ and $T_p = 19.5s$, is found to be 41.4m. This is considerably smaller than the most probable largest response during a storm with 10^{-4} year waves and 10^{-2} year wind. The fitted Gumbel distribution to maximum responses in this sea state is given in Appendix E.3.

Chapter 8

Comparing characteristic responses from POT, all sea states and traditional design conditions

The characteristic responses predicted by the POT method, all sea states approach and the original design conditions are listed in Table 8.1.

Table 8.1: Comparing characteristic responses by the three methods

	100-year [m]	10,000-year [m]
POT (threshold, $H_s = 9m$)	34.9	44.0
All sea states	36.7	52.1
Original design conditions	37.9	47.7

Recommended practice is that design conditions are conservative compared to the ‘true’ q-probability responses. The design conditions overestimate the ULS and ALS responses resulting from the POT analysis with about 8-9%. The ULS response predicted by design conditions is close to the 100-year response obtained from the all sea states approach, but under-predicts the

10,000-year response. This last observation is in line with the findings in Meling et al. (2000). Meling et al. (2000) estimated q-probability line tensions by original design conditions and all sea states approach. He found that the ULS line tension was approximately the same for the two methods, but the ALS line tension predicted by design conditions was less conservative than predicted by the all sea states approach.

The all sea states approach is expected to yield more conservative longterm responses than the POT method since it neglects correlation between successive sea states. This is also the case for the present study. The all sea states 100 and 10,000-year response are respectively 5% and 18% larger than the longterm responses resulting from the POT analysis. Keep in mind that the ULS responses obtained from the POT and all sea states approach are consistent since the same set of response surfaces are used for both long term analyses, while the ALS responses were calculated with two different sets of response surfaces.

In the present study, all environmental forces are conservatively assumed to act in surge direction, but directional variability of environmental forces can easily be included in the POT analysis. It is possible to model each storm step as it appears in the hindcast data, i.e. let each environmental parameter act in its actual direction. This would be more computational demanding than herein since each storm step would be calculated as it appears, without using response surfaces. For the present problem, there are e.g. 778 unique storm steps for threshold $H_s = 9m$. It follows that $40 \cdot 778 = 31120$ time domain simulations are required to identify the distribution of maximum response for each storm step.

The all sea states approach is less flexible in introducing directional variability, and it is often limited by the amount of hindcast data available. If directional variability is to be included, a possible approach is to divide the hindcast data into sectors and obtain the joint distribution of H_s , T_p and W within each sector. The probability that wind and waves acts in a given direction, i.e. occurs in one specific sector, is then given by the number of observations in this sector divided by the number of total observations, Bitner-Gregersen and Haver (1991). Such an approach assumes that wind and waves are collinear. This assumption is questionable for low and moderate sea, but can be reasonable in storm sea Haver (2013).

Chapter 9

Conclusion

The motivation for the present work was to compare characteristic responses resulting from a peak over threshold analysis with the more conventional all sea states approach and design conditions. The all sea states approach neglects correlation between successive sea states and are therefore expected to be more conservative than the POT method. This study demonstrates that the POT method is less conservative than the all sea states approach, at least for the present problem.

Original design conditions were expected to give conservative estimates of the characteristic responses compared to the POT method and all sea states approach. Design conditions give almost the same ULS response than the all sea states approach, but are conservative compared to the POT analysis. Further, the ALS response resulting from original design conditions are conservative compared to the POT method and non-conservative compared to the all sea states approach.

The estimates of q-probability responses calculated herein are conservative since all forces are assumed to act in the same direction. Neglecting current is a non-conservative assumption, and should be included in similar studies.

The practical implication of less conservative q-probability responses obtained from the POT analysis is a more optimized design of offshore structures without compromising the safety aspect.

Chapter 10

Further Work

Current forces and directional variability of environmental forces

Current forces and directional variability of the environment should be included in the analysis to provide a better representation of a real ocean climate. Here, current forces were non-conservatively neglected and directional variability of the environment was conservatively assumed to act in surge direction.

One of the advantages of the POT method is that it is easy to include more variables in the analysis than for the all sea states approach. It is of interest to see the impact of directional variability of waves and wind on 100-year and 10,000-year responses. The impact of current is also important, especially since neglecting current is a non-conservative assumption.

Correction of T_p in the hindcast data

The T_p values in the hindcast data for Haltenbanken are given with discrete logarithmic spacing. This is not a correct representation of the true spectral peak periods. Therefore, a dataset of ‘observed’ T_p was generated according to the procedure outlined in Haver (2015b). These corrected hindcast data are used in the longterm analysis. If another sample of ‘observed’ T_p values in the hindcast data is generated, it is expected that the results from the longterm analysis will

change (probably only with some few percent). It would, however, be advantageous to study the effect of generating a new sample of T_p on the overall longterm results.

β_G response surfaces

A challenging part of this study was to obtain reasonable β_G response surfaces, and it was convenient to assume that β_G is independent of the wind speed. The accuracy of this approximation should be further validated for this response case.

α_G response surfaces

α_G for any sea state within the sample space is found by bi-harmonic interpolation between H_s and T_p together with linear interpolation between discrete W values. Instead of using this combination of 2D spline for $H_s - T_p$ combinations and linear interpolation between sampled W values, it would be advantageous to use some kind of spline interpolation in 3D. It might improve the accuracy of the interpolation.

Storm as sequence of stationary sea states with smaller duration

The distribution of the maximum response of a storm is obtained by modeling each storm as a sequence of 3-hour stationary sea states. A more accurate representation of the storm may be obtained by describing the storm as a sequence of stationary sea states with a smaller duration. It is especially important to model the storm peak with reasonable accuracy since the most probable response occurs at the storm peak and the maximum response usually occurs in vicinity of the storm peak, Haver (2013). Of course, this is only possible if such hindcast data exists.

Correlated storms

Let each storm be modeled as a sequence of consecutive stationary sea states above the selected threshold. In the hindcast data for Haltenbanken, there are 446 such storms for threshold $H_s = 8m$. Some of these storms have two storm peaks that can result in two counted storms when it should have been counted as one. This results in some correlated storms in the sample of 446 observed storms. In this thesis, the storms are defined as correlated if the second storm begins within a 24-hour time window after the first storm ended. Such correlated storms are merged to one independent storm event. This results in 398 observed storms with threshold $H_s = 8m$.

The number of independent storm events is further reduced to 360 if the time window between correlated storms is increased to 48 hours. This might indicate that the selected criteria for correlated storms in this thesis needs further investigation. An alternative approach, as suggested by Tromans and Vandersohuren (1995), is to consider the through in H_s between two storms. If this through is less than 80% of the lowest peak, the storms are broken at the through to form two independent events.

Consistency in the response surfaces

Two sets of response surfaces were used in this project. One set of response surfaces was used for the POT analysis (to calculate ULS and ALS response). To preserve consistency in the results, this set of response surfaces was also used to calculate the ULS response in the all sea states analysis. However, later it became evident that the all sea states ALS design point lies outside the response surfaces used in the POT analysis and another set of response surfaces was therefore required.

If a similar study is conducted in the future, it is advisable to operate with one set of response surfaces that captures both observed and non-observed sea states with a reasonable margin.

Bibliography

(2003). *MOMISA - User's Documentation Program Version 5.7*.

(2007). N-003, Norsok, Action and action effects.

(2010). DNV-RP-F205, Global Performance Analysis of Deepwater Floating Structures.

(2013). *SIMO Theory Manual Version 4.0 rev. 3*.

(2014). DNV-RP-C205, Environmental conditions and environmental loads.

Battjes, J. A. (1972). Long-term wave height distributions at seven stations around the british isles. *Deutsche Hydrografische Zeitschrift*, 25(4):179–189.

Bitner-Gregersen, E. M. and Haver, S. (1991). Joint environmental model for reliability calculations. In *Proceedings of the First (1991) International Offshore and Polar Engineering Conference (ISOPE)*.

Coles, S. (2001). *An Introduction to Statistical Modeling of Extreme Values*. Springer.

Faltinsen, O. M. (1990). *Sea loads on ships and offshore structures*. Cambridge ocean technology series. Cambridge University Press, Cambridge.

Faltinsen, O. M. and Løken, A. E. (1980). Slow drift oscillations of ship in irregular waves. *Modeling, Identification and Control*, Vol. 1, No 4,:195–213.

Greco, M. (2012). Lecture Notes: TMR4215, Sea Loads. *Dept. of Marine Hydrodynamics*.

Haring, R. E., . H. J. C. (1978). Gulf of mexico rare wave return periods. In *Offshore Technology Conference. doi:10.4043/3230-MS*.

- Haug, O. and Guddal, J. (1981). Hindcasting the wind and wave climate of norwegian waters. *Det Norske Meteorologiske Institutt, Norwegian Meteorological Institute.*
- Haver, S. (2004). On the prediction of extreme wave crests heights. *University of Stavanger.*
- Haver, S. (2013). *Prediction of Characteristic Response for Design Purposes (PRELIMINARY VERSION).* Statoil.
- Haver, S. (2015b). *Lecture Note Draft 3 October 2015.* UiS.
- Haver, S. (2016). Private communication.
- Haver, S. (October, 2015a). Description of metocean characteristics for planning of marine operations. *Lecture Notes, UiS.*
- Haver, S. and Winterstein, S. R. (2008). Environmental contour lines: A method for estimating long term extremes by a short term analysis. In *Transactions - Society of Naval Architects and Marine Engineers.*
- Jahns, H. and Wheeler, J. (1973). Long-term wave probabilities based on hindcasting of severe storms. *JPT, Journal of Petroleum Technology*, 25:473–486.
- Johannessen, K., Meling, T., and Haver, S. (2002). Joint distribution for wind and waves in the northern north sea. *Statoil.*
- Larsen, K. (2015). *Mooring and station keeping of floating structures, part 2 of 2, Lecture Notes.* NTNU.
- Larsen, K. (2016). Private communication.
- Madsen, H. O., Krenk, S., and Lind, N. C. (1986). *Methods of structural safety.* Prentice-Hall international series in civil engineering and engineering mechanics. Prentice-Hall, Englewood Cliffs, NJ.
- Meling, T., Johannessen, K., Haver, S., and Larsen, K. (2000). Mooring analysis of semi-submersible by use of IFORM and contour surfaces. *Proceedings of ETCE/OMAE2000 Joint Conference.*

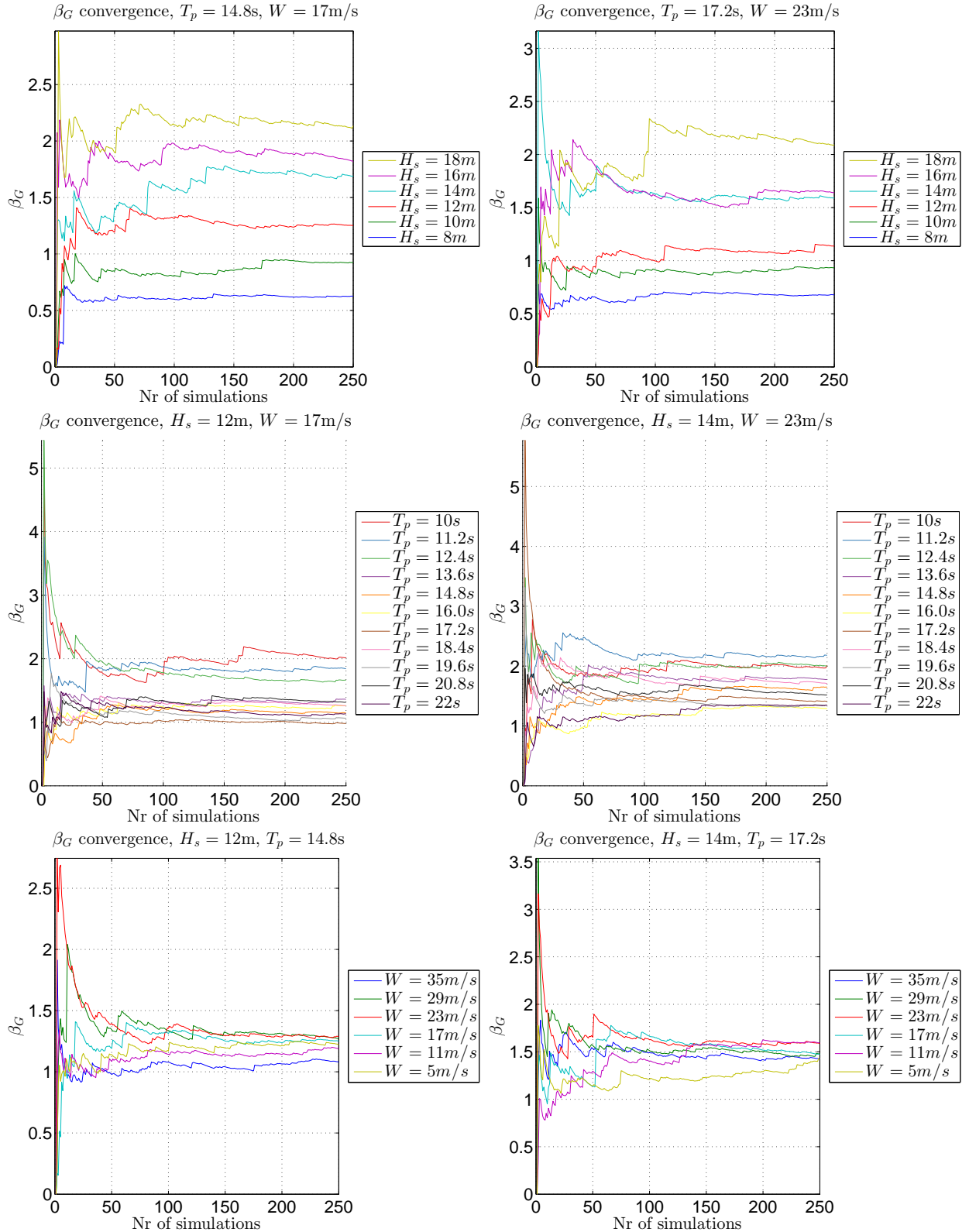
- Morgan, E. C., Lackner, M., Vogel, R. M., and Baise, L. G. (2011). Probability distributions for offshore wind speeds. *Energy Conversion and Management*, 52(1):15–26.
- Myrhaug, D. (2009). *Marin Dynamics TMR4182*. Akademika Forlag.
- Newman, J. N. (1974). Second-order, slowly-varying forces on vessels in irregular waves. *International Symposium on the Dynamics of Marine Vehicles and Structures in Waves*.
- Newman, J. N. (1977). *Marine Hydrodynamics*. MIT Press.
- Nordenstrøm, N. (1971). *Part 1 : environmental conditions and short term response*, volume 71-2-S of *Methods for predicting long term distributions of wave loads and probability of failure for ships*. Det norske Veritas, Oslo.
- Sandwell, D. T. (1987). Biharmonic spline interpolation of geos-3 and seasat altimeter data. *Geophysical Research Letters*.
- Tromans, P. S. and Vandersohuren, L. (1995). Response based design conditions in the north sea: Application of a new method. In *Offshore Technology Conference*. doi:10.4043/7683-MS.
- WolframMathWorld (2016). <http://mathworld.wolfram.com/hypersphere.html>, accessed 09.06.2016.

Appendices

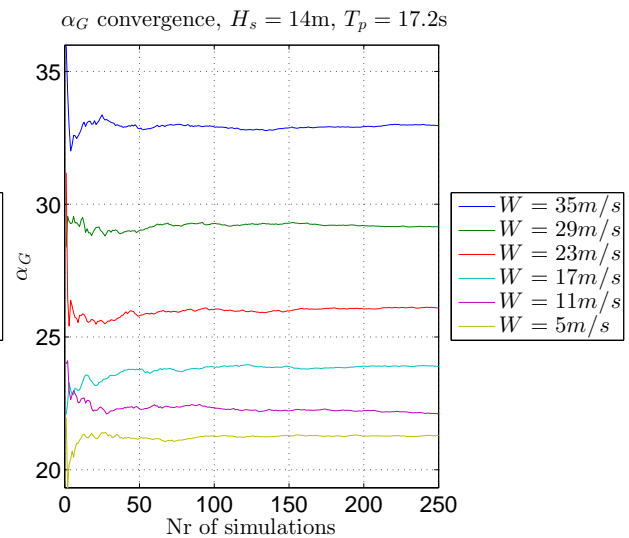
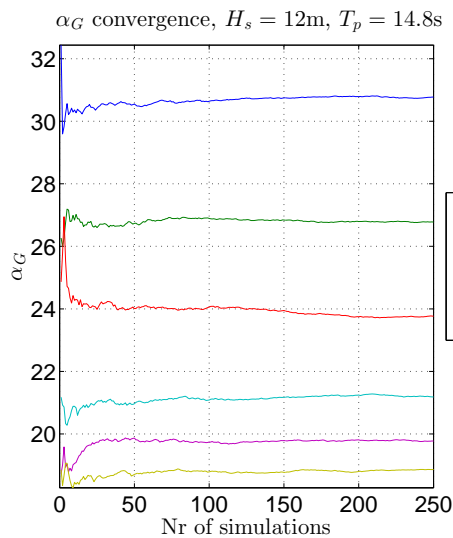
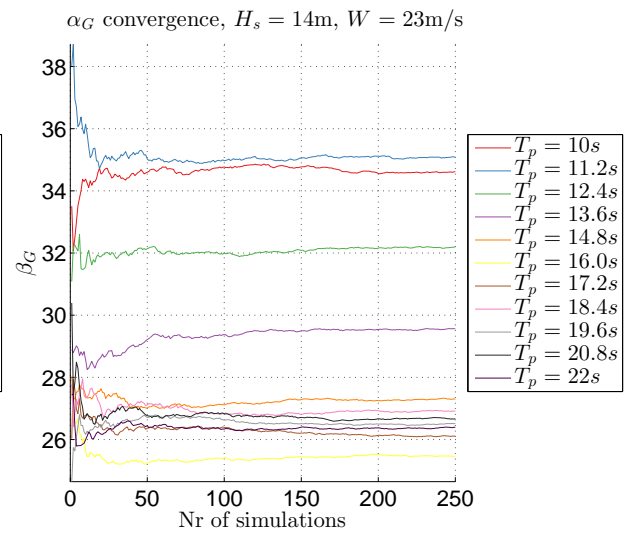
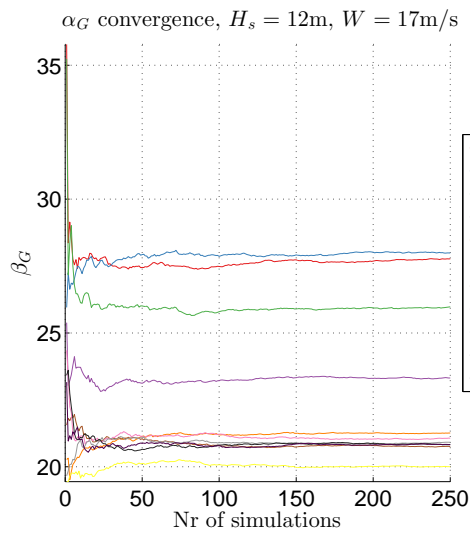
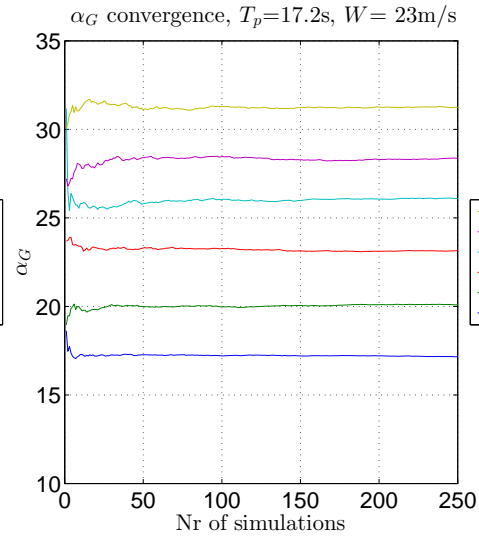
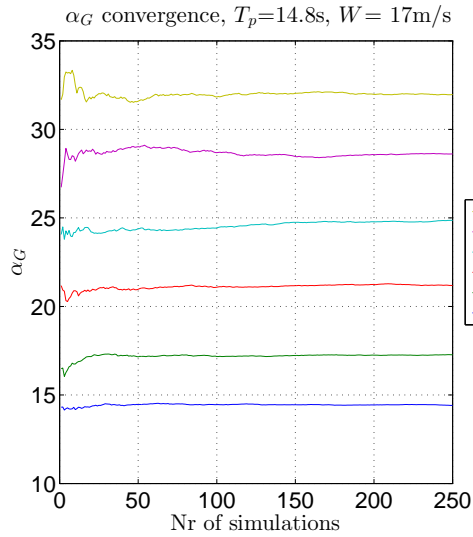
Appendix A

Response surfaces for the POT analysis

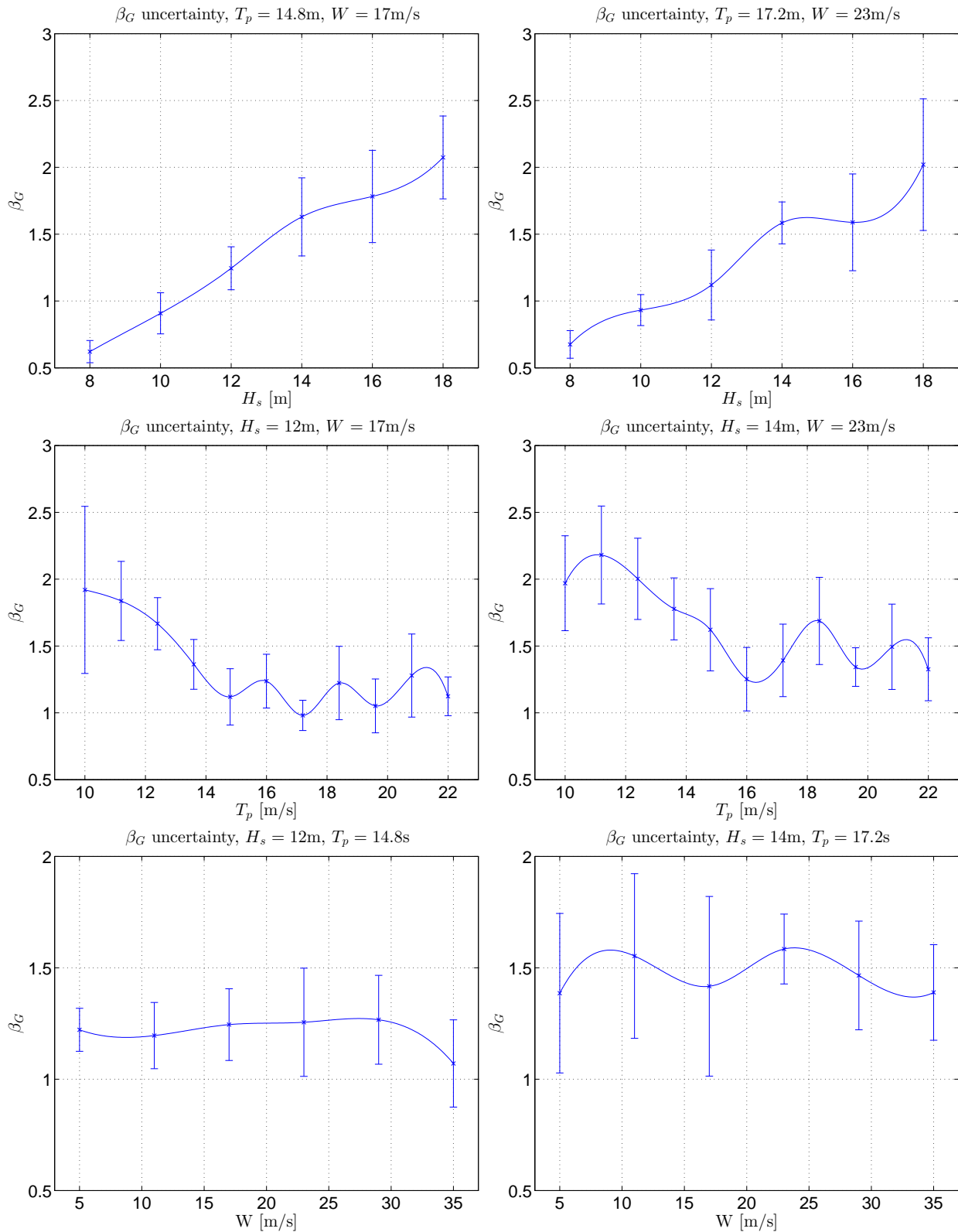
A.1 β_G convergence



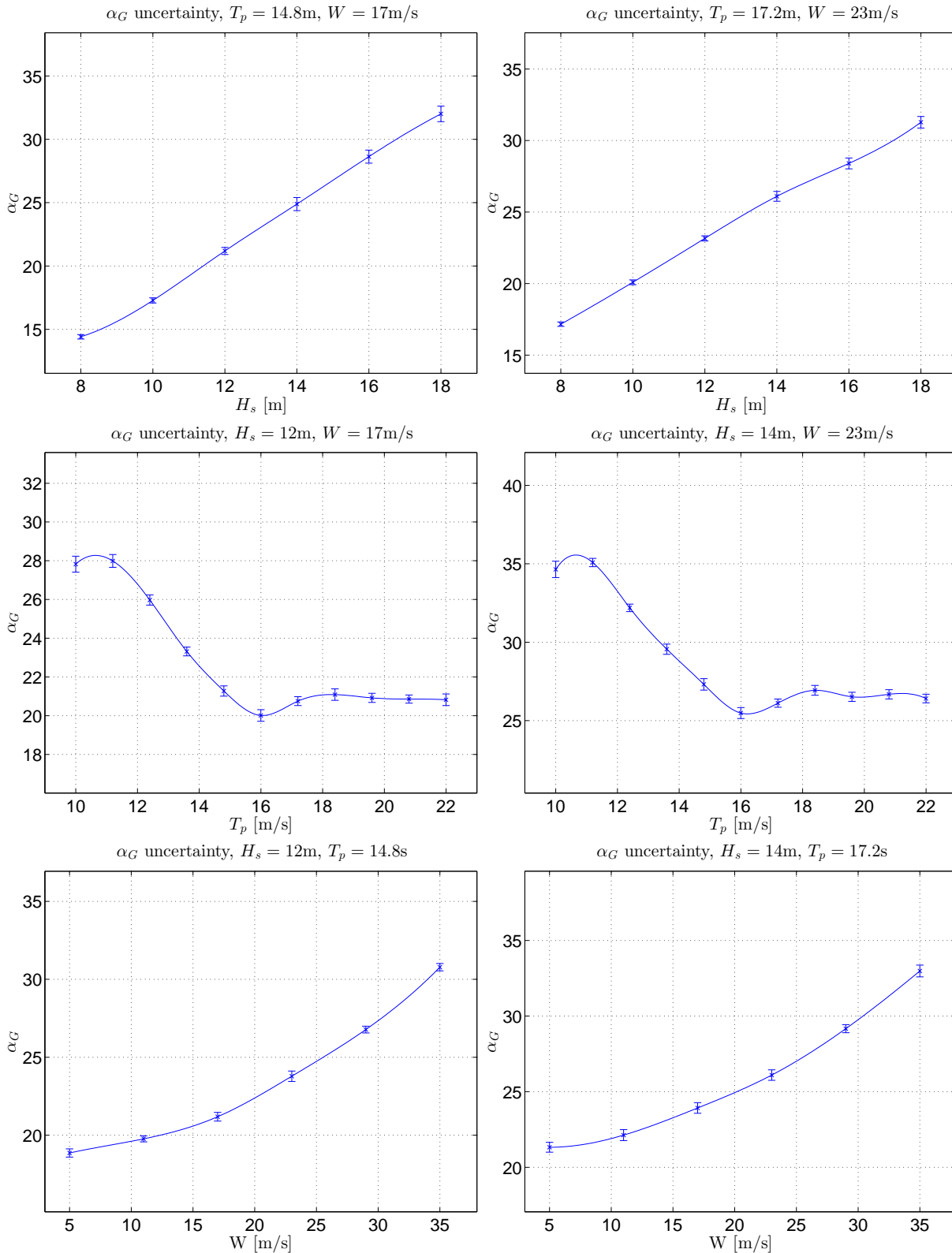
A.2 α_G convergence



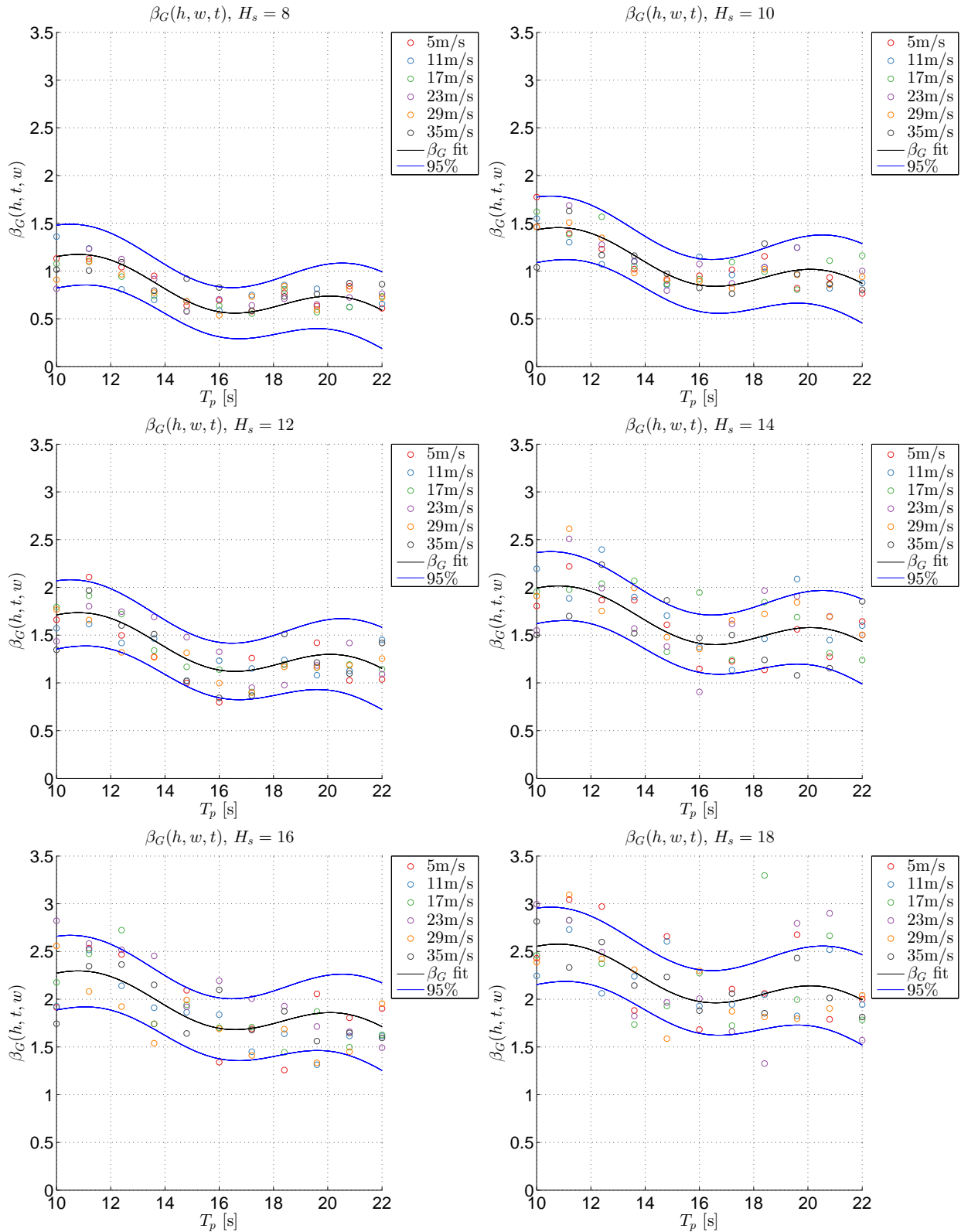
A.3 β_G dependency on H_s , T_p and W



A.4 α_G dependency on H_s , T_p and W

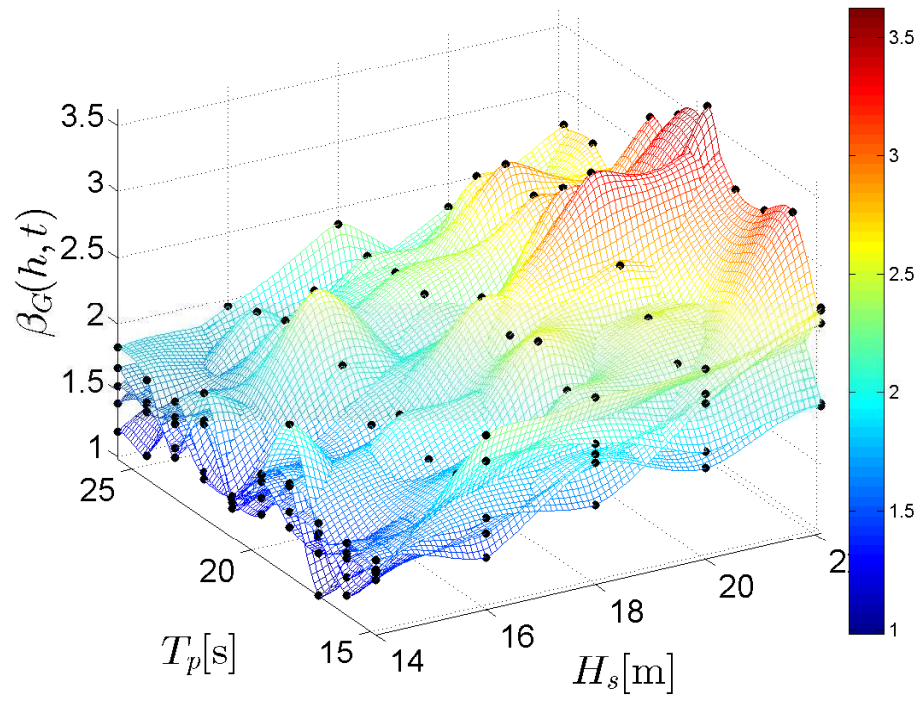


A.5 $\beta_G(h, t, w)$ fit to empirical data

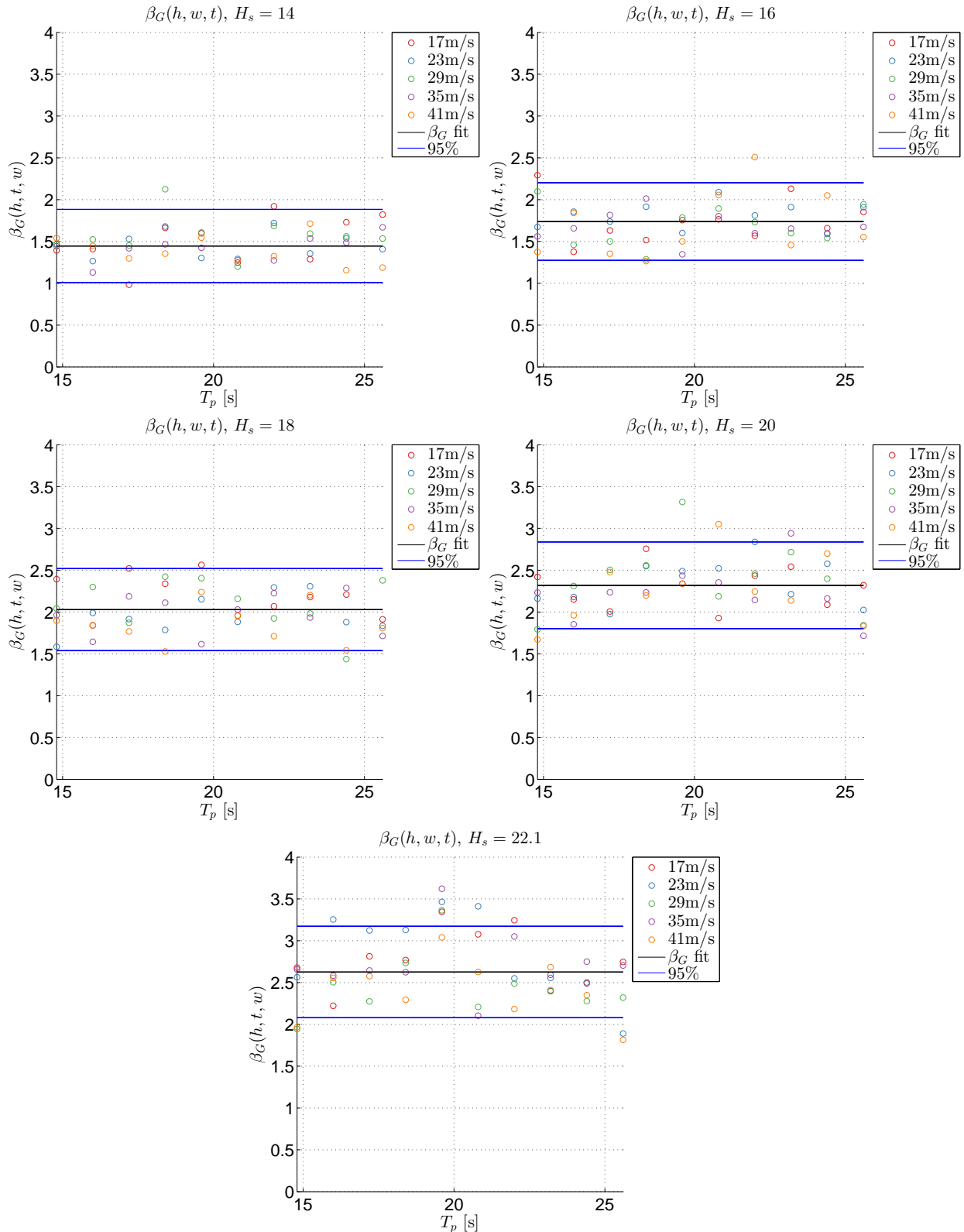


Appendix B

Additional response surfaces for the all sea states analysis

B.1 $\beta_G(h, t)$ response surfaces for different W values

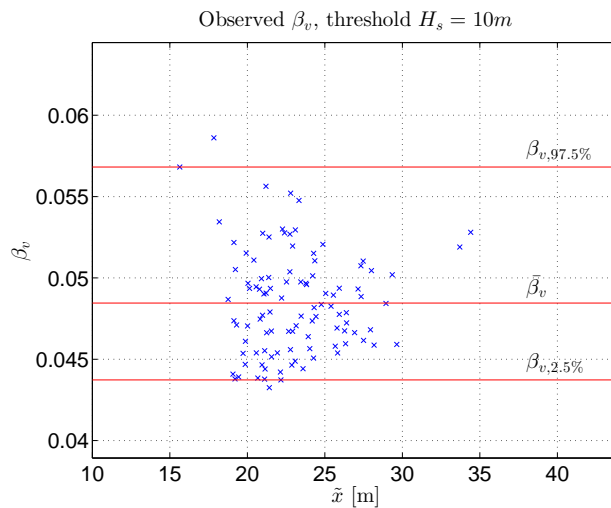
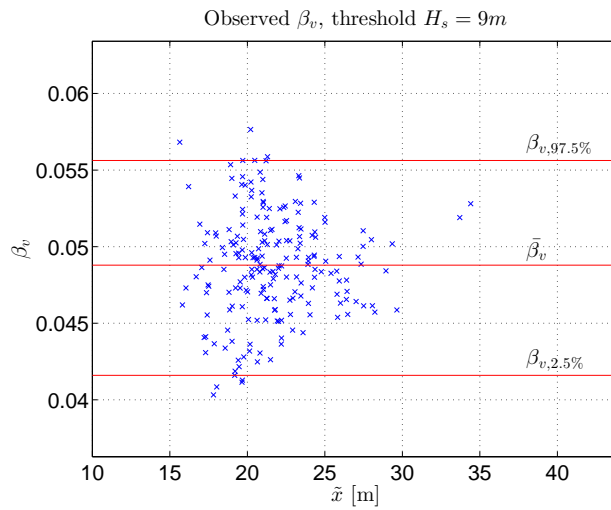
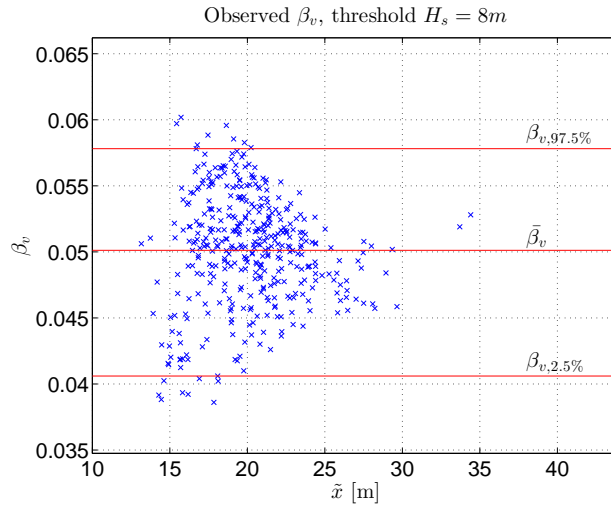
B.2 $\beta_G(h, t, w)$ fit to empirical data



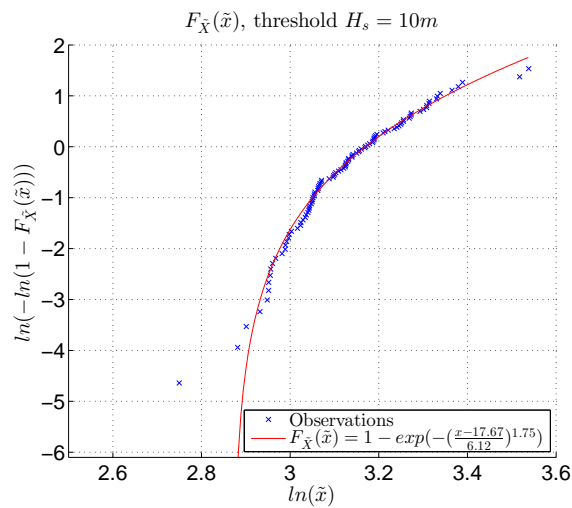
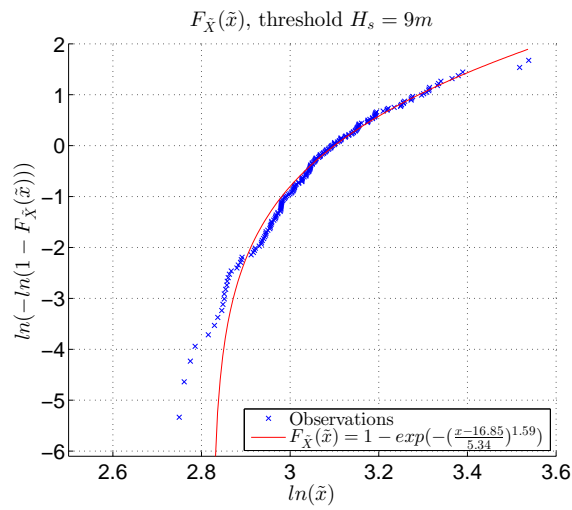
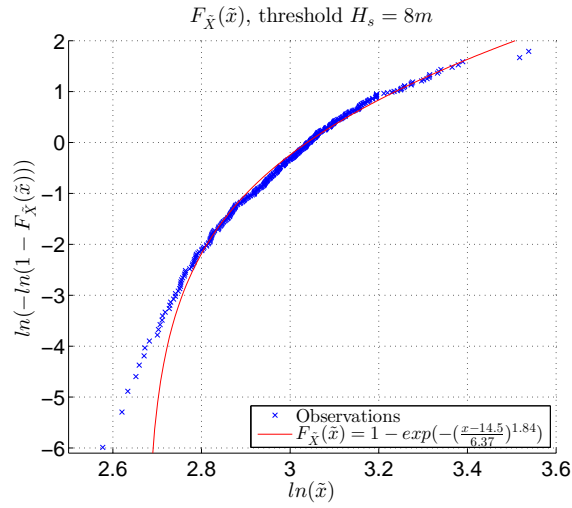
Appendix C

Peak Over Threshold

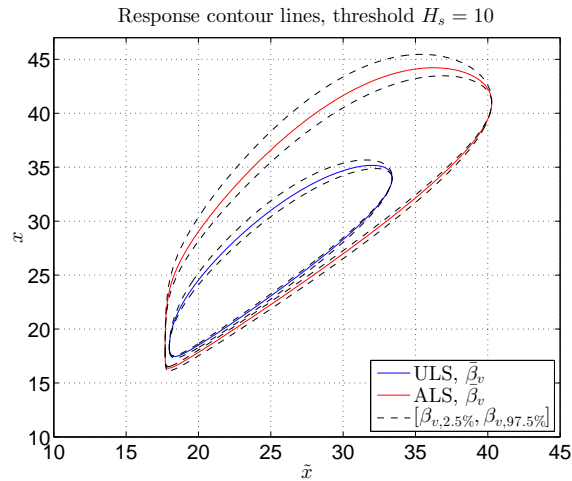
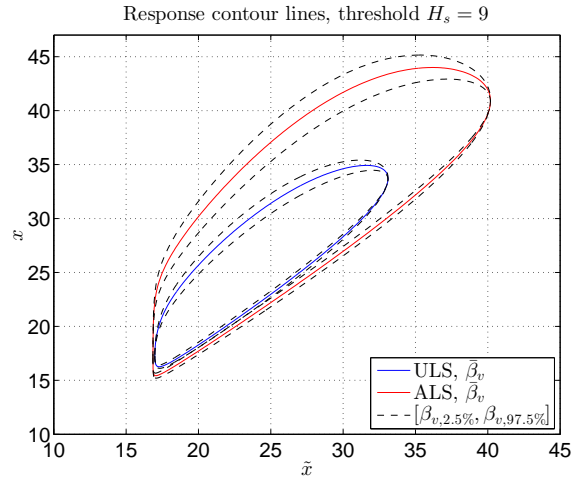
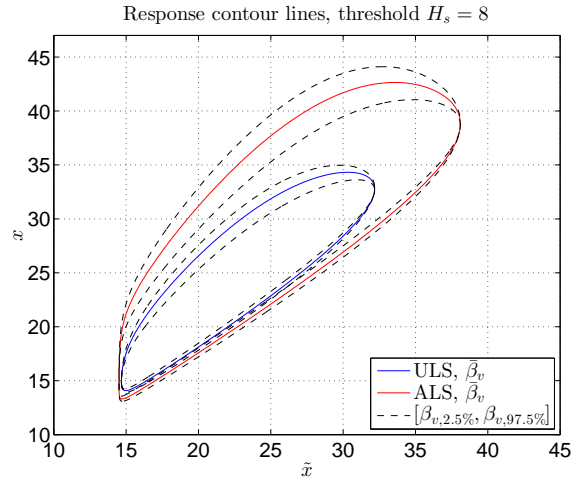
C.1 β_v for different thresholds



C.2 $F_{\tilde{X}}(\tilde{x})$ for different thresholds



C.3 Response contour lines for different threshold



Appendix D

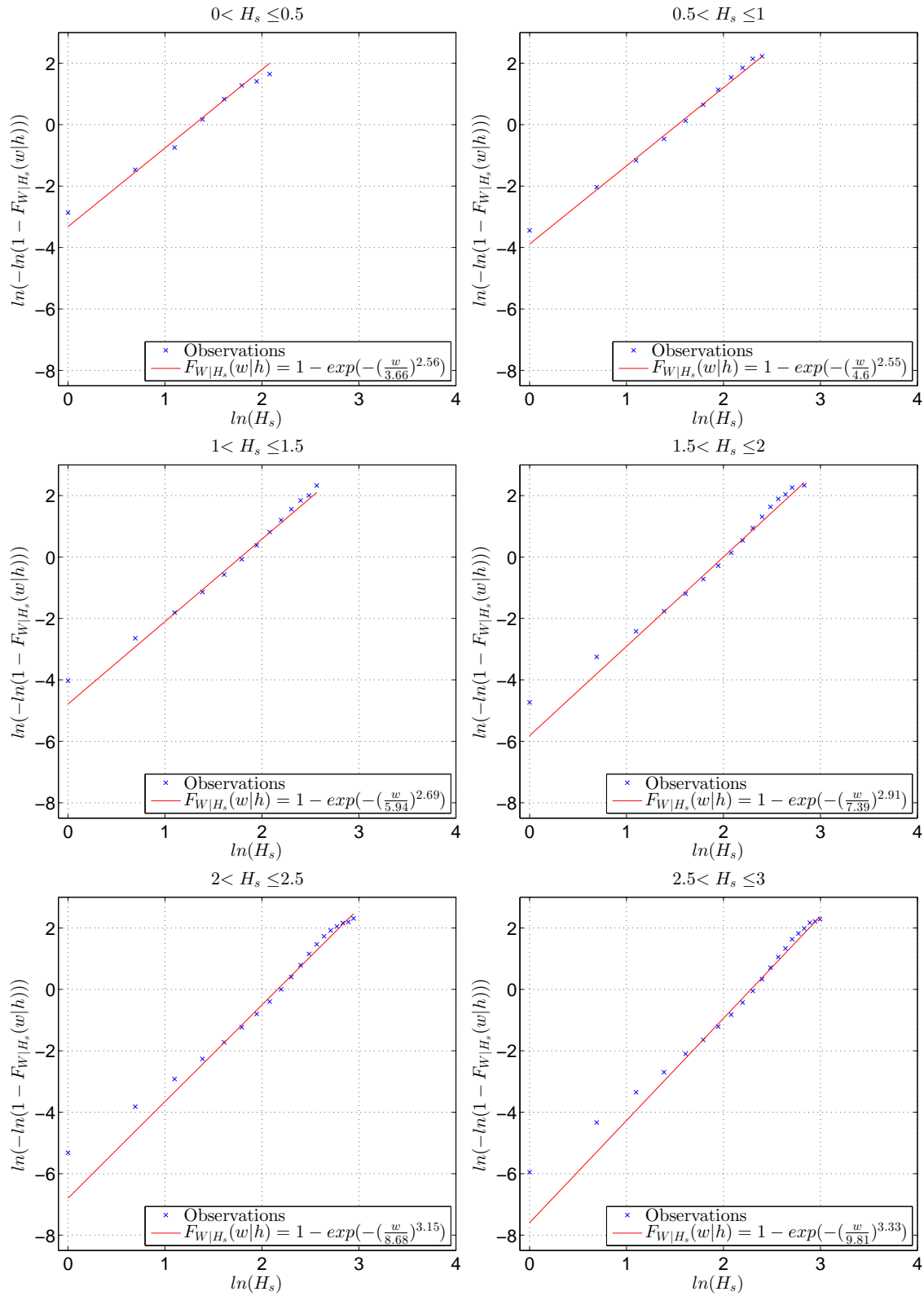
All sea states approach

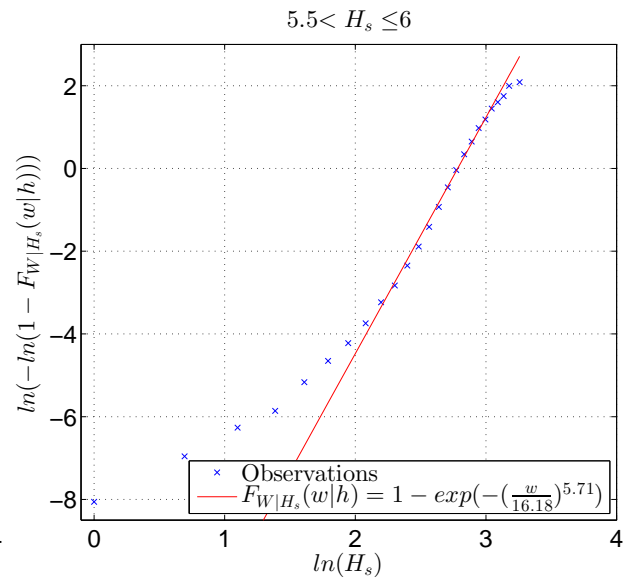
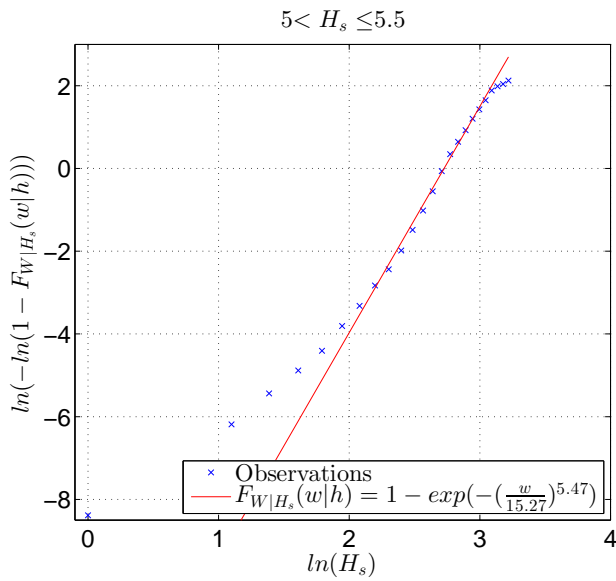
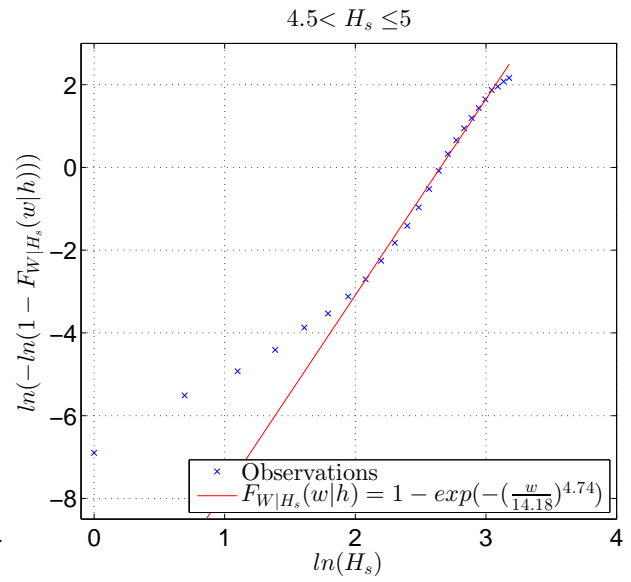
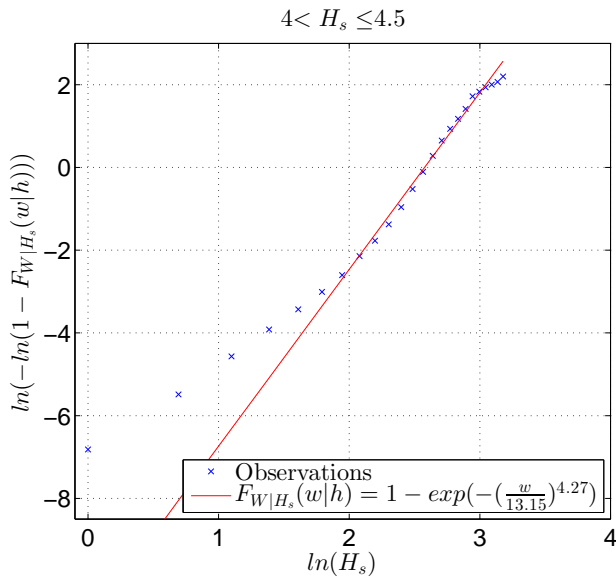
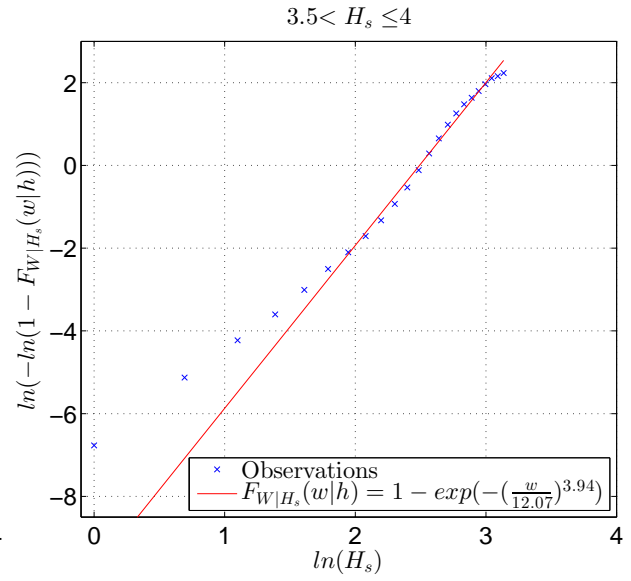
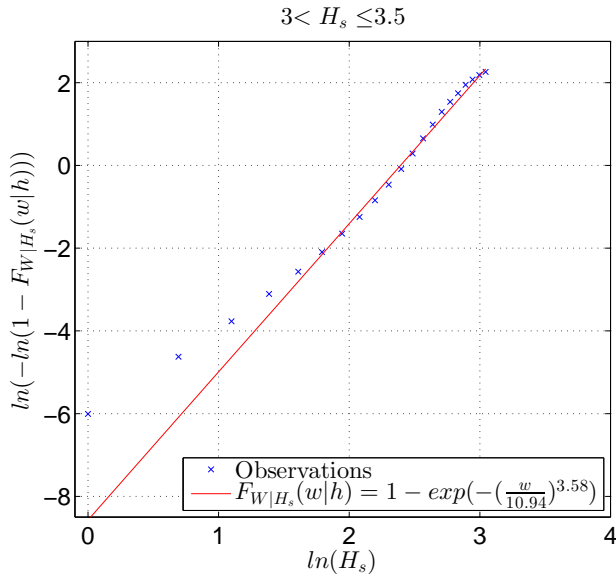
D.1 Scatter diagram

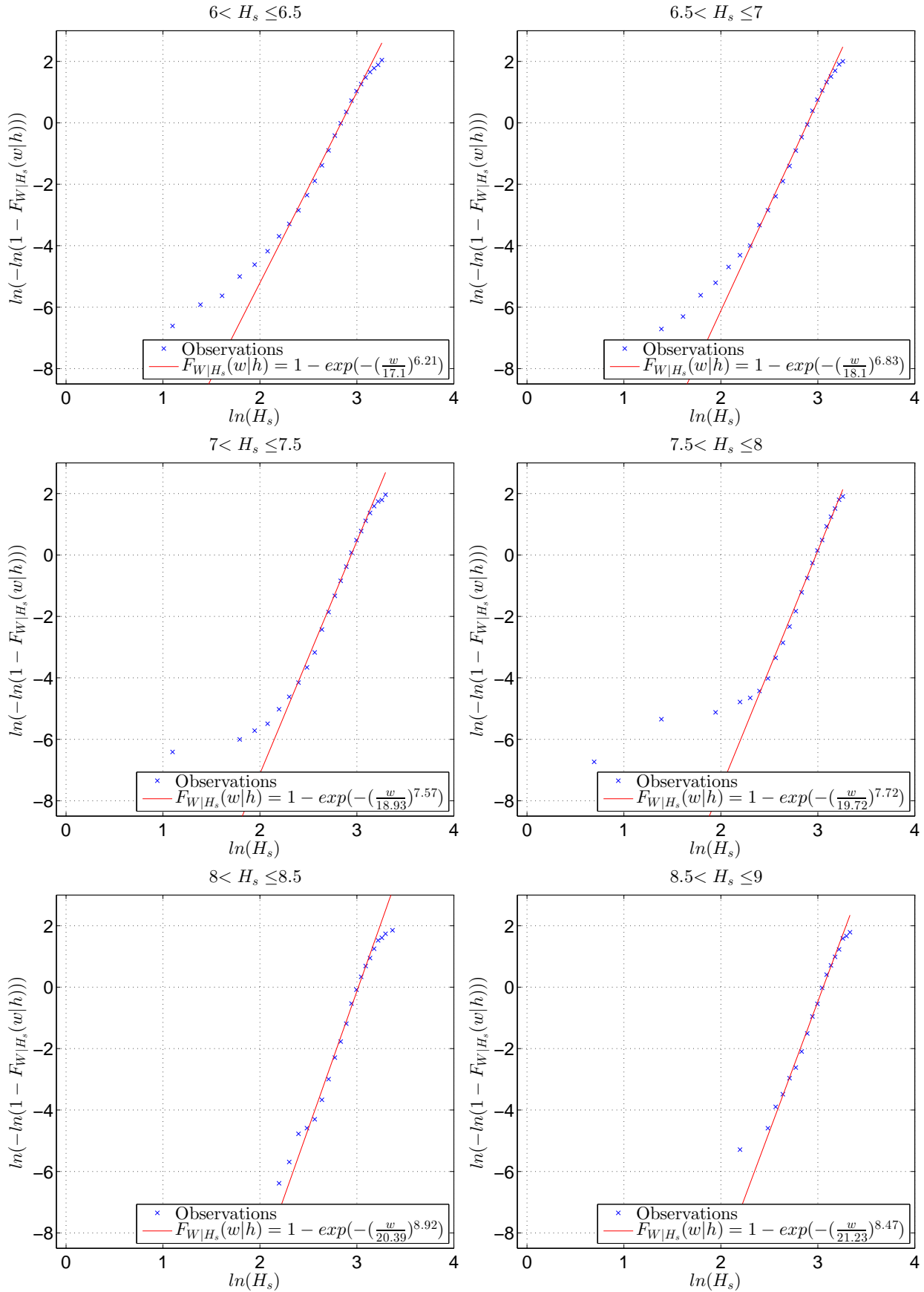
		0<W≤1.0																	Sum															
Hs\W	1	2	3	4	5	6	7	8	9	10	11	12	13	14	15	16	17	18	19	20	21	22	23	24	25	26	27	28	29	30	31	Sum		
0.5	10	27	31	57	37	13	2	2	0	0	0	0	0	0	0	0	0	0	0	0	0	0	0	0	0	0	0	0	0	0	0	179		
1.0	329	953	1525	2087	2202	1827	1076	362	82	16	1	0	0	0	0	0	0	0	0	0	0	0	0	0	0	0	0	0	0	0	0	10460		
1.5	500	1439	2328	3477	4426	4896	4647	3585	1949	766	194	34	16	0	0	0	0	0	0	0	0	0	0	0	0	0	0	0	0	0	0	28257		
2.0	257	857	1388	2128	3033	3668	4204	4466	4048	3035	1531	547	136	25	12	0	1	0	0	0	0	0	0	0	0	0	0	0	0	0	0	29336		
2.5	115	397	728	1084	1534	2105	2578	2996	3380	3400	2648	1625	677	225	59	16	6	1	2	0	0	0	0	0	0	0	0	0	0	0	0	23576		
3.0	49	196	406	579	946	1144	1537	1846	2328	2535	2615	2203	1404	651	309	75	26	10	1	1	0	0	0	0	0	0	0	0	0	0	0	18861		
3.5	36	107	191	307	440	616	865	1100	1459	1707	1962	2002	1702	1145	619	240	92	35	8	3	1	0	0	0	0	0	0	0	0	0	0	14637		
4.0	13	54	97	141	241	345	415	570	764	1057	1337	1658	1652	1328	877	442	195	75	40	18	6	1	1	0	0	0	0	0	0	0	0	0	11327	
4.5	9	25	51	77	100	134	191	323	378	547	780	1067	1198	1162	976	563	324	189	103	15	8	3	2	2	2	0	0	0	0	0	0	0	8227	
5.0	6	18	35	51	68	91	129	207	295	405	593	782	918	884	622	410	235	130	56	24	4	3	1	0	0	0	0	0	0	0	0	0	5955	
5.5	1	8	15	22	30	40	54	73	96	115	157	204	244	288	338	396	454	514	579	650	728	813	904	999	1099	1199	1299	1399	1499	1599	1699	1799	4374	
6.0	1	2	3	3	3	3	3	3	3	3	3	3	3	3	3	3	3	3	3	3	3	3	3	3	3	3	3	3	3	3	3	3	3158	
6.5	0	0	0	0	0	0	0	0	0	0	0	0	0	0	0	0	0	0	0	0	0	0	0	0	0	0	0	0	0	0	0	0	0	2237
7.0	0	0	0	0	0	0	0	0	0	0	0	0	0	0	0	0	0	0	0	0	0	0	0	0	0	0	0	0	0	0	0	0	0	1645
7.5	0	0	0	0	0	0	0	0	0	0	0	0	0	0	0	0	0	0	0	0	0	0	0	0	0	0	0	0	0	0	0	0	0	1217
8.0	0	0	0	0	0	0	0	0	0	0	0	0	0	0	0	0	0	0	0	0	0	0	0	0	0	0	0	0	0	0	0	0	0	840
8.5	0	0	0	0	0	0	0	0	0	0	0	0	0	0	0	0	0	0	0	0	0	0	0	0	0	0	0	0	0	0	0	0	0	593
9.0	0	0	0	0	0	0	0	0	0	0	0	0	0	0	0	0	0	0	0	0	0	0	0	0	0	0	0	0	0	0	0	0	0	396
9.5	0	0	0	0	0	0	0	0	0	0	0	0	0	0	0	0	0	0	0	0	0	0	0	0	0	0	0	0	0	0	0	0	0	281
10.0	0	0	0	0	0	0	0	0	0	0	0	0	0	0	0	0	0	0	0	0	0	0	0	0	0	0	0	0	0	0	0	0	0	193
10.5	0	0	0	0	0	0	0	0	0	0	0	0	0	0	0	0	0	0	0	0	0	0	0	0	0	0	0	0	0	0	0	0	0	122
11.0	0	0	0	0	0	0	0	0	0	0	0	0	0	0	0	0	0	0	0	0	0	0	0	0	0	0	0	0	0	0	0	0	0	68
11.5	0	0	0	0	0	0	0	0	0	0	0	0	0	0	0	0	0	0	0	0	0	0	0	0	0	0	0	0	0	0	0	0	0	44
12.0	0	0	0	0	0	0	0	0	0	0	0	0	0	0	0	0	0	0	0	0	0	0	0	0	0	0	0	0	0	0	0	0	0	27
12.5	0	0	0	0	0	0	0	0	0	0	0	0	0	0	0	0	0	0	0	0	0	0	0	0	0	0	0	0	0	0	0	0	0	12
13.0	0	0	0	0	0	0	0	0	0	0	0	0	0	0	0	0	0	0	0	0	0	0	0	0	0	0	0	0	0	0	0	0	0	10
13.5	0	0	0	0	0	0	0	0	0	0	0	0	0	0	0	0	0	0	0	0	0	0	0	0	0	0	0	0	0	0	0	0	0	8
14.0	0	0	0	0	0	0	0	0	0	0	0	0	0	0	0	0	0	0	0	0	0	0	0	0	0	0	0	0	0	0	0	0	0	3
14.5	0	0	0	0	0	0	0	0	0	0	0	0	0	0	0	0	0	0	0	0	0	0	0	0	0	0	0	0	0	0	0	0	0	2
15.0	0	0	0	0	0	0	0	0	0	0	0	0	0	0	0	0	0	0	0	0	0	0	0	0	0	0	0	0	0	0	0	0	0	0
15.5	0	0	0	0	0	0	0	0	0	0	0	0	0	0	0	0	0	0	0	0	0	0	0	0	0	0	0	0	0	0	0	0	0	0
16.0	0	0	0	0	0	0	0	0	0	0	0	0	0	0	0	0	0	0	0	0	0	0	0	0	0	0	0	0	0	0	0	0	0	0
16.5	0	0	0	0	0	0	0	0	0	0	0	0	0	0	0	0	0	0	0	0	0	0	0	0	0	0	0	0	0	0	0	0	0	0
17.0	0	0	0	0	0	0	0	0	0	0	0	0	0	0	0	0	0	0	0	0	0	0	0	0	0	0	0	0	0	0	0	0	0	0
Sum	1326	4076	6780	9987	13036	14840	15674	15485	14776	13574	11862	10342	8449	6740	5452	3800	2746	2086	1773	1108	796	564	307	217	124	68	36	16	8	2	3	166053		

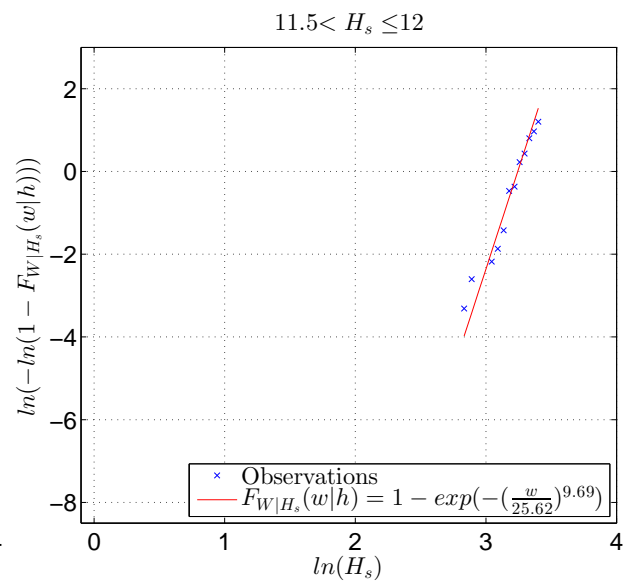
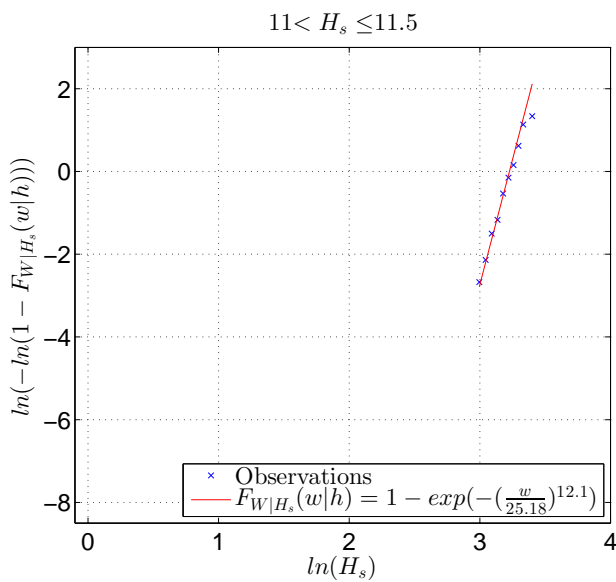
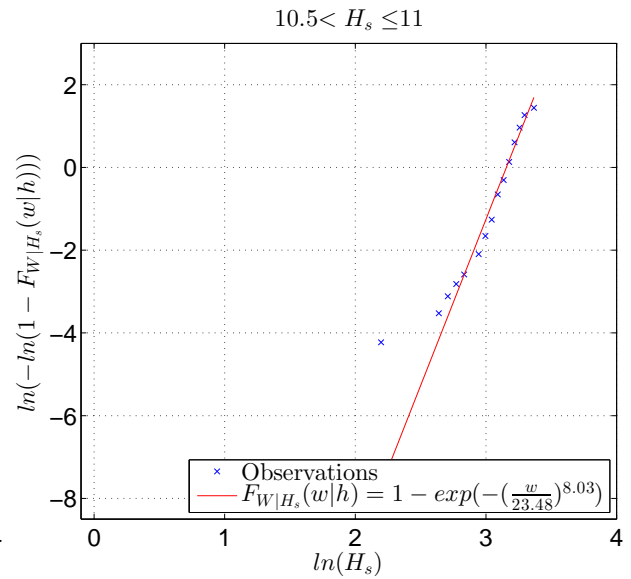
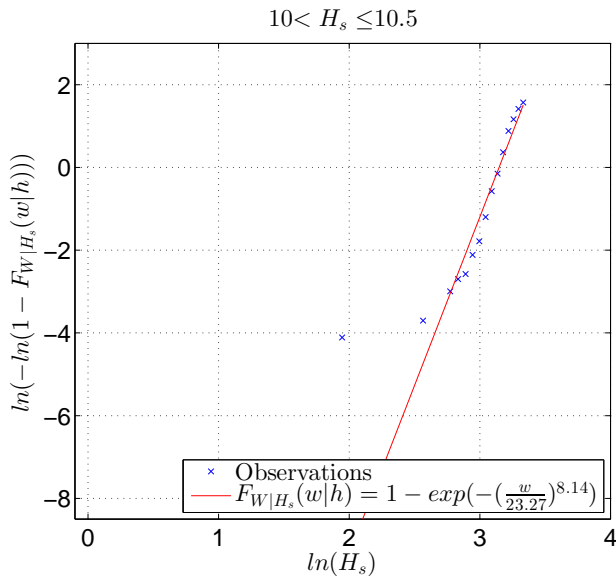
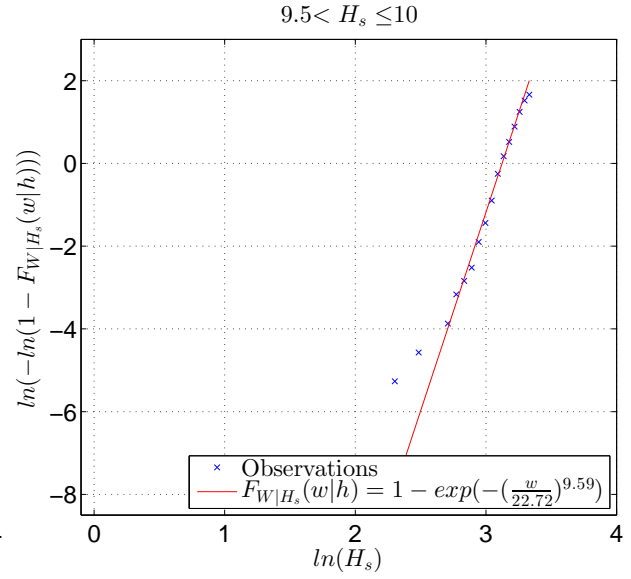
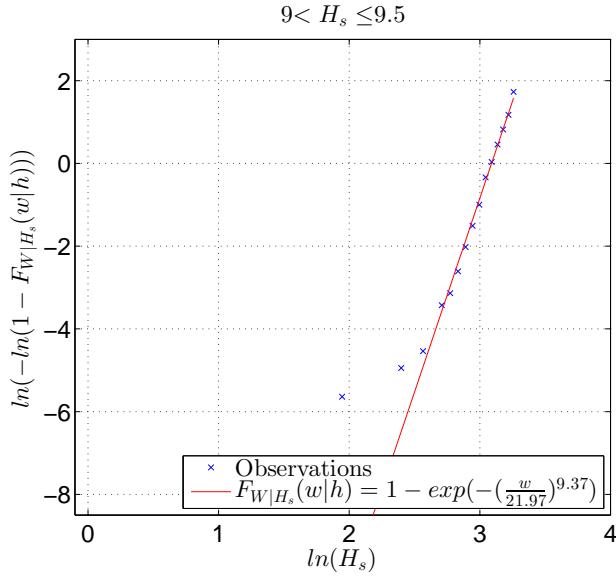
Scatter diagram (Heidrun hindcast 1957-2014)

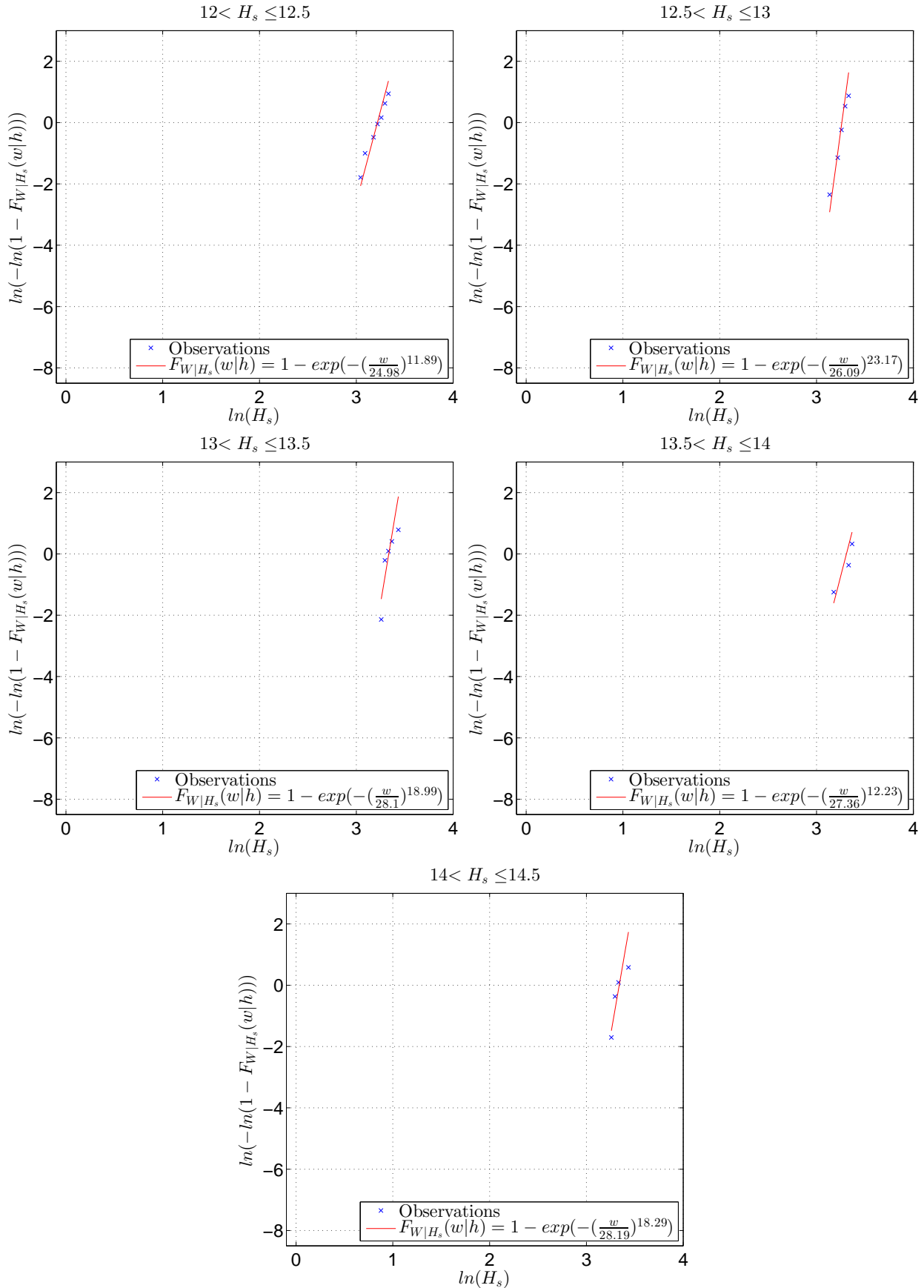
D.2 Conditional distribution of W



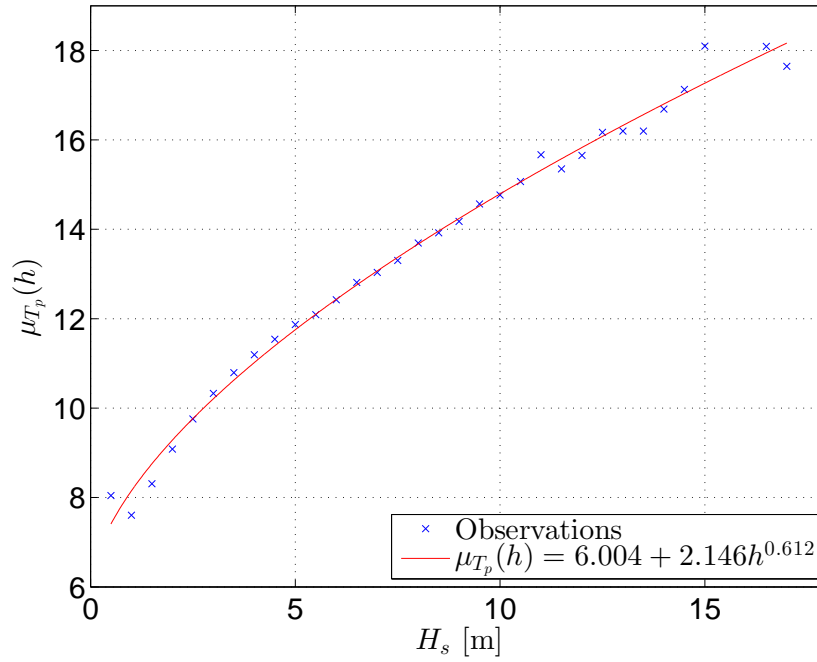




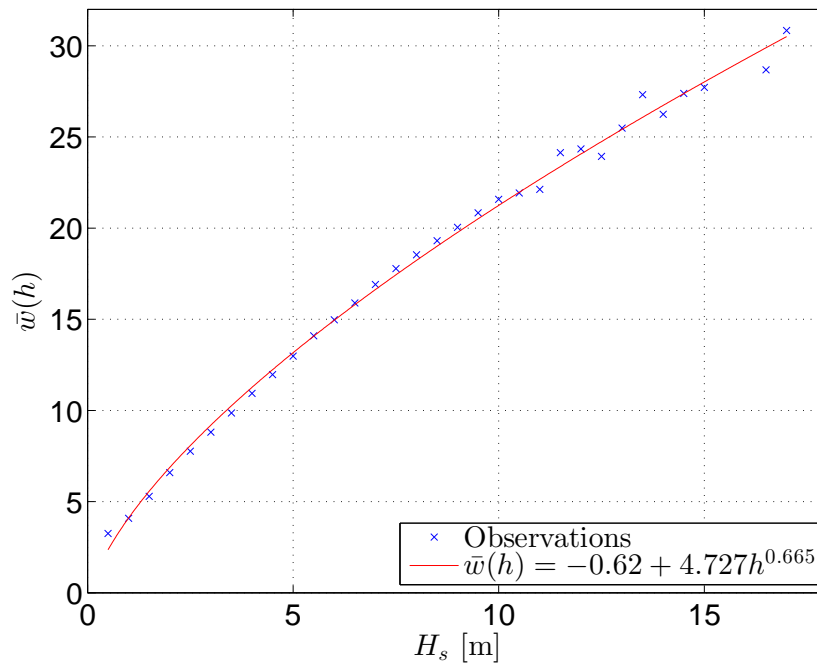




D.3 Conditional distribution of T_p

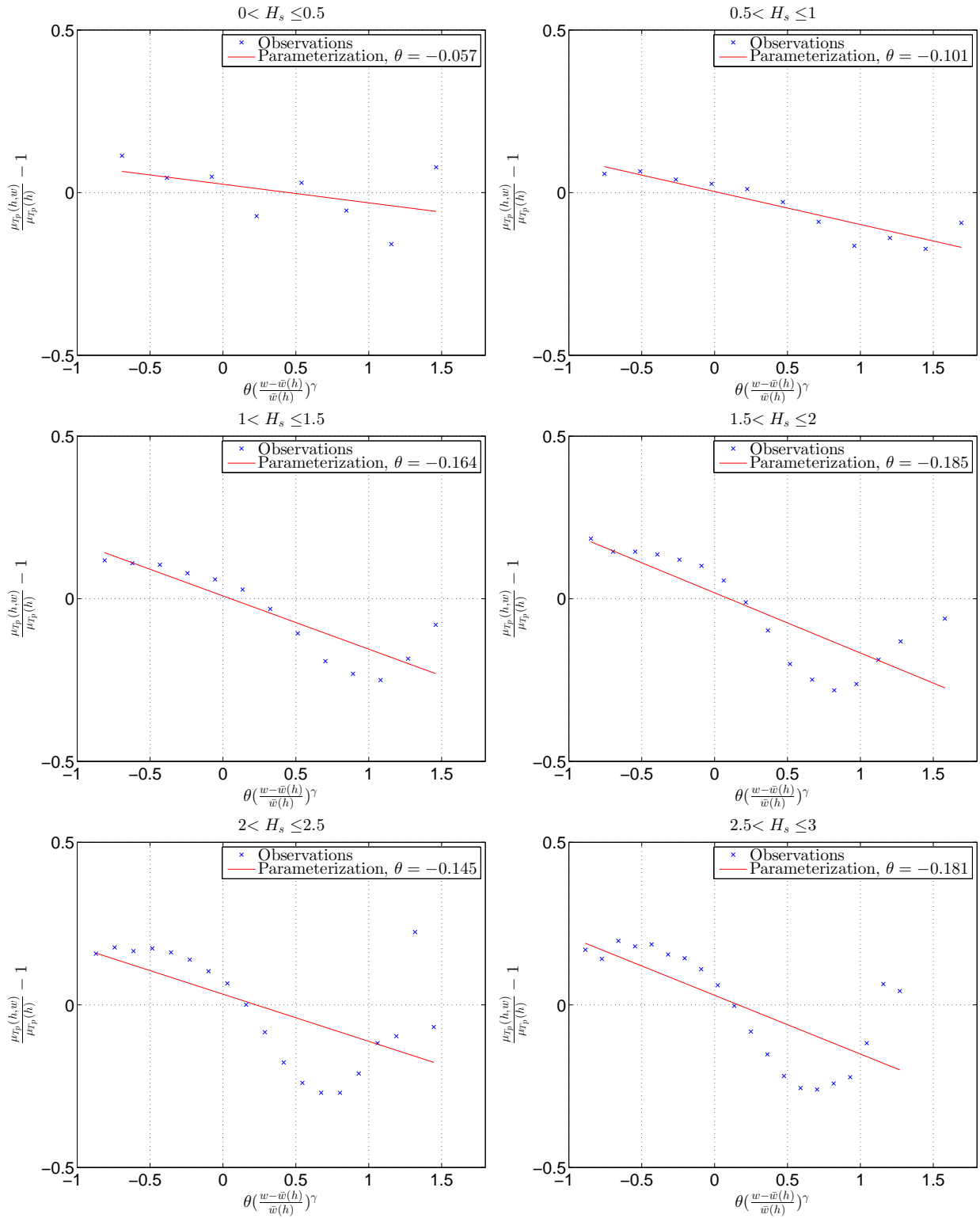


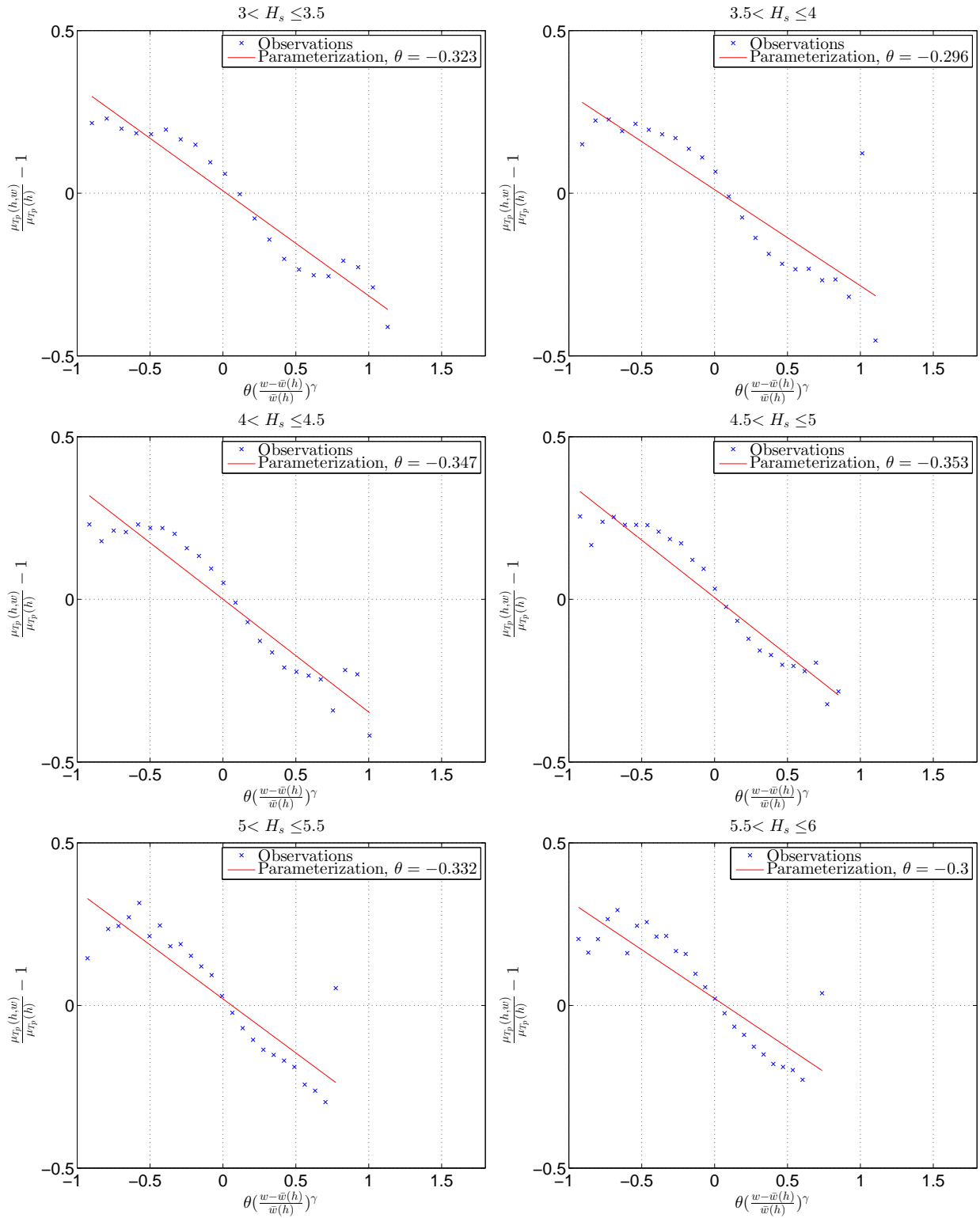
Parameterization of μ_{T_p} compared to empirical observations

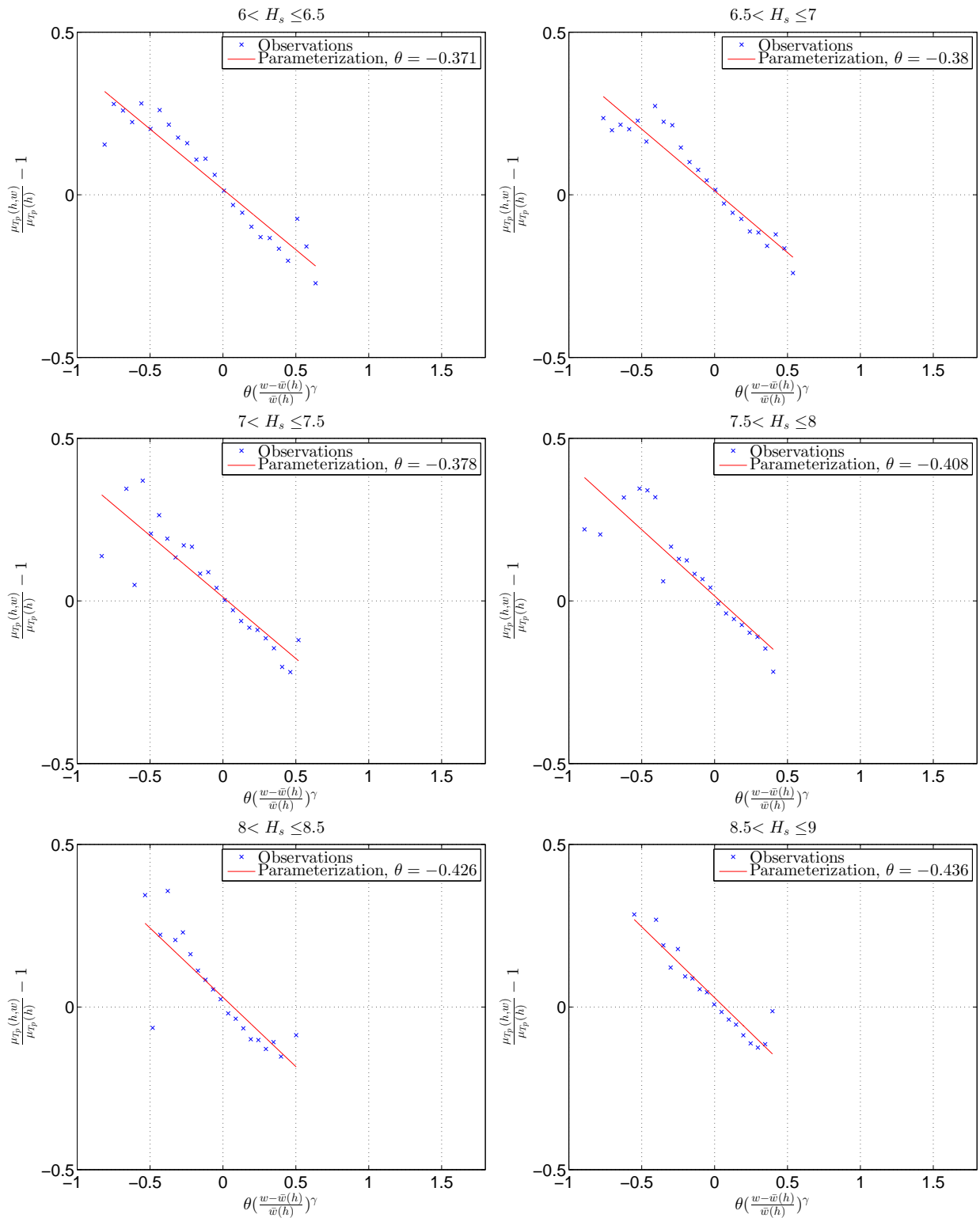


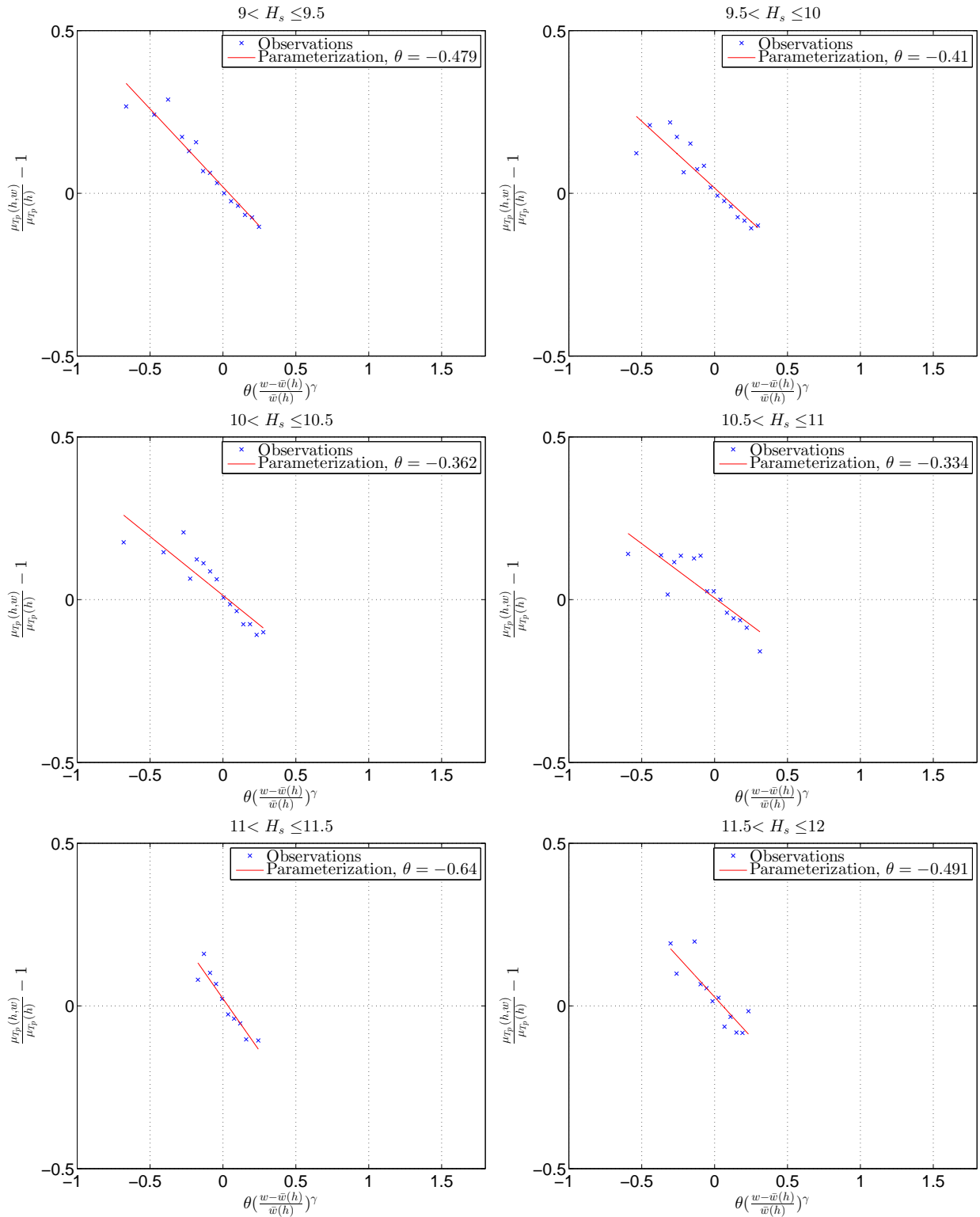
Parameterization of $\bar{w}(h)$ compared to empirical observations

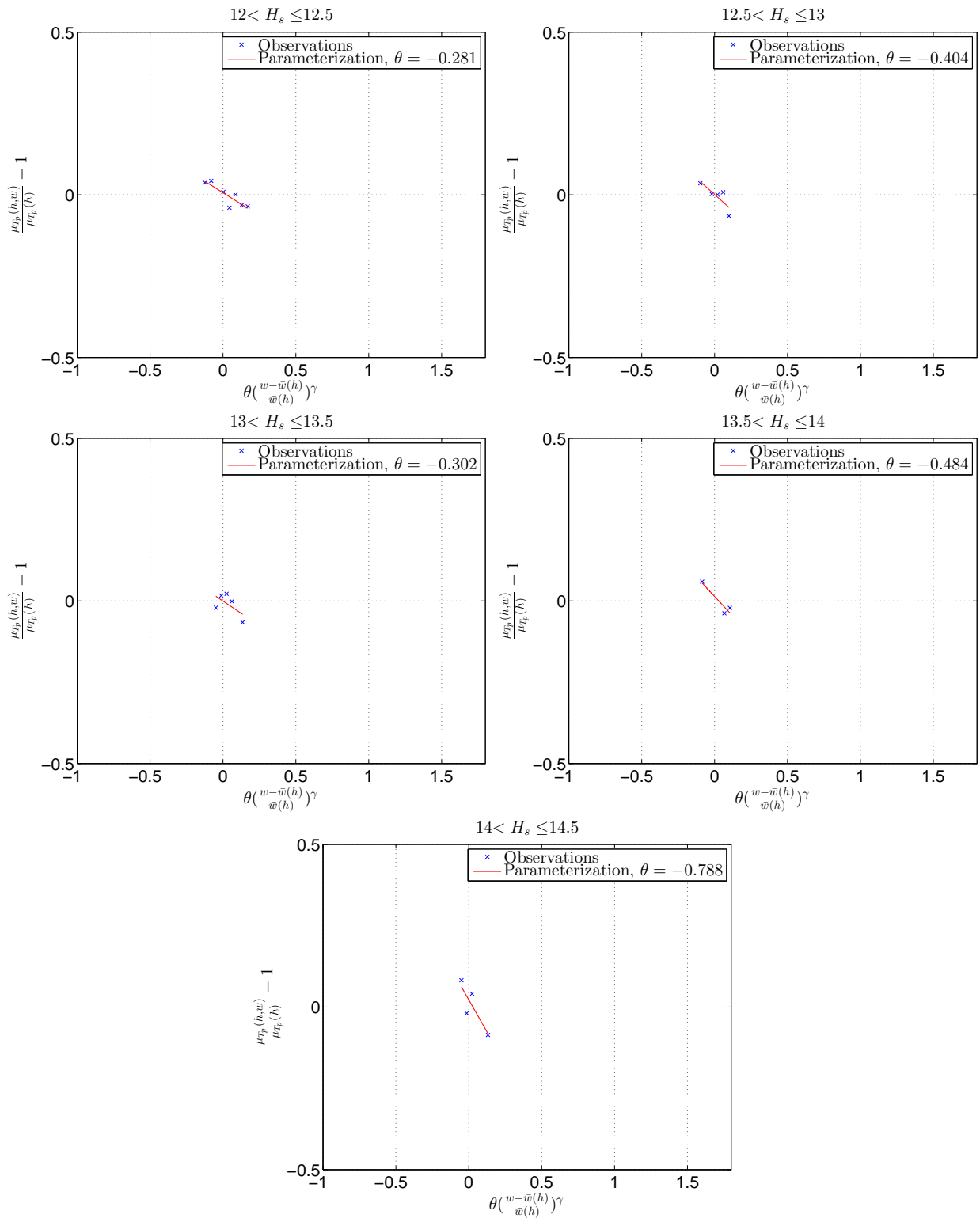
Normalized T_p as a function of normalized W







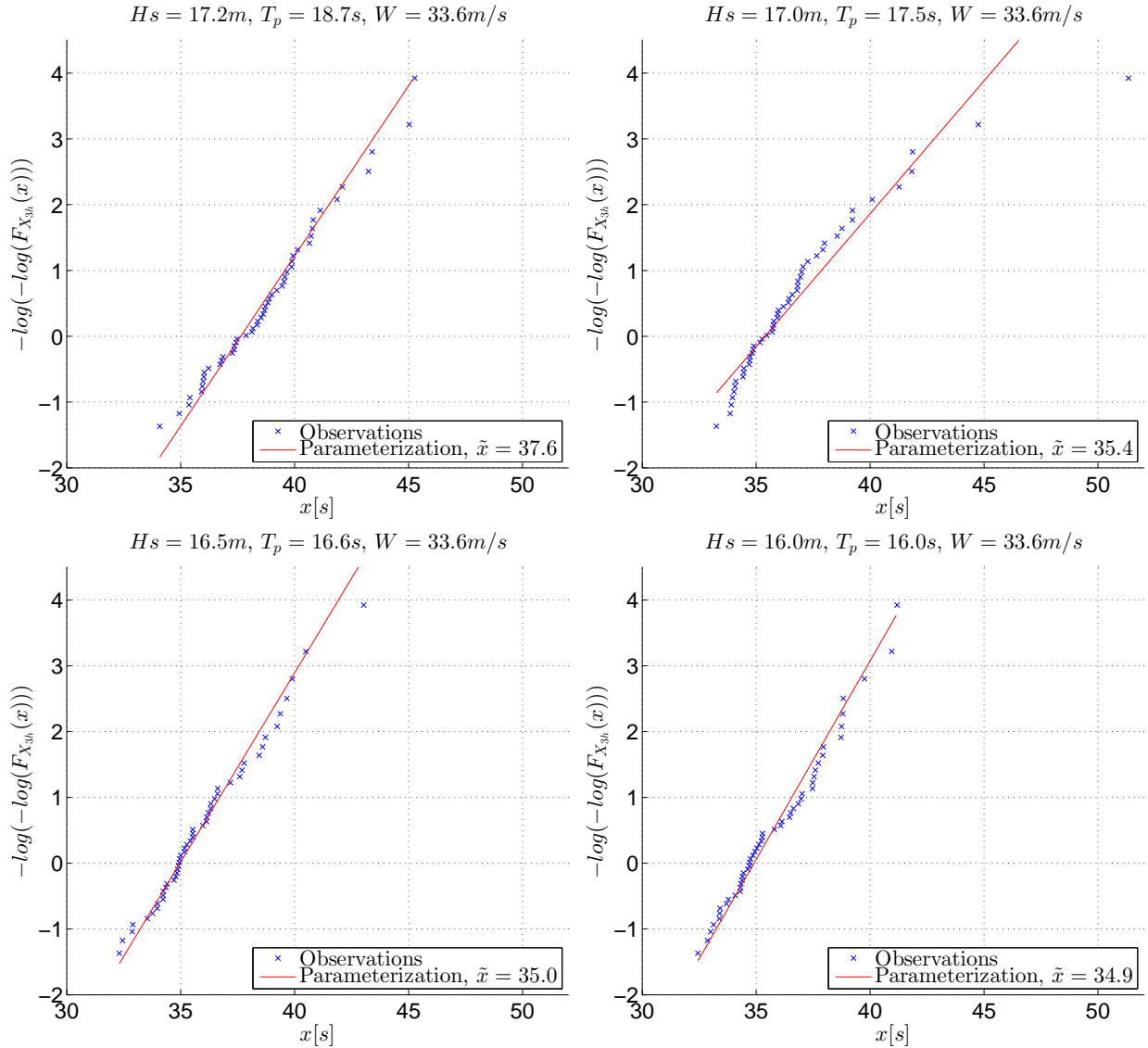




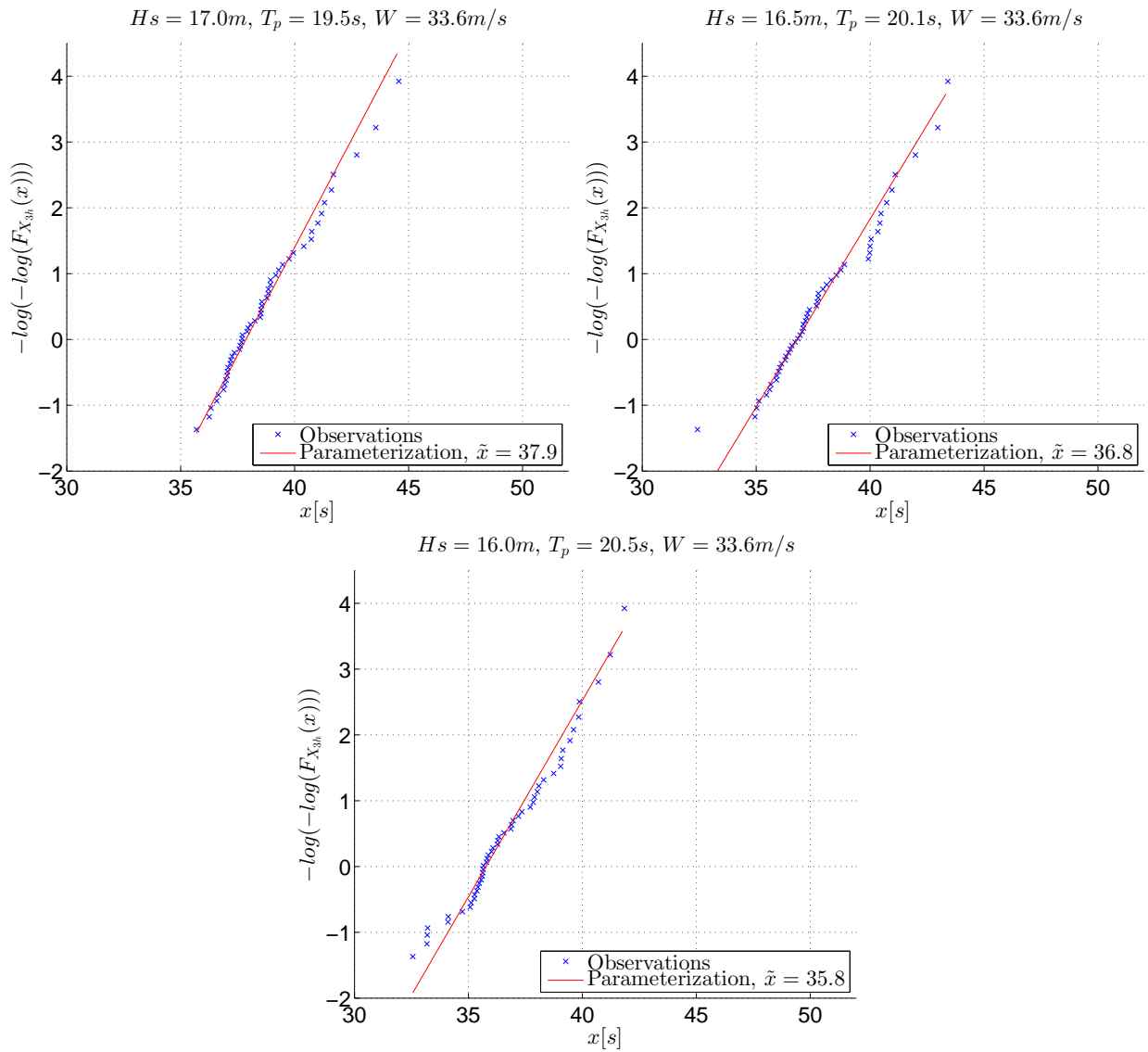
Appendix E

Traditional approach in estimating characteristic responses

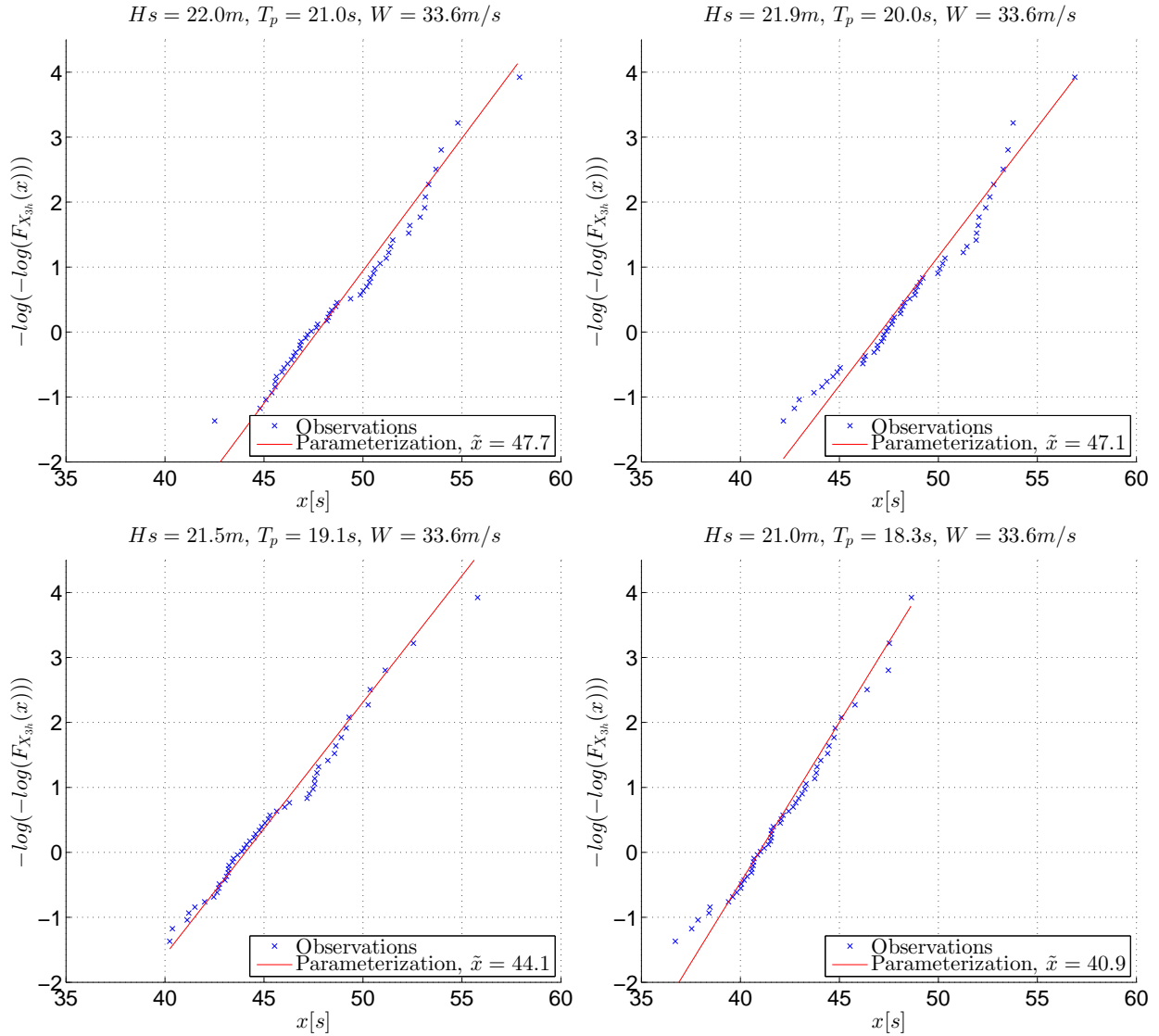
E.1 Responses along 100-year contour of H_s and T_p in combination with 100-year wind speed



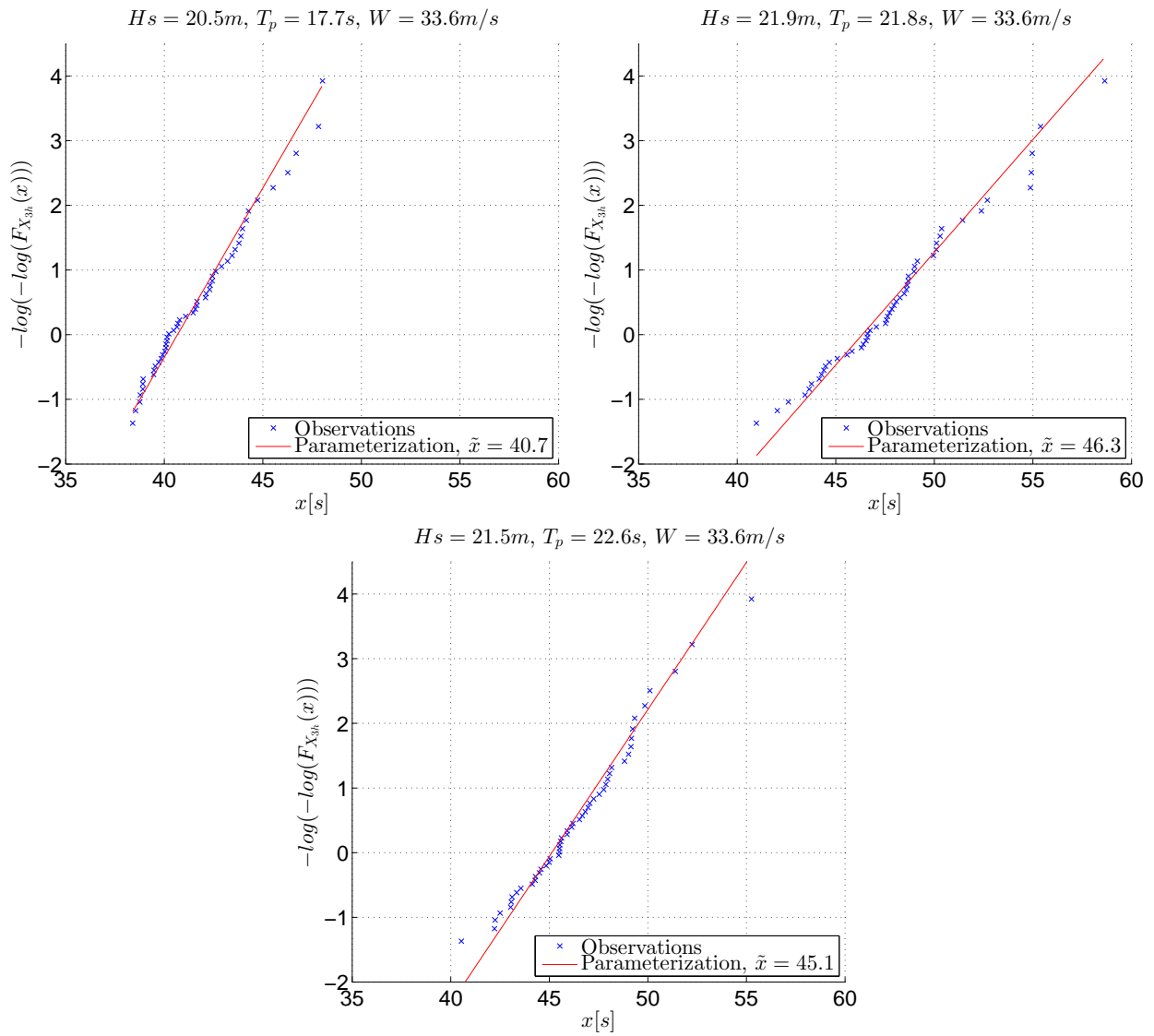
E.1. RESPONSES ALONG 100-YEAR CONTOUR OF H_S AND T_P IN COMBINATION WITH 100-YEAR WIND SPE



E.2 Responses along 10,000-year contour of H_s and T_p in combination with 100-year wind speed



E.2. RESPONSES ALONG 10,000-YEAR CONTOUR OF H_S AND T_p IN COMBINATION WITH 100-YEAR WIND S



E.3 Responses on 100-year contour of H_s and T_p in combination with 10,000-year wind speed

